Die approbierte Originalversion dieser Dissertation ist an der Hauptbibliothek der Technischen Universität Wien aufgestellt (http://www.ub.tuwien.ac.at).

The approved original version of this thesis is available at the main library of the Vienna University of Technology (http://www.ub.tuwien.ac.at/englweb/).

TECHNISCHE UNIVERSITÄT WIEN
Vienna University of Technology

DISSERTATION

HIGHER ORDER PRINCIPLES IN DISTRIBUTION PATTERNS OF SEROTONERGIC RECEPTOR SUBTYPES REVEALED BY POSITRON EMISSION TOMOGRAPHY

Ausgeführt zum Zwecke der Erlangung des akademischen Grades eines Doktors der technischen Wissenschaften unter der Leitung von

Ao.Univ.Prof. Dipl.-Ing. Dr.rer.nat. Dr.techn. Dr.scient.med. Frank Rattay
E101
Institut für Analysis und Scientific Computing
Computational Neuroscience and Biomedical Engineering

und

Assoc.Prof. PD Dr.med. Rupert Lanzenberger
Medizinische Universität Wien
Universitätsklinik für Psychiatrie und Psychotherapie
Functional, Molecular & Translational Neuroimaging Lab – PET & MRI

eingereicht an der Technischen Universität Wien
Fakultät für Mathematik und Geoinformation

von

Dipl.-Ing. (FH) Markus Savli
Matrikelnummer 0226759
Adalbert-Stifter-Straße 35/9/9
1200 Wien

Wien, am 19. September 2012

Danksagung

An dieser Stelle möchte ich mich bei vielen Personen bedanken, die mich bei der Erstellung dieser Arbeit unterstützt haben. Besonderer Dank gilt dabei zunächst Assoc.Prof. PD Dr.med. Rupert Lanzenberger, der nicht nur die wissenschaftliche Betreuung meiner Dissertation übernommen und dessen Fortschritt durch seine zielgerichtete Betreuung bereichert, sondern mich auch durch seine wertvollen Anregungen und Ratschläge hinsichtlich fachlicher und persönlicher Weiterentwicklung stets gefördert hat. Die Forschungstätigkeit in seinem Labor war eine äußerst fruchtbare Zeit – nicht zuletzt aufgrund der ausgesprochen angenehmen und kollegialen Atmosphäre. Ich möchte mich bei allen Kollegen der gesamten Arbeitsgruppe des Functional, Molecular and Translational Neuroimaging Labors bedanken, die nie abgeneigt waren, bei einfachen wie auch schwierigen Fragestellungen zu helfen, aber auch immer für einen guten Scherz aufgelegt waren. Hierbei möchte ich ebenfalls O.Univ.Prof. Dr.h.c.mult. Dr.med. Siegfried Kasper, Vorstand der Universitätsklinik für Psychiatrie und Psychotherapie erwähnen, der stets wohlwollend meiner Forschungstätigkeit gegenüberstand.

Nicht weniger zu danken gilt es Ao.Univ.Prof. Dipl.-Ing. Dr.rer.nat. Dr.techn. Dr.scient.med. Frank Rattay für seinen positiven Einfluss auf die Arbeit, vor allem seinen ermutigenden Zuspruch von Beginn an, den Sprung ins kalte Wasser zu wagen. Er hat mich in jeglicher Hinsicht unterstützt und ohne ihn hätte ich den Schritt in die Welt der Wissenschaft wahrscheinlich nicht riskiert.

Nicht versäumen will ich auch meinen Dank für viele Freunde auszusprechen, die mir während dieser Zeit ermutigend und unterstützend beistanden. Besonders danken möchte ich Renate, die nicht müde wurde mich immer wieder anzuspornen, sowie Gudrun, unter deren Fittichen ich einen Unterschlupf als Maulwurfskönig fand. Es war eine lustige und angenehme Zeit bei ihr, die ich nie vergessen werde. Dank auch an Benjamin für viele Ge-

spräche und spontane Kochaktionen. Ferner möchte ich mich bei Andrés und seiner Familie für viele Sonntagnachmittage bedanken. Ebenfalls möchte ich mich bei Bernd für die sportlichen Ausflüge und Wettkämpfe bedanken.

Ein herzlicher Dank gilt vor allem meiner Familie, die während der Zeit meines Studiums eine stets hilfreiche und ermunternde Stütze waren, obwohl sie mich aufgrund der Entfernung nur selten zu Gesicht bekamen. Danke für euer vorbehaltloses Vertrauen in guten sowie herausfordernden Phasen und dass ihr immer für mich da wart!

Jenseits der menschlichen Hilfestellung möchte ich meinen besonderen Dank an Gott, den Vater und Herrn Jesus Christus aussprechen, der mir Kraft, Gesundheit, Ausdauer sowie Weisheit schenkte diese Arbeit erfolgreich durchzuführen.

Zusammenfassung

Das äußerst umfangreiche serotonerge System mit seinen mindestens 16 Rezeptorsubtypen ist in der Pathophysiologie von vielen neuropsychiatrischen Erkrankungen involviert. Unterschiede in den Verhältnissen zwischen den verschiedenen prä- und postsynaptischen Rezeptoren gelten als wahrscheinliche Ursachen dieser Erkrankungen. Bisher gibt es jedoch kaum umfassende *in vivo* Werte, die mit standardisierten Verfahren erfasst wurden. In dieser Positronenemissionstomographie (PET) Studie wurden 3 Rezeptorsubtypen des serotonergen Systems mit den wichtigsten inhibitorischen (5-HT_{1A}, und 5-HT_{1B}) und exzitatorischen Rezeptoren (5-HT_{2A}), sowie des Serotonintransporter (5-HTT) bei gesunden Menschen quantifiziert. Ziel der Studie war es 1) eine Datenbank mit standardisierten Werten zu erstellen, 2) Zusammenhänge mit post-mortem Daten zu untersuchen und 3) Wechselwirkungen zwischen den inhibitorischen und exzitatorischen Rezeptoren festzustellen. Die PET Messungen wurden insgesamt an 95 gesunden Probanden durchgeführt (Alter=28.0±6.9 Jahre; 59% männlich) wobei die selektiven Radioliganden [*carbonyl*-^{11}C]WAY-100635, [^{11}C]P943, [^{18}F]altanserin und [^{11}C]DASB verwendet wurden. Eine standardisierte Vorlage im stereotaktischen Raum diente zur Bestimmung der Zielregionen. Diese Vorlage beinhaltete zwei anatomische Parzellierungschemata: 1) 41 Brodmann Areale und 2) 52 AAL (automated anatomical labeling) Regionen. Die daraus berechneten durchschnittlichen kortikalen und subkortikalen Bindungspotentialwerte (BP) ergaben eine gute Übereinstimmung mit den bisher publizierten *in vivo* und post-mortem Daten. Mittels linearer Gleichungen wurden Zusammenhänge zu den post-mortem Bindungen hergestellt, welche 5.89 pmol/g (5-HT_{1A}), 23.5 pmol/g (5-HT_{1B}), 31.44 pmol/g (5-HT_{2A}) und 11.33 pmol/g (5-HTT) als Äquivalent für ein BP von 1 ergaben. Darüber hinaus wurden rezeptorspezifische BP Mittelwertsmaps auf Voxelebene erstellt. Signifikante partielle Korrelationen zwischen den BP Werten zweier Rezeptoren korrigiert für den dritten sowie den 5-HTT zeigten systemische Wechselwirkungen anstatt unabhängiger Mechanismen einzelner Rezeptoren. Diese Erkenntnisse können die Interpretation über Veränderungen im serotonergen System, die während neuropsychiatrischer Erkrankungen stattfinden, verbessern.

Abstract

The highly diverse serotonergic system with at least 16 different receptor subtypes is implicated in the pathophysiology of most neuropsychiatric disorders. Alterations of the interplay between various pre- and postsynaptic receptor subtypes might be involved in the pathogenesis of these disorders. However, there is a lack of comprehensive *in vivo* values using standardized procedures. In the current PET study 3 receptor subtypes, including the major inhibitory (5-HT_{1A} and 5-HT_{1B}) and excitatory (5-HT_{2A}) receptors, and the transporter (5-HTT) were quantified in the brain of healthy human subjects to 1) provide a database of standard values; 2) establish associations to post-mortem data; and 3) examine the interaction between inhibitory and excitatory receptors. PET scans were performed on 95 healthy subjects (age=28.0±6.9 years; 59% males) using the selective radioligands [*carbonyl*-^{11}C]WAY-100635, [^{11}C]P943, [^{18}F]altanserin and [^{11}C]DASB, respectively. Data analysis was uniformly carried out using a unique template in stereotactic space. This template follows two anatomical parcellation schemes: 1) Brodmann Areas including 41 regions and 2) AAL (automated anatomical labeling) including 52 regions. Mean cortical and subcortical binding potential (BP) values were in good agreement with previously published human *in vivo* and post-mortem data. By means of linear equations, PET binding potentials were translated to post-mortem binding (provided in pmol/g), yielding 5.89 pmol/g (5-HT_{1A}), 23.5 pmol/g (5-HT_{1B}), 31.44 pmol/g (5-HT_{2A}), and 11.33 pmol/g (5-HTT) being equivalent to the BP of 1, respectively. Furthermore, individual voxel-wise maps with BP values were computed from average tracer-specific whole-brain binding maps. Significant partial correlations were found between the binding potentials of receptors pairs controlled for the third and the transporter, emphasizing a systemically organized interaction instead of independent receptor mechanisms. This knowledge might improve our interpretation of the alterations taking place in the serotonergic system during neuropsychiatric disorders.

Vorwort

Die vorliegende Dissertation wurde im Jahr 2012 verfasst und ist während meiner Tätigkeit als Wissenschaftlicher Mitarbeiter im Functional, Molecular & Translational Neuroimaging Lab – PET & MRI an der Medizinische Universität Wien, Universitätsklinik für Psychiatrie und Psychotherapie unter der Leitung von Assoc.Prof PD Dr.med. Rupert Lanzenberger sowie Ao.Univ.Prof. Dipl.-Ing. Dr.rer.nat. Dr.techn. Dr.scient.med. Frank Rattay (Institut für Analysis und Scientific Computing, Technische Universität Wien) entstanden. Die Ergebnisse dieser Arbeit resultieren aus Erkenntnissen, die ich im Rahmen meiner Forschungstätigkeit in den vergangenen Jahren gewinnen konnte. Die dafür verwendete Literatur habe ich bis Juli 2012 berücksichtigt. Außerdem möchte ich erwähnen, dass Teile dieser Arbeit im Journal *NeuroImage* unter dem Titel „Normative database of the serotonergic system in healthy subjects using multi-tracer PET“ (NeuroImage 63 (1) (2012) 447–459) als Fachartikel erschien. Weitere Artikel über die in dieser Arbeit erörterten Themen sind in Planung und werden vorrausichtlich demnächst publiziert.

Wien, September 2012

It is the heart which perceives God, and not the reason.

Blaise Pascal

(1623-1662) French Scientist, Religious Philosopher

Abbreviations

5-HT	5-Hydroxytryptamin, Serotonin
$5\text{-}HT_{1A}$	Serotonin-1A receptor
$5\text{-}HT_{1B}$	Serotonin-1B receptor
$5\text{-}HT_{2A}$	Serotonin-2A receptor
5-HTT	Serotonin transporter
AAL	Automated anatomical labeling
BBB	Blood-brain barrier
BGO	Bismuth Germanate, Bismuth Germanium Oxide
B_{max}	Absolute number of binding sites
BP	Binding potential
CT	Computed tomography
DOI	Depth of interaction
FBP	Filtered backprojection
FOV	Field of view
FWHM	Full width at half maximum
GSO	Gadolinium Oxyorthosilicate
keV	Kilo electron volts
K_D	Affinity, dissociation constant
LOR	Line of response
LSO	Lutetium Oxyorthosilicate
LYSO	Lutetium Yttrium Oxyorthosilicate
ML	Maximum likelihood
MNI	Montreal Neurological Institute
MRI	Magnetic resonance imaging
MRTM	Multilinear reference tissue model
NaI(Tl)	Sodium iodide doped with thallium
OSEM	Ordered subset expectation maximization
PET	Positron emission tomography
ROI	Region of Interest
SNR	Signal to noise ratio
SPECT	Single-photon emission tomography
TAC	Time activity curve
TOF	Time of flight
YSO	Yttrium Oxyorthosilicate

Table of contents

Danksagung ii
Zusammenfassung iv
Abstract v
Vorwort vi
Abbreviations viii
Table of contents ix

1 Introduction.....1
1.1 Positron Emission Tomography.....1
1.1.1 Positrons.....2
1.1.2 Positron Decay.....3
1.1.3 Positron Annihilation.....4
1.1.4 Scintillation detectors.....5
1.1.5 Coincidence detection.....9
1.1.6 True and Random Coincidences.....10
1.1.7 Scatter.....10
1.1.8 Attenuation.....11
1.1.9 Time-of-Flight PET.....14
1.1.10 Spatial Resolution.....16
1.1.11 Tomographic Reconstruction.....19
1.1.11.1 Projections.....19
1.1.11.2 The Sinogram.....20
1.1.11.3 The Radon Transformation.....21
1.1.11.4 Image reconstruction.....23
1.1.11.5 Fourier slice theorem.....23
1.1.12 Backprojection.....23
1.1.13 Other reconstruction methods.....26
1.1.14 2D and 3D PET.....27
1.2 The serotonergic system.....29
1.2.1 5-HT_{1A} receptor.....32
1.2.2 5-HT_{1B} receptor.....34
1.2.3 5-HT_{2A} receptor.....36

1.2.4 The serotonin transporter 37
1.3 Brain receptor imaging 38
1.3.1 Receptor Quantification 40
1.4 Neuroanatomy 42
1.5 Databases 44

2 Experimental Setup and Methods 45
2.1 Participants 45
2.2 Radiosynthesis and data acquisition 47
2.2.1 [carbonyl-^{11}C]WAY-100635 47
2.2.2 [^{11}C]P943 50
2.2.3 [^{18}F]altanserin 53
2.2.4 [^{11}C]DASB 55
2.3 Image preprocessing 59
2.4 Region of interest definition 59
2.5 Data quantification 62
2.6 Statistical analysis 63

3 Results 65
3.1 PET Binding Potential 67
3.2 Comparison with *in vivo* data 73
3.3 Comparison with post-mortem data 76
3.4 Interaction between binding proteins 82
3.4.1 Brodmann Areas 83
3.4.2 AAL Regions 86

4 Discussion 89
4.1 Database of standard values 89
4.2 Comparison with post-mortem data 92
4.3 Interaction between inhibitory and excitatory receptors 92
4.4 Limitations and outlook 95

5 References 97

6 Curriculum Vitae 111

1 Introduction

1.1 Positron Emission Tomography

Positron emission tomography (PET) is a non-invasive nuclear medicine imaging technique to image specific biomolecules in the living brain (Bailey et al., 2003). Since the introduction of the first human PET tomograph in the year 1974 (Phelps et al., 1975; Ter-Pogossian et al., 1975), PET has emerged as an important clinical tool in oncology, neurology, and cardiology (Rohren et al., 2004; Walker et al., 2004). More specifically, PET is used to examine brain disease, most notably brain tumors, strokes and neurodegenerative diseases (dementia/Alzheimer' disease). Furthermore, it can also show perfusion, blood flow, oxygen extraction and glucose metabolism of the working brain (Jones and Rabiner, 2012). The sensitivity of PET in detecting and quantifying small amounts of substances in concentrations down to the picomolar range is unmatched by any other imaging method currently available (Heiss and Herholz, 2006). In recent years PET has become a suitable method for clinical studies on psychiatric disorders, as well as early stage drug development (Walker et al., 2004) and neurosurgical examinations (Frankle et al., 2005; Wahl and Buchnan, 2002). Figure 1 depicts the increasing number of articles being published.

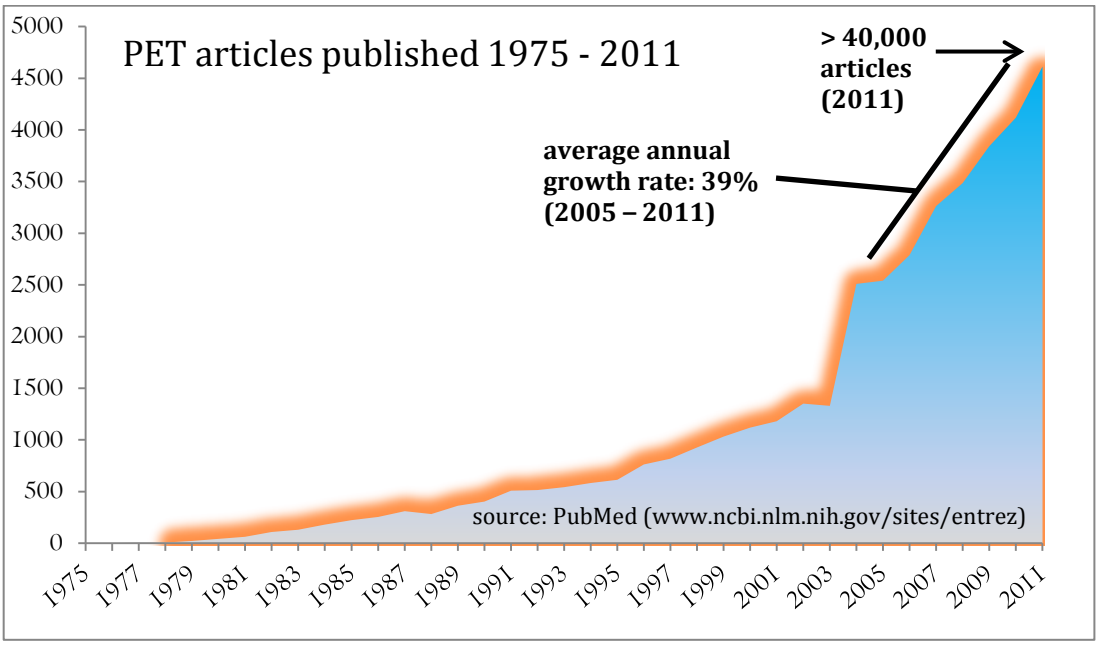

Figure 1: Number of articles using positron emission tomography accessible within PubMed (www.ncbi.nlm.nih.gov/sites/entrez).

1.1.1 Positrons

By its very nature, PET imaging relies on positrons and positron decay. Positrons are the antimatter counterpart of electrons with equal mass but positively charged. Combining quantum mechanics and special relativity, Paul A.M. Dirac was the first to propose the existence of these particles in 1928. A few years later, positrons were detected experimentally by Carl D. Anderson using a cloud chamber. Both were awarded the Nobel Prize in Physics for their achievements. Positrons also were the first antimatter particles to be demonstrated.

Isotope	Half-life $t_{1/2}$	Production	Maximum Energy	Positron range in water (mm)	
	min		MeV	mean	max
^{15}O	2.01	$^{14}N(d,n)^{15}O$	1.72	1.5	7.3
^{13}N	9.98	$^{16}O(p,\alpha)^{13}N$	1.19	1.4	5.1
^{11}C	20.4	$^{14}N(p,\alpha)^{11}C$	0.96	1.1	4.1
^{18}F	109.8	$^{18}O(p,n)^{18}F$	0.64	1.0	2.4

Table 1: Properties of positron emitting isotopes used in nuclear medicine.

1.1.2 Positron Decay

Positrons are emitted from radionuclides, i.e. radioactive atomic nuclei which are proton-rich. In an attempt to stabilize, they decay by giving off a positive charge (Bailey et al., 2003). This is also known as positive beta decay and is the more prevalent mode of decay for lower atomic weight nuclei (e.g. Oxygen-15 (^{15}O), Carbon-11 (^{11}C), Nitrogen-13 (^{13}N), and Fluorine-18 (^{18}F)), while higher atomic weight nuclei (e.g. ^{123}I) decay by electron capture. The general equation for positron decay from an atom is:

$$ {}^{A}_{Z}X_{N} \xrightarrow{decay} {}_{Z-1}^{A}Y_{N+1} + e^{+} + \upsilon \qquad (1) $$

The decay of the positron results in a new nuclide of the same mass number but with one atomic number less than the parent, hence 1 proton is converted into 1 neutron. The emission of a neutrino accompanies this conversion as first postulated by W. Pauli 1930. Neutrinos are very light particles without charge. Since it interacts very weakly with other particles or the surrounding material, the neutrino escapes without direct relevance to PET imaging.

Particle accelerators are necessary to produce positron emitting radionuclides. Nuclides suitable for medical use are usually short living isotopes which are analogues of components found in nature involved in biochemical processes (Price, 2003). The most commonly used isotopes are ^{11}C, ^{13}N, ^{15}O, ^{18}F. However, the synthesis of isotopes requires the in-house production of those positron emitters. Nowadays cyclotron units (Ernest O. Lawrence; Nobel Prize 1939) are installed at hospitals which paved the way for the on-site production of target molecules applied in nuclear medicine (see Figure 2). Table 1 summarizes some positron emitting isotopes used in nuclear medicine.

Figure 2: *Cyclotron unit at the AKH Wien.*

1.1.3 Positron Annihilation

After ejection from the nucleus, positrons travel through matter until they collide with an electron. The travelling distance depends on the initial positron energy and is usually a few millimeters (see Table 1), because the positron first has to lose kinetic energy and decelerate before it can interact with an electron. When encountering with a nearby electron, both the positron and the electron annihilate, and their masses are converted into a pair of photons of identical energy. Figure 3 illustrates the annihilation process. The final energy results from the kinetic and mass energy of both particles according to Einstein's famously described mass-energy equivalence (mass times the speed of light squared) (Einstein, 1905). The two annihilation γ-ray photons, each with an energy of 511keV, are emitted simultaneously in opposite directions of approximately 180 degrees.

$$e^{+} + e^{-} \xrightarrow{\text{annihilation}} \gamma + \gamma \tag{2}$$

$$E = m \cdot c^{2} \tag{3}$$

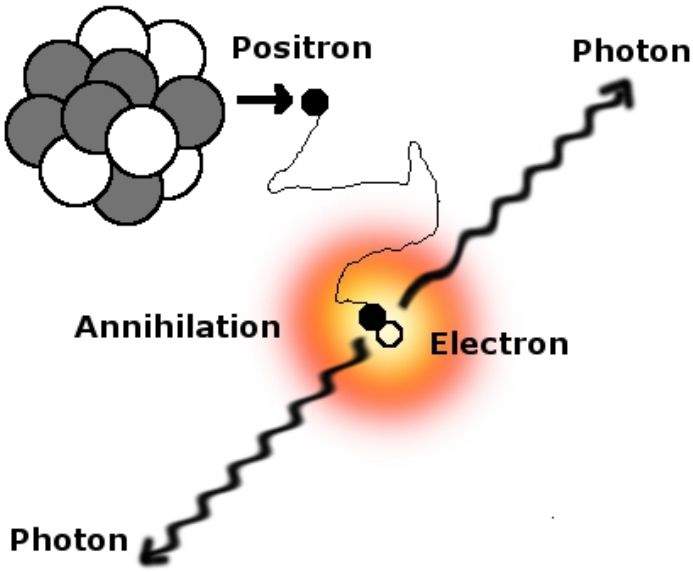

Figure 3: Emission of 2 γ-ray photons with an energy of 511keV in opposite directions after annihilation of a position and an electron.

1.1.4 Scintillation detectors

Scintillators have luminescence properties that generate light in fluorescent tubes when excited by ionizing radiation (see Figure 5). In order to count the photons, scintillators are connected to an electronic light sensor, such as photomultiplier tubes or semiconductor-based photodiodes (e.g. avalanche photodiodes) (see Figure 5). Scintillator materials used for detectors in PET scanners are often inorganic chemical compounds grown in high temperature furnaces such as BGO (Bismuth Germinate), GSO (Gadolinium Oxyorthosilicate), LSO (Lutetium Oxyorthosilicate) or LYSO (Lutetium Yttrium Oxyorthosilicate). Sodium iodide doped with thallium (NaI(Tl)) and BGO became the first generation (about the 1980s and through the 1990s) of scintillators in a conventional PET scanner (Basu et al., 2011). While NaI(Tl) fur-

nished very high light output, and hence good energy resolution, BGO provided very high sensitivity. In spite of the individual strengths and weaknesses of each scintillator, the long decay time limited the performance of these scanners, especially at high count rates (Basu et al., 2011). The introduction of GSO brought slight improvements regarding light output, sensitivity, and decay time compared to the earlier generation of scintillators. In the latest generation of scintillators, LSO and LYSO are the preferred materials for PET detectors (Kimble et al., 2003). Both have very similar properties featuring very high light output (close to that of NaI(Tl)), high sensitivity (close to BGO), and very fast decay times. Their cerium-doped silicate analogues additionally obtain high stopping power and fast bright scintillation light (Cerium-doped Lutetium Oxyorthosilicate and Cerium-doped Lutetium Yttrium Orthosilicate) (Humm et al., 2003). Table 2 gives an overview of commonly used scintillator materials.

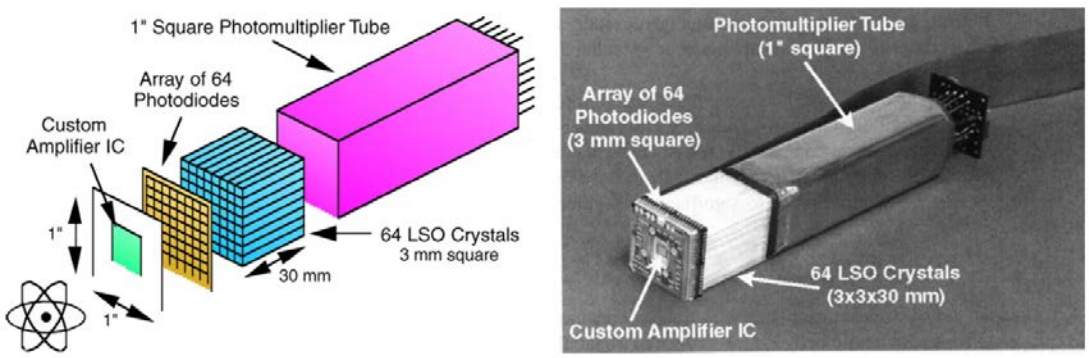

Figure 4: Components of scintillator and photomultiplier tube. Reproduced from (Lewellen, 2008).

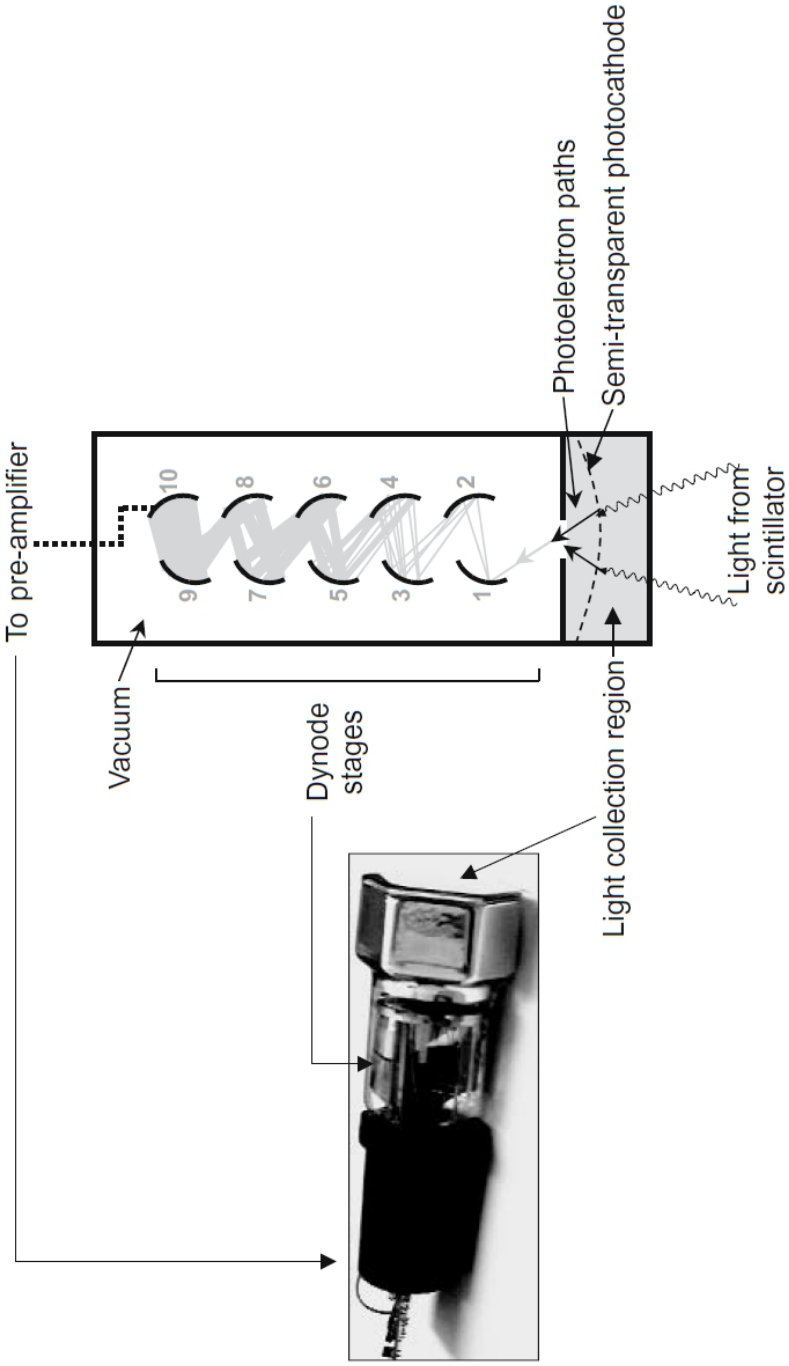

Figure 5: Scheme of scintillation of photon and amplification of photoelectron in the photomultiplier. The photoelectron finally is converted into an electrical signal. Reproduced from (Bailey et al., 2005).

Table 2: Physical properties of commonly used scintillator materials in PET.

Compound	Chemical Formula	Density	Decay Time	Melting Point	Peak Emission Wave Length λ	Light yield	Hydroscopic
		g/cm³	ns	°C	nm	% NaI(Tl)	
NaI(Tl)	NaI(Tl)	3.67	230	651	415	100	yes
BGO	$Bi_4Ge_3O_{12}$	7.13	300	1050	480	15	no
GSO	Gd_2SiO_5:Ce	6.71	50-60	1950	440	25	no
LSO	Lu_2SiO_5:Ce	7.4	40	2050	420	75	no
YSO	Y_2SiO_5:Ce	4.53	40	2470	420	118	no
LYSO	$Lu_{(2-x)}Y_xSiO_5$:Ce	7.4	40	2100	420	75	no
BaF2	BaF_2	4.89	630/0.8	1368	220 (195)	5	slightly

Sodium iodide doped with thallium (NaI(Tl)), Bismuth germanate $Bi_4Ge_3O_{12}$ (BGO), Gadolinium oxyorthosilicate doped with cerium Gd_2SiO_5:Ce (GSO), Lutetium oxyorthosilicate doped with cerium, Lu_2SiO_5:Ce (LSO), Yttrium oxyorthosilicate doped with cerium Y_2SiO_5:Ce (YSO), Lutetium yttrium oxyorthosilicate doped with cerium, $Lu_{(2-x)}Y_xSiO_5$:Ce (LYSO), and barium fluoride (BaF_2). *Barium fluoride possesses a fast-decaying and a slow-decaying component. Data from Cherry et al. 2003, Lewellen 2008, and Lecomte 2009.

1.1.5 Coincidence detection

Simultaneous detection of two annihilation photons in opposite directions is the basic principle of PET imaging with substantially higher sensitivity than conventional single-photon emission tomography (SPECT) imaging. The opposing detectors register the arrival of photons. If two photons are detected within a narrow time frame (typically 3-15ns), this coincidence event is recorded. Such a coincidence window is fundamental as the photons travel different distances from the annihilation event to the detectors. One can further infer that the annihilation occurred somewhere along a line between the two detectors, because the photons leave the annihilation point in opposite directions (see Figures 3 and 10). This line between the detectors is called line of response (LOR). Depending on the radioactivity applied, millions of coincidence events are registered providing a large number of LOR for PET image quantification. In order to increase the sensitivity of scanners a detector ring is used instead of two single detectors, and placed around the patient. Today, commercial PET scanners typically are multi-ring scanners, i.e. they have several rings to simultaneously scan multiple planes. This allows imaging of an axial field-of-view (FOV) of 10 to 25cm which is sufficient for the human brain. Figure 6 shows the PET facility at the AKH Wien.

Figure 6: Human PET facility at the AKH Wien.

1.1.6 True and Random Coincidences

Thus far it is assumed that the coincidence emerges from the same pair of photons produced from the same annihilation event, within the detector ring, somewhere along the LOR. This event is called a *true coincidence* (see Figure 7). However, other coincident events from unrelated photons, which are temporally within the given coincidence window too, may occur and be recorded. These events are called *random or false coincidences*. Figure 7 shows examples of random coincidences. Random coincidences add background noise to the acquired PET image and decrease the image contrast if no correction is applied (Cherry et al., 2003). While true coincidences only occur from a source within the volume between the detector pairs, random coincidences can arise from activities at any location between the detectors, including locations outside the FOV of the system. They are inevitable and constitute the majority of registered coincidence events. Since the occurrence of random coincidences is proportional to the timing window, narrow windows are desirable to improve the image contrast without reducing its signal-to-noise ratio. However, fast scintillators with good timing resolution are required to reduce the number of random coincidences (Bailey et al., 2003).

1.1.7 Scatter

Scattered coincidences are one category of nonvalid registrations. Scatter occurs when one of the photons leaves the body from the annihilation event unscattered and the other photon experiences scatter, i.e. it changes direction before leaving the body. Consequently, this photon is detected in a detector different from the appropriate for a true coincidence event. Thus, according to the resulting LOR between these detectors, the annihilation event may falsely appear outside the body (see Figure 7), however not all photons undergo scatter to this extent. For the detector system it is impossible to distinguish these from valid events. In brain imaging studies the scatter ranges

from 30%-60% of all collected events (Turkington, 2001). Scattered events can be in-plane or out-of-plane. To prevent out-of-plane scatter, lead shields are placed on either side of the detector ring or flat ring-shaped tungsten septa are placed between the detector rings. This can effectively reduce the likelihood of accepting scattered photons down to approximately 10%-20%.

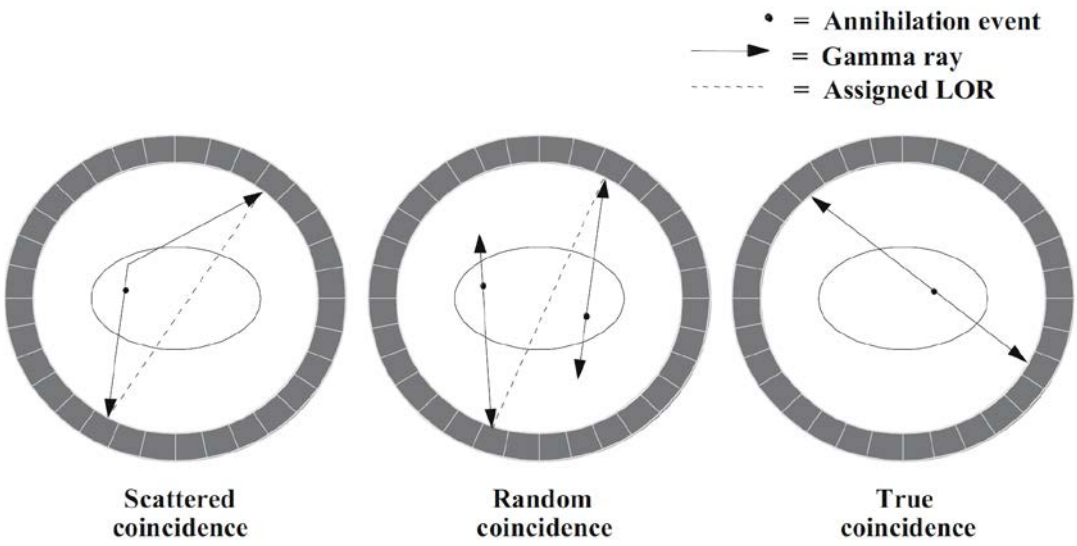

Figure 7: Classification of coincidences. Scattered coincidences (left) occur when one photon deflects (scatters) and changes its direction. Random coincidences (center) emerge from two unrelated annihilation photons. Both scatter and random coincidences lead to incorrect line of response information resulting in a loss of contrast. True coincidences (right) are from a single annihilation event. Reproduced from (Bailey et al., 2003).

1.1.8 Attenuation

When annihilation photons travel in tissue they interact with matter thereby losing energy. Often photons are deflected (scatter) or even absorbed (stopped), and finally may not be detected in any detector (see Figure 7). This loss of true coincidences, due to scatter and absorption, is commonly known as attenuation, and results in degraded PET images since fewer photons are detected. It also increases noise and inaccurate quantification of

radioactivity distributions. The degree of loss depends on the patient's size and increases in heavier patients, since the probability that an event will be attenuated is much higher (Basu et al., 2011). Attenuation takes place in form of a mono-exponential function:

$$I_x = I_0 \cdot e^{-\mu x} \tag{4}$$

where *I* represents the photon beam intensity, the subscript "*0*" the unattenuated beam intensity, the subscript "*x*" the intensity measured through a thickness of a material with thickness *x*, and *μ* refers to the attenuation coefficient of the material (*unit:* cm^{-1}). Each material is characterized by a different attenuation coefficient which is a measure of the probability that a photon will attenuate by a unit length of the material (Bailey et al., 2003). Fortunately, attenuation correction can be relatively easily performed. In a modern integrated PET/CT system (PET with an CT (computed tomography) scanner), adequate attenuation correction can be obtained from the low dose CT scan (X-rays) and applied to the emission scan (Lokitz et al., 2006). The other approach measures the correction by performing an additional transmission scan with an external radioactive source (Humm et al., 2003) which frequently is ^{68}Ge (parent of ^{68}Ga, $t_{1/2}$=273 days). This method is usually applied in PET scanners without integrated CT. Figure 8 depicts both methods of attenuation correction.

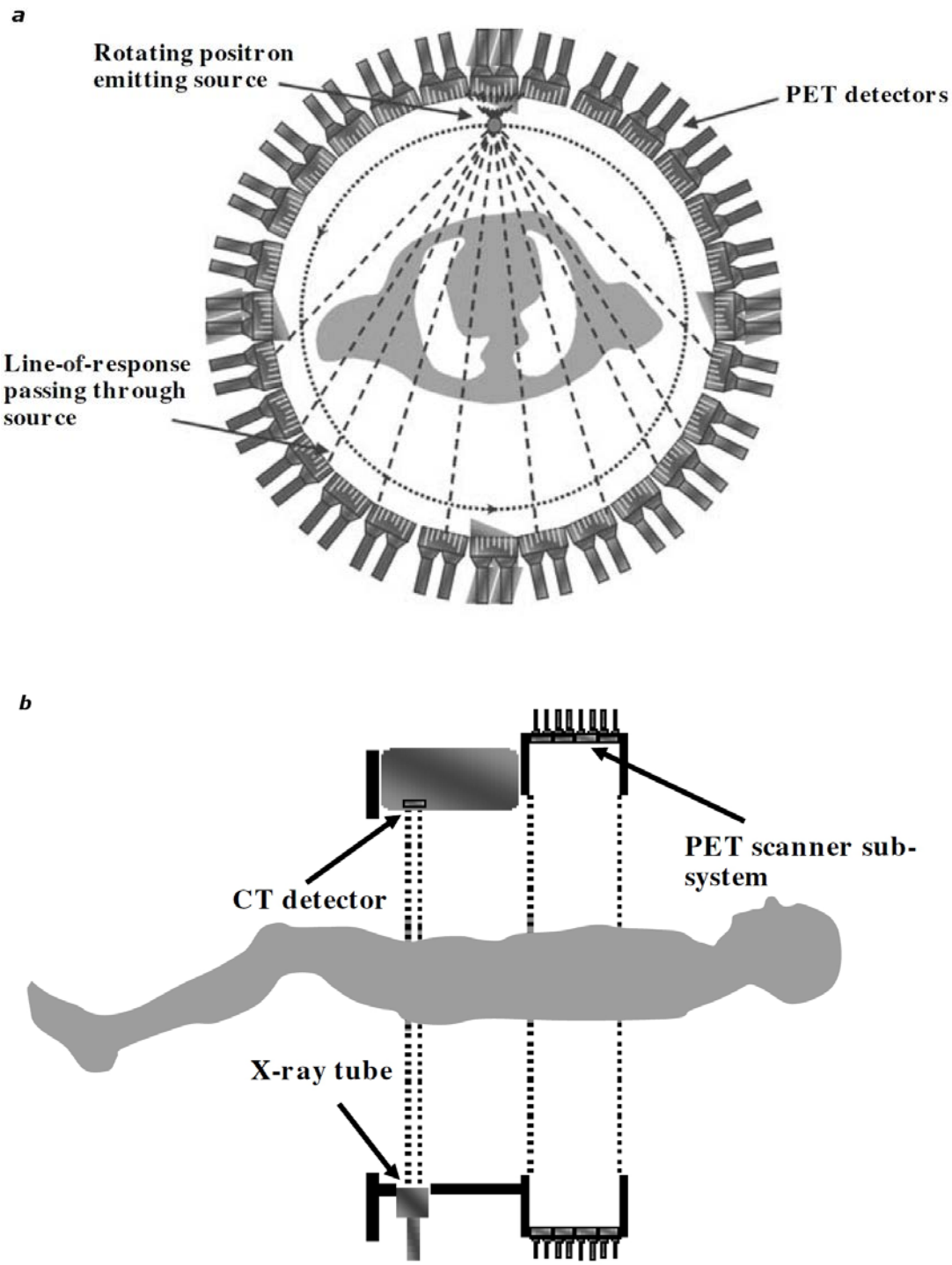

Figure 8: Attenuation correction in PET systems. Before the introduction of PET/CT scanners, a rotating positron-emitting rod source was used to acquire transmission data (a). In dual modality PET/CT systems the X-ray CT performs these measurements. Reproduced from (Bailey et al., 2003).

1.1.9 Time-of-Flight PET

Like most other imaging modalities, PET is affected by statistical noise (Moses, 2007). Accurate measurement of the arriving time of the two annihilation photons between the coincidence detectors can better determine their location along the LOR. This technique is known as time-of-flight PET and would theoretically allow the formation of tomographic images without mathematical reconstruction algorithms (Cherry et al., 2003). Although the first of PET cameras incorporating time-of-flight measurement were built in the 1980's, detection performance was limited by the materials and technologies available at that time (Moses, 2007). Thanks to the advance in electronics, the availability of cheaper computer power, the improvement in reconstruction methods and the discovery of new fast scintillators (Moses and Derenzo, 1999), TOF PET cameras are becoming the new standard technology for all major PET scanner manufactures (Conti, 2011). A good timing resolution also helps reducing the number of random coincidences. The TOF difference is proportional to the path length difference of the two photons, and can be used to estimate the annihilation point along the straight line connecting the detectors. Although time resolution uncertainties caused by several instrumental factors blur the position of the photons, TOF measurement, however, can improve the image quality due to increased signal-to-noise ratio (SNR). The smaller the time resolution (faster scintillator), the smaller the error on the localisation (Conti, 2011). The position of the annihilation event along the line with respect to the midpoint is given by:

$$\Delta x = \frac{c}{2} \cdot \Delta t \tag{5}$$

where Δx is the position error, c is the velocity of light (3×10^{8} m/s), and Δt is the difference in the arrival times of the photons. In order to achieve a sub-centimeter resolution, timing resolution of less than 50 picoseconds (1 psec = 10^{-12} sec) would be required, which is impossible to obtain so far. With the fastest available scintillators and careful design of electronic components,

the achievable timing resolution constrains the positron position to a line segment of about 7.5 cm (Moses, 2007). Nonetheless, this level of timing resolution is already beneficial to acquire images with higher SNR than images reconstructed without TOF information (Cherry et al., 2003). See Figure 9 for a schematic illustration of TOF.

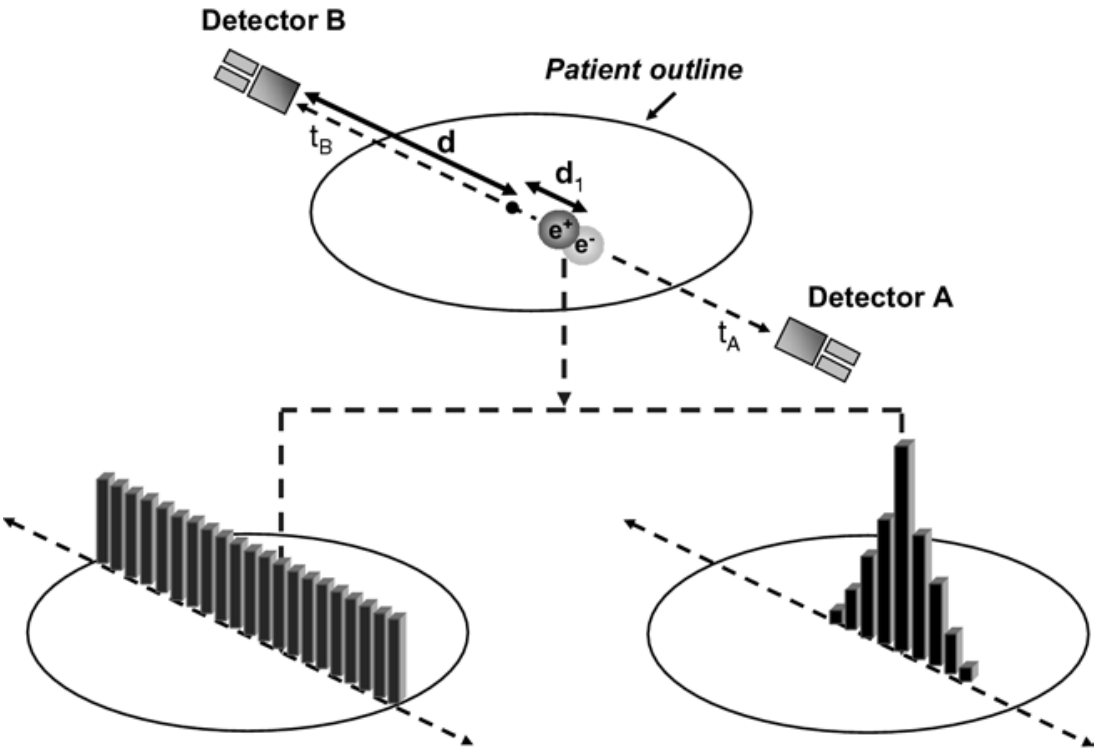

Figure 9: Schematic illustration incorporating time-of-flight (TOF) for PET data acquisition. Conventional PET cameras (left) localize the position of the annihilation event with equal probability along the line joining the two detectors (line of response, LOR), whereas in TOF PET cameras (right) the arrival time difference is used to further restrict the annihilation point to a limited range. Reproduced from (Townsend, 2008).

1.1.10 Spatial Resolution

Spatial resolution is an important factor in PET imaging and is influenced by several degrading factors:

1. **Positron physics**. Before positrons undergo annihilation they travel a distance from the location of decay to the point of annihilation, depending on their initial energy. The initial energy is specific for each nuclide and determines the range of travel for a positron (see Table 1), which is known as *positron range* (Humm et al., 2003). The maximum distance a positron travels, lies within a few millimetres, although its pathway is significantly obstructed with multiple large-angle deflections. However, the distance of interest is the effective positron range which is the average distance from the emitting nucleus measured perpendicularly to the line defined by the direction of the annihilation photons (see Figure 10). Although this distance is always smaller than the maximum range, it is not precisely indicating the location from which the decaying radioactive nucleus emitted the positron. This results in a LOR adjacent to the true annihilation point (Cherry et al., 2003).

2. **Noncollinearity**. A second factor also pertaining to the physics of positrons is that the annihilation photons are almost never emitted strictly at a 180 degree angle from each other due to some residual momentum of the positron just before annihilation (Cherry et al., 2003). This contributes further uncertainty to the localisation of the nuclear decay event of about 0.5° FWHM, and is approximately Gaussian distributed (Bailey et al., 2003; Humm et al., 2003). The effect on spatial resolution is linearly dependent on the distance between the two coincidence detectors. In a typical whole-body PET scanner (~80-90cm diameter), noncollinearity can degrade resolution by a further 1.5-2mm (see Figure 10). This effect and the abovemen-

tioned positron range constitute a fundamental lower limit of the spatial resolution achievable in PET. (Bailey et al., 2003).

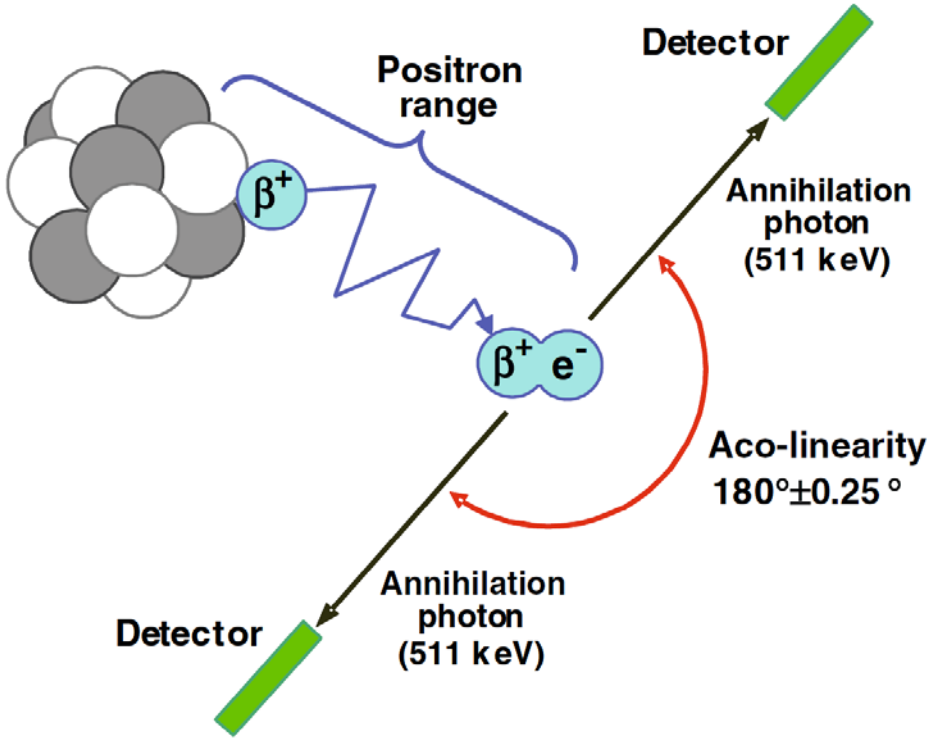

Figure 10: Blurring due to positron physics. The effective positron range is defined as the perpendicular distance from the decaying atom to the line of the two 511keV annihilation photons. The effect that the annihilation photons are almost never emitted at exactly 180° degrees is known as noncollinearity and leads to further positioning errors. Reproduced from (Lecomte, 2009).

3. **Detectors**. The spatial resolution of the multidetector PET system with discrete elements is determined mainly by the size of the individual detector elements or by the intrinsic resolution of the camera detector (Cherry et al., 2003). Although it should ideally be approximately half the width of an individual crystal, there are several interfering factors that limit the resolution feasible in a real detector module (Lewellen, 2008). These are *scatter* within the detector and the *depth-*

of-interaction (DOI) effect. Both effects are related to the density of the scintillator material used in the scanner. In very short crystals the gamma ray Compton scatters in the detector, and will often exit without a second photoelectric interaction (total absorption) (Lewellen, 2008). In order to improve overall sensitivity, an appropriate thickness of scintillator material is required to give good detection efficiency for 511keV annihilation photons (Cherry et al., 2003). Typically, PET systems employ 2- to 3cm thick scintillators. On the other hand, the short distance a photon travels after it enters a detector leads to so-called DOI uncertainties (see Figure 11), since the measured position of energy deposition is projected to the entrance surface of the detector (Bailey et al., 2003). One solution would be to measure the DOI of the photon in the detector (Turkington, 2001) or, alternatively, the implementation of statistical estimation techniques to determine the point of interaction in the crystal array instead of linear algorithms (Lewellen, 2008).

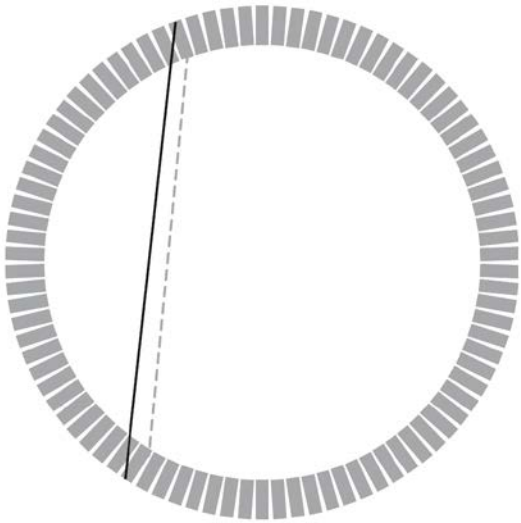

Figure 11: Schematic illustration of parallax error due to unknown depth-of-interaction (DOI) of the photons within a ring detector system. The solid line represents the flight path of the photons, the dashed line the assigned line of response. Reproduced from (Bailey et al., 2003).

1.1.11 Tomographic Reconstruction

Thanks to the discovery of X-rays or Röntgen rays at the end of the 19th century by C. Röntgen (awarded the first Nobel Prize in Physics in 1901), the view into the human body became possible without opening it. These 2-dimensional projections, however, only provided limited insights of the 3-dimensional anatomy in the body. Superior insight has been realized by tomographic images, which constitute 2D-representations of 3D objects showing structures within a specific plane. The term tomography is the composite of the two Greek words *τομή* (section, cut) and *γράφειν* (to write). The underlying mathematical basis for tomographic imaging was first published by the Viennese mathematician Johann Radon in 1917 (Radon, 1986), however it was not until the 1960s that his work found practical application. In the early 1970s the development of the first X-ray computed tomograph (CT) by A.M. Cormack and G. Hounsfield (Nobel Prize 1979) brought Radon's theory into the field of medical imaging (Cormack, 1973; Hounsfield, 1973, 1977, 1980). Later it also came to PET imaging since its basic principles apply to all kinds of tomography.

1.1.11.1 Projections

In a modern PET scanner ring detectors are placed around the object of observation. Theoretically, coincidences between all pairs of detectors are possible. More precisely, for a ring of n detectors these are:

$$\frac{n(n-1)}{2} \tag{6}$$

trajectories (Kalman, 2002; Turkington, 2001). During a PET scan hosts of events are recorded (>10^6). These numerous trajectories can be arranged as sets of parallel LOR, thus one set represents one view of the radioactive distribution of a particular angle at the respective slice. A full set of such line integrals (measured counts) is also called *projection* or *projection profile*

(Cherry et al., 2003), and would be similar from the one by one collection with a collimated gamma camera.

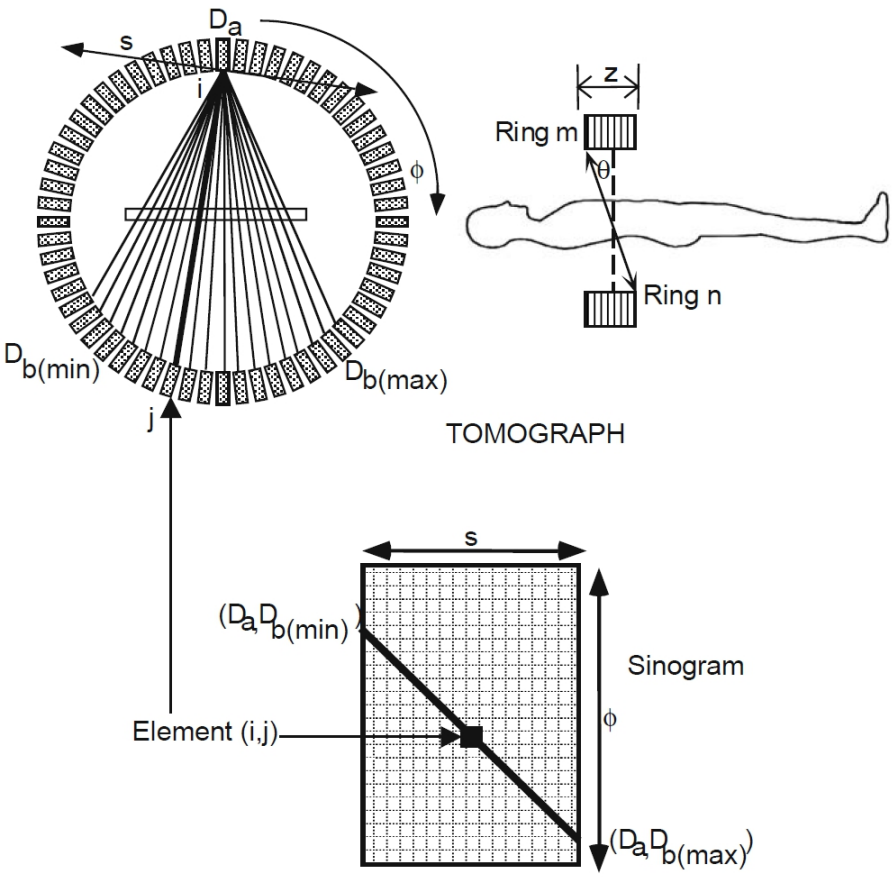

Figure 12: Illustration of Sinogram. Reproduced from (Bailey, 2005)

1.1.11.2 The Sinogram

As abovementioned the projection of an object *f(x,y)* is recorded at a given angle *θ*. This is repeated for the other angles between *θ* and *θ* + 180 degrees at discrete steps of equal space resulting in N projections (see Figure 12). In conventional computer tomography, the collected profiles between 180 and 360 degrees would be redundant, however for practical reasons they are recorded too (Cherry et al., 2003). The calculation of line integrals for a specific point requires the introduction of a new coordinate system. Assuming a stationary coordinate system relative to the camera detector sys-

tem (i.e. in plane), the transformation for a point *p(x,y)* projected at angle *θ* can be performed by the rotation matrix:

$$\begin{pmatrix} \rho \\ s \end{pmatrix} = \begin{pmatrix} \cos\theta & -\sin\theta \\ \sin\theta & \cos\theta \end{pmatrix} \begin{pmatrix} x \\ y \end{pmatrix} \tag{7}$$

Subsequently, all projections of each angle can be displayed in form of a matrix *p(ρ,θ)*. The graphical representation of this matrix is also known as *sinogram* (see Figure 13), and provides a convenient way to collect the acquired data. In the sinogram of each row represents the number of counts of a single angle position. Its name stems from the fact that a point object *p(x,y)* follows a sinusoidal path down the matrix (Cherry et al., 2003).

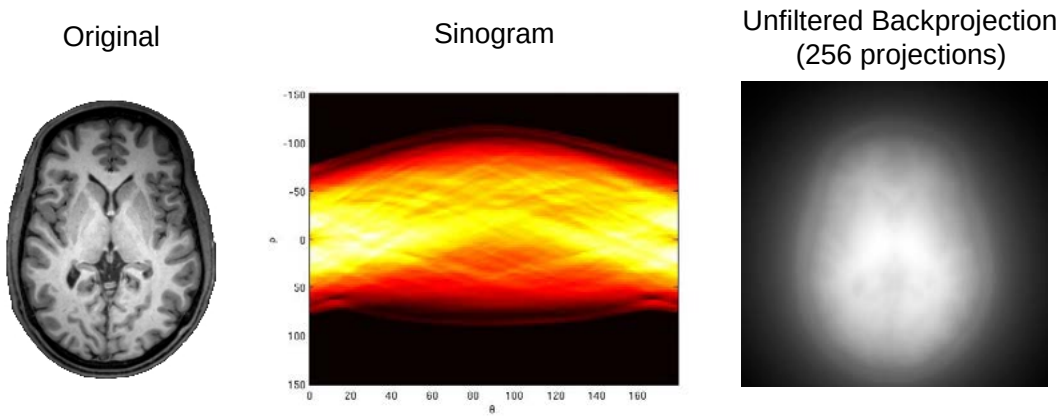

Figure 13: Sinogram from a set of 256 projection profiles of the left image. Each column represents one projection profile in sequential order from 0 to 180 degrees. Simple (unfiltered) backprojection provides blurred images regardless the number of projection profiles.

1.1.11.3 The Radon Transformation

In mathematics the radon transformation is applied for the calculation of line integrals and subsequent conversion into a transversal image representing the object. The projection of a two-dimensional function *f(x,y)* at a given an-

gle θ is a set of line integrals of parallel beams in a certain direction. In general, the Radon transform of *f(x,y)* is the line integral of *f* parallel to the *s* axis. The Radon transformation is given by

$$\mathcal{R}_f(\rho,\theta) = \int_{-\infty}^{\infty} f\,(\rho\cos\theta - s\sin\theta, \rho\sin\theta + \cos\theta)\mathrm{ds} \tag{8}$$

Applying the Dirac delta function, the formula can be rewritten as

$$\mathcal{R}_f(\rho,\theta) = \int_{-\infty}^{\infty}\int_{-\infty}^{\infty} f\,(x,y)\delta(\rho - x\cos\theta - y\cos\theta)\,\mathrm{dx}\,\mathrm{dy} \tag{9}$$

The advantage of the transformation with the Dirac delta function is based on the fact that all values outside the considered domain are multiplied by zero, i.e. are eliminated, whereas all remaining values are multiplied by one, hence all relevant values can be filtered for further processing.

At the first glance his discovery did not seem of great importance. Indeed, it took more than 55 years until his contribution found practical application. In his inauguration speech as rector of the University of Vienna 1954 he even mentioned:

> *"Oft liegen Dinge so, daß mathematische Theorien in abstrakter Form bereits vorliegen, vielleicht als unfruchtbare Spielerei betrachtet, die sich plötzlich als wertvolles Werkzeug für physikalische Erkenntnisse entpuppen und ihre latente Kraft in ungeahnter Weise offenbaren".*

Unfortunately he never witnessed himself the manifold potential slumbering in his discoveries and died just a few years before the beginning of the era of modern medical imaging.

1.1.11.4 Image reconstruction

Given the projections of the object as Radon transforms, the most obvious method for reconstruction would be the inverse Radon transformation. There are two options to perform the inversion: Fourier slice theorem and (filtered) backprojection (FBP).

1.1.11.5 Fourier slice theorem

According to the projection-slice theorem, an infinite number of one-dimensional projections of an object, at infinite number of angles, can reconstruct the original object. This inversion is carried out by means of the 2D Fourier transformation.

$$(\mathcal{F}f)(v_x, v_y) = F(v_x, v_y) = \int_{-\infty}^{\infty}\int_{-\infty}^{\infty} f(x,y) \cdot e^{-2\pi i(xv_x + yv_y)} dxdy \qquad (10)$$

In this context, the projection-slice theorem connects the Fourier transformation to the Radon transform. To get the image back from the projections means finding the inverse Radon transform from the abovementioned equation 10. J. Radon already provided an explicit formula as a solution. His approach, however, turned out to be unstable regarding noisy data, which usually is the case in a PET scanner. Soon, it has been replaced by a more stable approach for reconstruction, the filtered backprojection (FBP).

1.1.12 Backprojection

The simple backprojection became the first but not accurate reconstruction algorithm used in PET. From a given set of projection profiles $p(\rho,\theta_i)$ at discrete angles θ_i, assuming each profile sampled at discrete intervals, the image will be reconstructed on a 2D image, i.e. a discrete matrix of pixels. For mathematical simplification, matrix sizes are often a power of 2 (e.g. 256 × 256, 512 × 512). The amount of a particular element from the projection profile is divided uniformly by the number of matrix elements and projected

along the path of the matrix. This is why it is called *backprojection*. When this operation is repeated for all profiles, an approximation of the original image can be created. The basic concept is demonstrated in Figure 13. One major drawback is that counts are inevitably projected outside the true location of an object, yielding blurred images (Cherry et al., 2003). Obviously, a greater number of angles around the object and samples within the projections (number of detectors) improve the image quality (see Figure 13). Although this can diminish the influence of blurring, it remains at an unsatisfactory degree in the final image. Furthermore, blurring radially increases towards the peripheral space. Thus, the relationship between the original and the reconstructed image can mathematically be described by:

$$f'(x,y) = f(x,y) \otimes \frac{1}{\rho} \tag{12}$$

where $\otimes$ denotes the process of convolution, and ρ the distance from the centre. Despite numerous attempts to eliminate or at least suppress blurring, simple backprojection is only useful for high contrast objects relative to surrounding tissues. In practice, this is seldom the case, hence more powerful reconstruction algorithms are required.

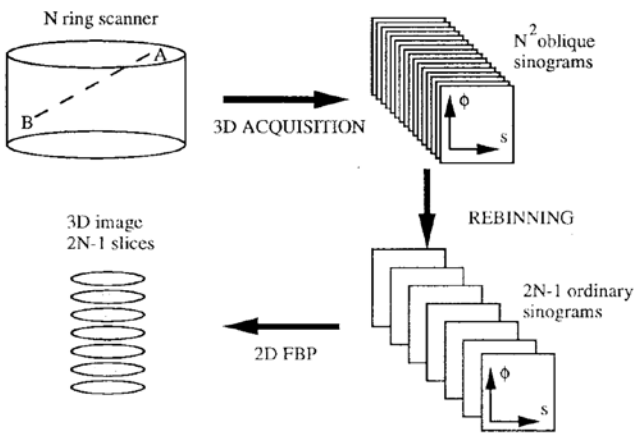

Figure 14: The principle of a rebinning algorithm. Reproduced from (Defrise et al., 1997)

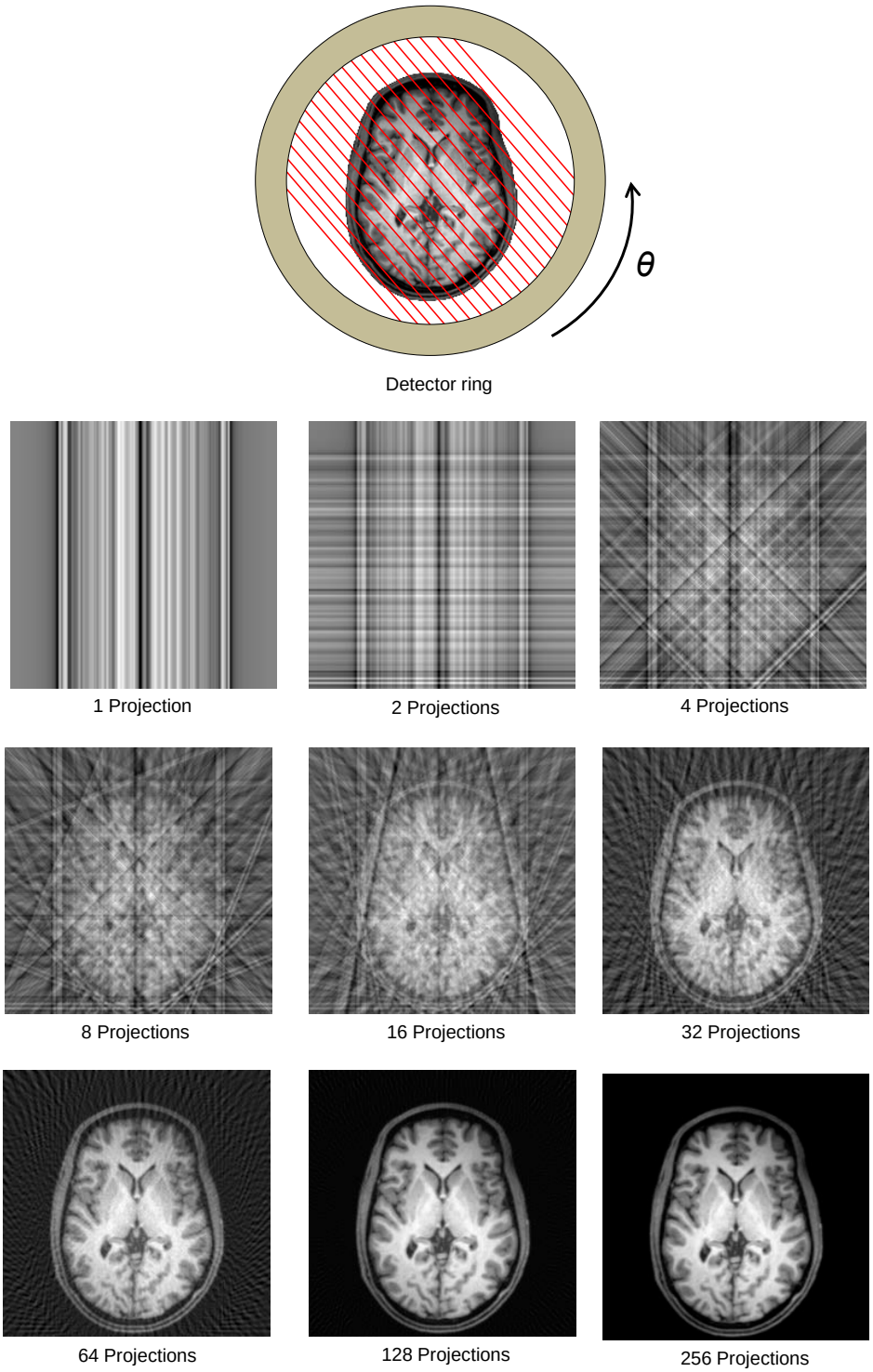

***Figure 15*:** Demonstration of filtered backprojection for a single brain slice of the author at various projection profiles.

1.1.13 Other reconstruction methods

A more sophisticated approach that successfully eliminates blurring is called *filtered backprojection (FBP)* (see Figure 15). Similarly to another advanced method called the *Fourier transform reconstruction* method (Lewitt, 1983), FBP employs the projection slice theorem in combination with the backprojection technique. The application of reconstruction filters in the frequency domain ought to eliminate 1/r blurring. This produces “sharpened” images, however accompanied with the disadvantage of lower signal-to-noise ratio. Therefore, FBP images are usually noisier compared to images produced by simple backprojection. Improved reconstruction filters (e.g. Shepp-Logan, Hann, Hamming, etc.) were designed to reduce the influence of noise and artefacts with varying degree of success. In the recent years, they have again been superseded by an even more powerful class of methods, known as *iterative algorithms* (Cherry et al., 2003). Among these computational more intensive techniques, the *maximum-likelihood* (ML) (Shepp and Vardi, 1982) and *ordered subset expectation maximization* (OSEM) (Hudson and Larkin, 1994) emerged as the most popular iterative algorithms (Basu et al., 2011). They provide more precise reconstruction images compared to FBP featuring several advantages e.g. better signal-to-noise ratio, and less streak artefacts (see Figure 16).

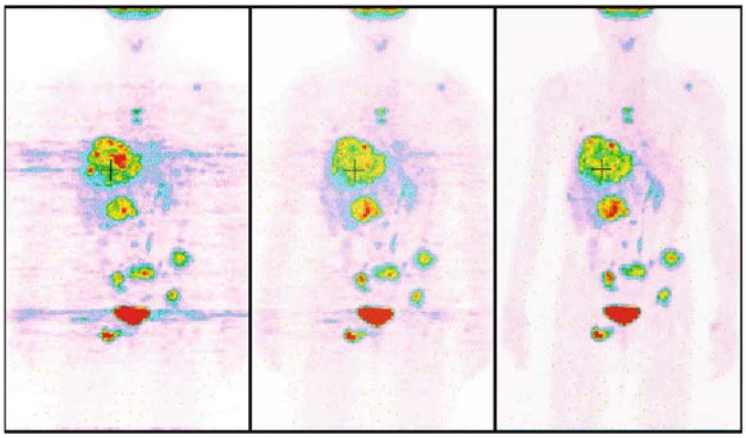

Figure 16: Whole-body 2D PET study. Comparison between different reconstruction algorithms of transmission and emission scan. Filtered backprojection (FBP) – FBP (left), OSEM-FBP (centre), OSEM-OSEM (right). Reproduced from (Defrise et al., 2005)

1.1.14 2D and 3D PET

Early PET scanners were constructed with only one ring of detectors in order to restrict data acquisition and reconstruction to a single axial slice. Later, more rings were added, which allowed simultaneous scanning of larger object spans. Thereby, collimators or septa were often placed between the individual rings to reduce the interplane scatter. These were thin lead or tungsten rings of ~1mm size to efficiently reject annihilation photons coming from oblique lines. The separate collection of coincidences from a single traverse plane is also known as 2D PET (Cherry et al., 2003). Applying this technique, 3D PET images were reconstructed from a stack of independent 2D planes since the lack of suitable algorithms prevented fully 3D imaging at that time (Basu et al., 2011). In 3D PET the interplane septa are retracted from the PET scanner allowing coincidences for all possible LOR, as shown in Figure 17. This modification leads on the one hand to a substantial improvement in sensitivity (typically between 4-8 fold), however at the same time it increases the number of scattered photons as well as random coincidences (Fahey, 2002). Although reconstruction of 3D data typically is more complex and time consuming, 3D acquisition became the standard mode on all commercial PET systems through the advances in computer technology (Basu et al., 2011), the availability of convenient algorithms (Cherry et al., 1991; Colsher, 1980; Daube-Witherspoon and Muehllehner, 1987; Defrise et al., 1997; Kinahan et al., 1997; Kinahan and Rogers, 1989) and above all the dramatic improvement in sensitivity (Cherry et al., 2003). Among several algorithms the OSEM method emerged as the most popular mainly due to its easy implementation (Defrise, 2001; Hudson and Larkin, 1994; Johnson et al., 1997).

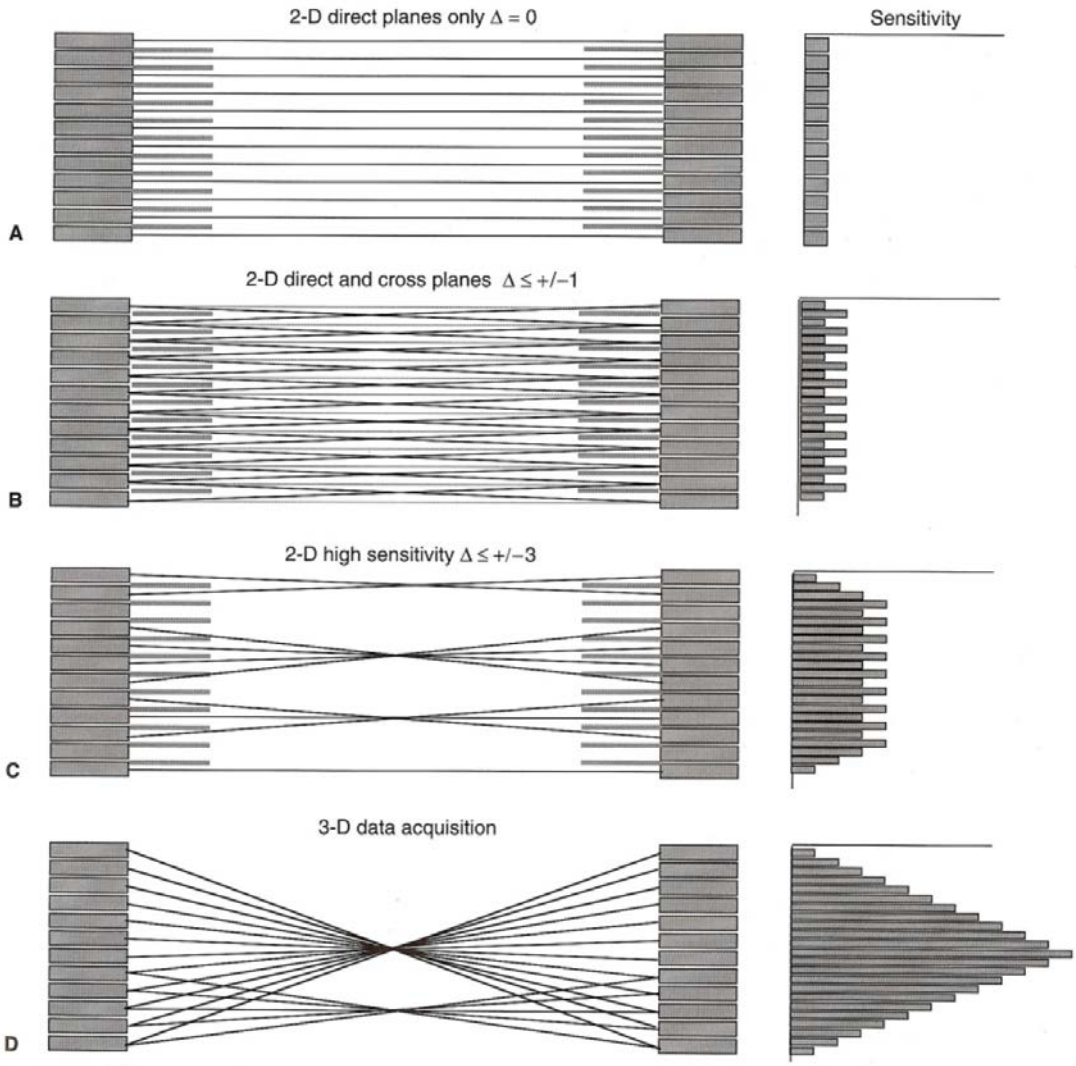

Figure 17: 2D and 3D acquisition schemes. Left side shows axial cross sections through a multiring scanner, right side the corresponding sensitivity profiles. In 2D PET axial collimators of septa between each ring of detector prevented the coincidence detection from other rings (A) was limited to adjacent rings (B) or more rings (C). In 3D acquisition mode, all septa were removed resulting in a 4-8 fold higher sensitivity (D). In C and D only selected LOR are shown. Reproduced from (Cherry et al., 2003).

1.2 The serotonergic system

Serotonin was isolated and characterized for the first time in 1948 (Rapport, 1997; Rapport et al., 1948) and later determined to be named 5-hydroxytryptamine (5-HT). In addition to its involvement in platelet aggregation and mobility of the gastrointestinal tract, 5-HT is a neurotransmitter and plays a central role in the regulation of various cerebral functions. In the central nervous system the highest concentration of 5-HT is detectable in the raphe nuclei located in the brain stem (Lundberg et al., 2005; Palkovits et al., 1974; Varnäs et al., 2004). The amino acid tryptophan is the substrate for the 2-step reaction of serotonin synthesis. In the brain it is synthesized in the raphe nuclei of the midbrain. From the raphe nuclei, projections run to the areas in the basal ganglia, neocortex, limbic and paralimbic cortex (Hornung, 2003), reaching almost the entire brain.

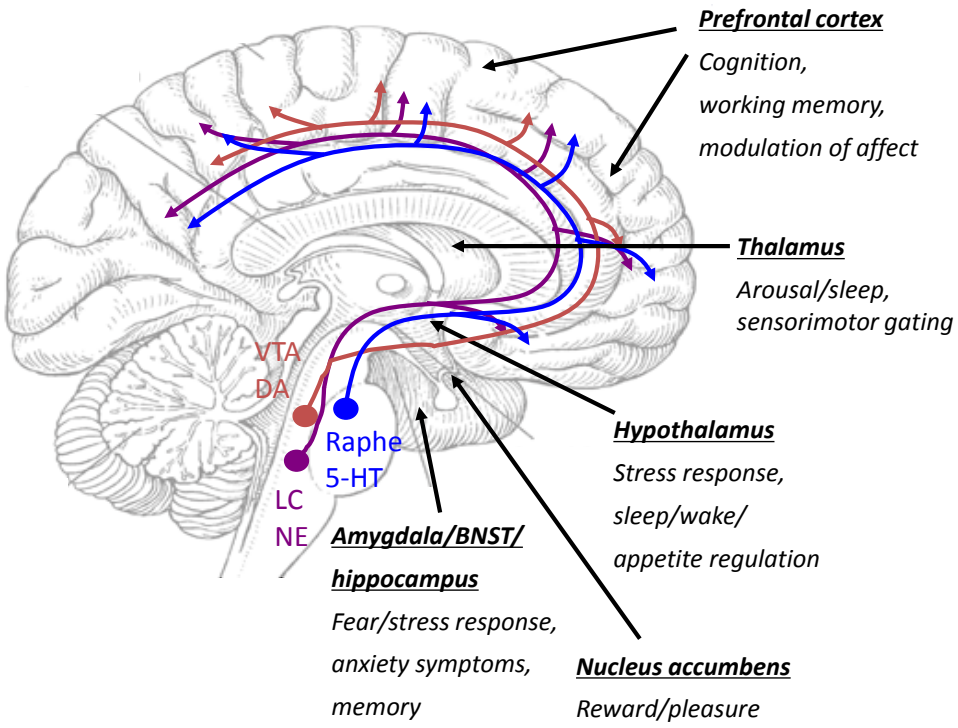

Figure 18: Projection pathways of neurotransmitter systems. Red, dopaminergic system; purple, noradrinalergic system; blue, serotonergic system.

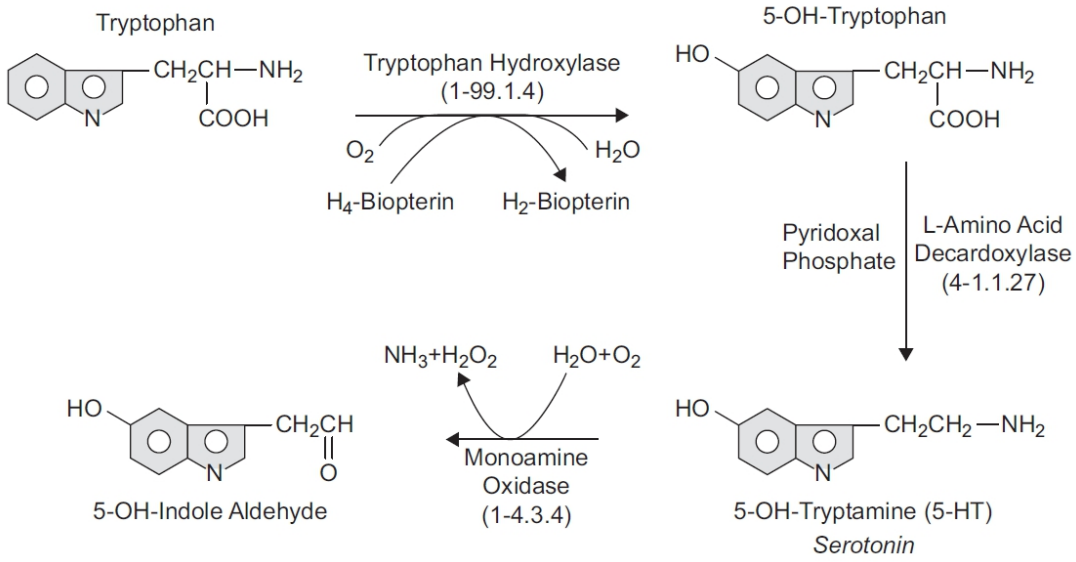

Figure 19: Biosynthetic pathway of serotonin (5-hydroxytryptamine, 5-HT) from L-tryptophan. Reproduced from (Azmitia, 2010)

The serotonergic system is involved in the regulation of a variety of neurophysiological and psychological functions including neuronal development (Lauder et al., 1983) and neuroplasticity (Benninghoff et al., 2012), thermoregulation (Feldberg and Myers, 1964), pain (Tenen, 1967), motor regulation (Jacobs, 1991), different stages of the sleep cycle (Jouvet, 1967), appetite (Haleem, 1993), sexual behavior (Gorzalka et al., 1990; Olivier et al., 1998), aggression (Manuck et al., 1998; Sheard, 1969; Soubrie, 1986; Witte et al., 2009), reward processing (Kranz et al., 2010), impulsivity (Miyazaki et al., 2012; Winstanley et al., 2005), anxiety (Briley et al., 1990) as well as mood and temperament (Mann, 1999). This system works in concert with various environmental and endogenous signals such as day light intensity and length (Spindelegger et al., 2011) and several hormones as cortisol (Lanzenberger et al., 2010), progesterone (Lanzenberger et al., 2011) and dehydroepiandrosterone sulfate (Moser et al., 2010). Furthermore, it has shown an integral role in the pathophysiology of common neuropsychiatric disorders including major depression (Mann, 1999; Staley et al., 1998), bipolar disorder (Chee et al., 2001), obsessive compulsive disorder (Adams et al.,

2005), anxiety disorders (Akimova et al., 2009; Lanzenberger et al., 2007; van der Wee et al., 2008), post-traumatic stress disorder (Davis et al., 1997; Murrough et al., 2011a; Murrough et al., 2011b), eating disorders (Bailer et al., 2005; Mayer and Walsh, 1998), sleep disturbance (Portas et al., 1998), attention deficit hyperactivity disorder (Quist et al., 2003), drug addiction (Carey et al., 2005; Muller et al., 2007), suicidal behavior (Mann, 1999), schizophrenia (Abi-Dargham, 2007; Aghajanian and Marek, 2000; Hurlemann et al., 2005; Hurlemann et al., 2008), Alzheimer (Ouchi et al., 2009), migraine (Panconesi, 2008) and epilepsy (Assem-Hilger et al., 2010).

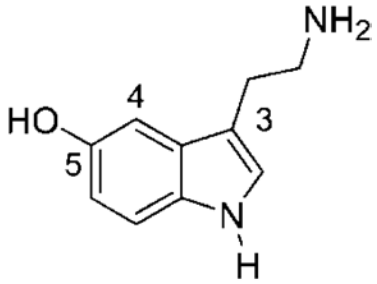

Figure 20: Structural formula of 5-hydroxytryptamine (5-HT, serotonin). Reproduced from (Nichols and Nichols, 2008).

Serotonin mediates its numerous effects by binding to a large family of receptors categorized according to their structural diversity, mode of action and pharmacologic specifications. So far seven major families of serotonin receptors (5-HT1 to 5-HT7) and at least 16 subtypes of 5-HT receptors and a serotonin transporter (5-HTT) have been identified (Hoyer et al., 2002; Melke et al., 2003). Different receptor subtypes do not show homogenous functions and distribution in the brain (Saulin et al., 2012). Therefore, mapping of 5-HT receptor subtypes is a substantial step to understand the pathophysiology of psychiatric disorders. Currently, the serotonergic system is one of the main targets of pharmacologic treatment interventions and is also under focus for the purpose of developing new psychoactive drugs. Interestingly, many established serotonin-related compounds such as tricyclic and

tetracyclic antidepressants, and atypical neuroleptics have been discovered by serendipity. Nonetheless, continuous investigation of treatment strategies relies on fundamental and refined knowledge about this system.

1.2.1 5-HT_{1A} receptor

The 5-HT1 receptor family consists of five subtypes (1A, 1B, 1D, 1E and 1F) that inhibit the formation of cyclic adenosine monophosphate (cAMP) and play an inhibitory function. The 5-HT_{1A} receptor is a G-protein-coupled receptor. Among the 5-HT1 receptors, 5-HT_{1A} is of special interest because it is the most widespread receptor type in the mammalian brain (Herold et al., 2012). It appears as somatodendritic autoreceptor on serotonin neurons in the raphe nuclei controlling serotonergic cell firing (Evans et al., 2008; Hajos et al., 2001) and as heteroreceptors in projection areas inhibiting postsynaptic cell firing (Fink and Gothert, 2007). Quantitative determination of 5-HT_{1A} receptors in the human brain has become possible using PET and selective radioligands such as [c*arbonyl*-^{11}C]WAY-100635 (Pike et al., 1995), [^{18}F]FCWAY (Carson et al., 2000), [^{18}F]MPPF (Shiue et al., 1997), and [^{11}C]CUMI-101 (Milak et al., 2008).

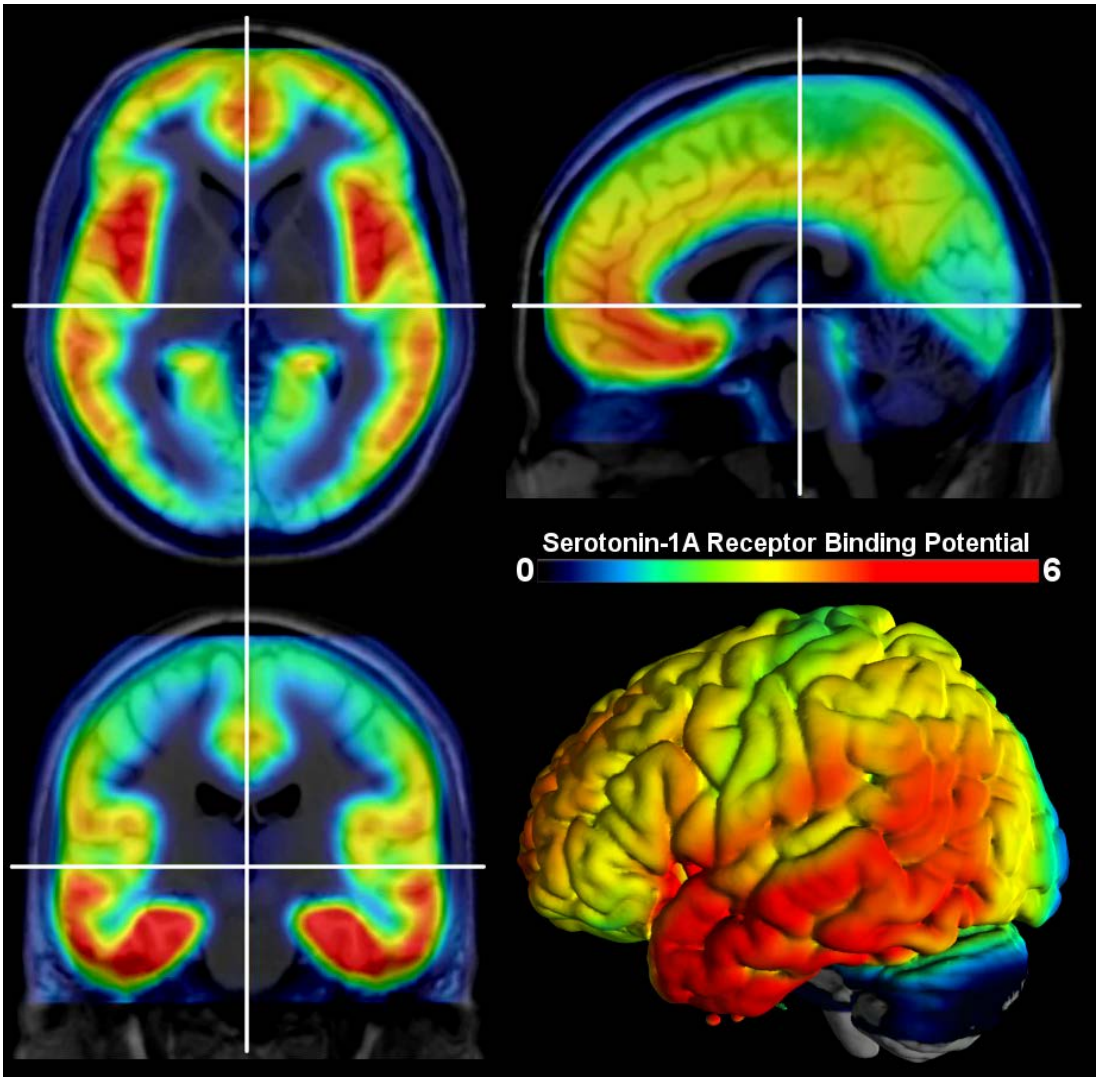

Figure 21: Average **distribution of the serotonin 1A (5-HT$_{1A}$) receptor** in the human brain measured with PET and the radioligand [c*arbonyl*-^{11}C]WAY-100635. The color table indicates receptor binding potentials. Reproduced from (Saulin et al., 2012); created by Savli.

1.2.2 5-HT_{1B} receptor

5-HT_{1B} receptors are located presynaptically on both serotonergic neurons as autoreceptors and on non-serotonergic neurons as heteroreceptors (Boschert et al., 1994; Clark and Neumaier, 2001; Sari et al., 1999), where they are involved in the release of a range of neurotransmitters such as serotonin (Martin et al., 1992), dopamine (Sarhan et al., 1999), acetylcholine (Maura and Raiteri, 1986), glutamate (Muramatsu et al., 1998), noradrenaline (Hoyer et al., 1990) and GABA (Bramley et al., 2005; Tanaka and North, 1993). So far two 5-HT_{1B} radioligands, [^{11}C]P943 (Gallezot et al., 2010; Nabulsi et al., 2010) and [^{11}C]AZ10419369 (Varnäs et al., 2011), suitable for human PET imaging have been developed to study the function of these receptors *in vivo* and to investigate their role in the pathophysiology of neuropsychiatric disorders.

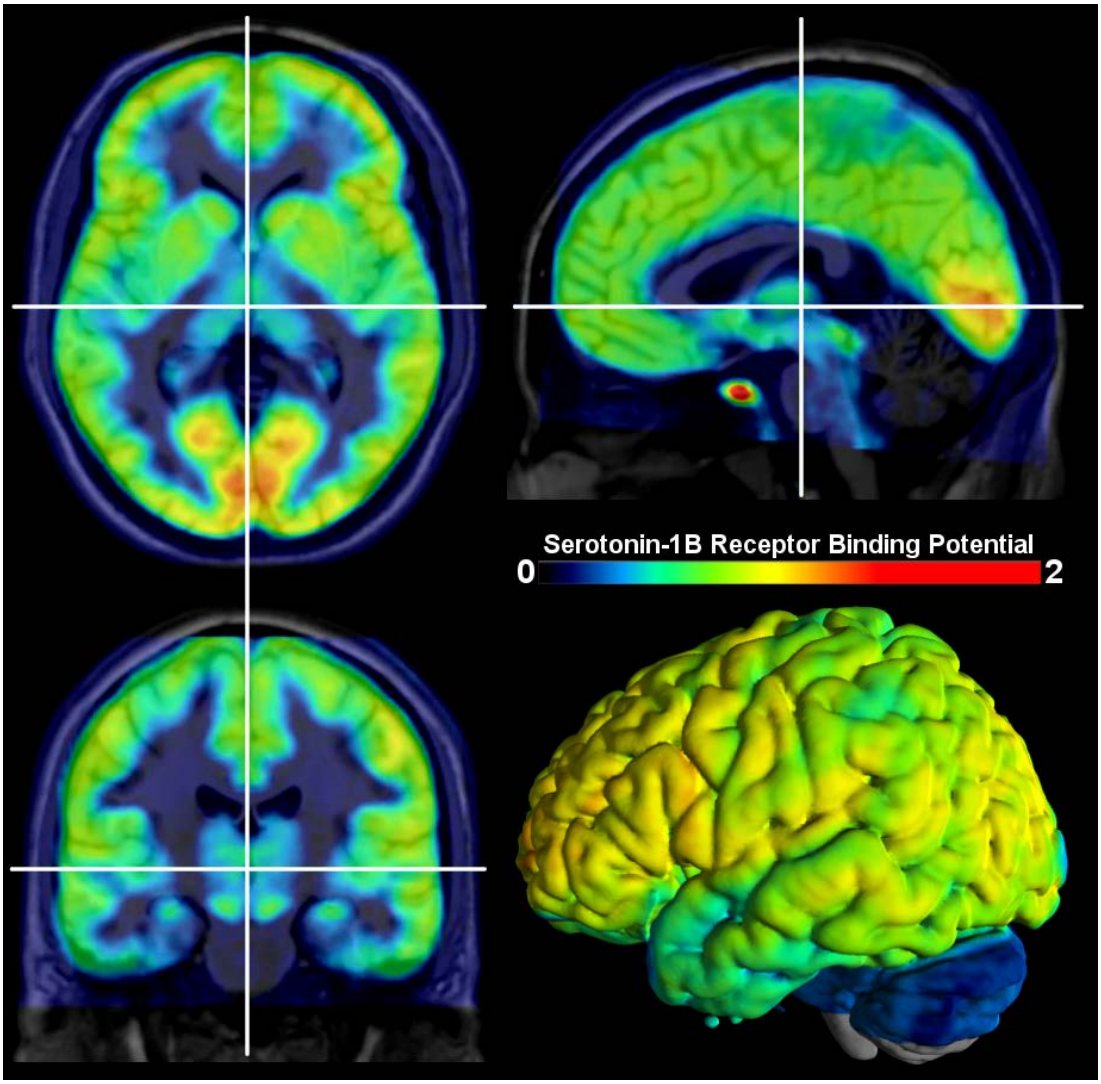

Figure 22: Average **distribution of the serotonin 1B (5-HT_{1B}) receptor** in the human brain measured with PET and the radioligand [^{11}C]P943. The color table indicates receptor binding potentials. Reproduced from (Saulin et al., 2012); created by Savli.

1.2.3 5-HT_{2A} receptor

The 5-HT2 receptor group includes excitatory receptors. The most extensively studied and characterized among them is 5-HT_{2A} which is the main excitatory receptor subtype in the serotonergic system. Located postsynaptically, the 5-HT_{2A} receptor is a G-protein-coupled receptor. [^{18}F]altanserin is the most frequently used radioligand for evaluating 5-HT_{2A} receptors *in vivo* (Lemaire et al., 1991), while [^{11}C]MDL100907 studies are rare (Talbot et al., 2012).

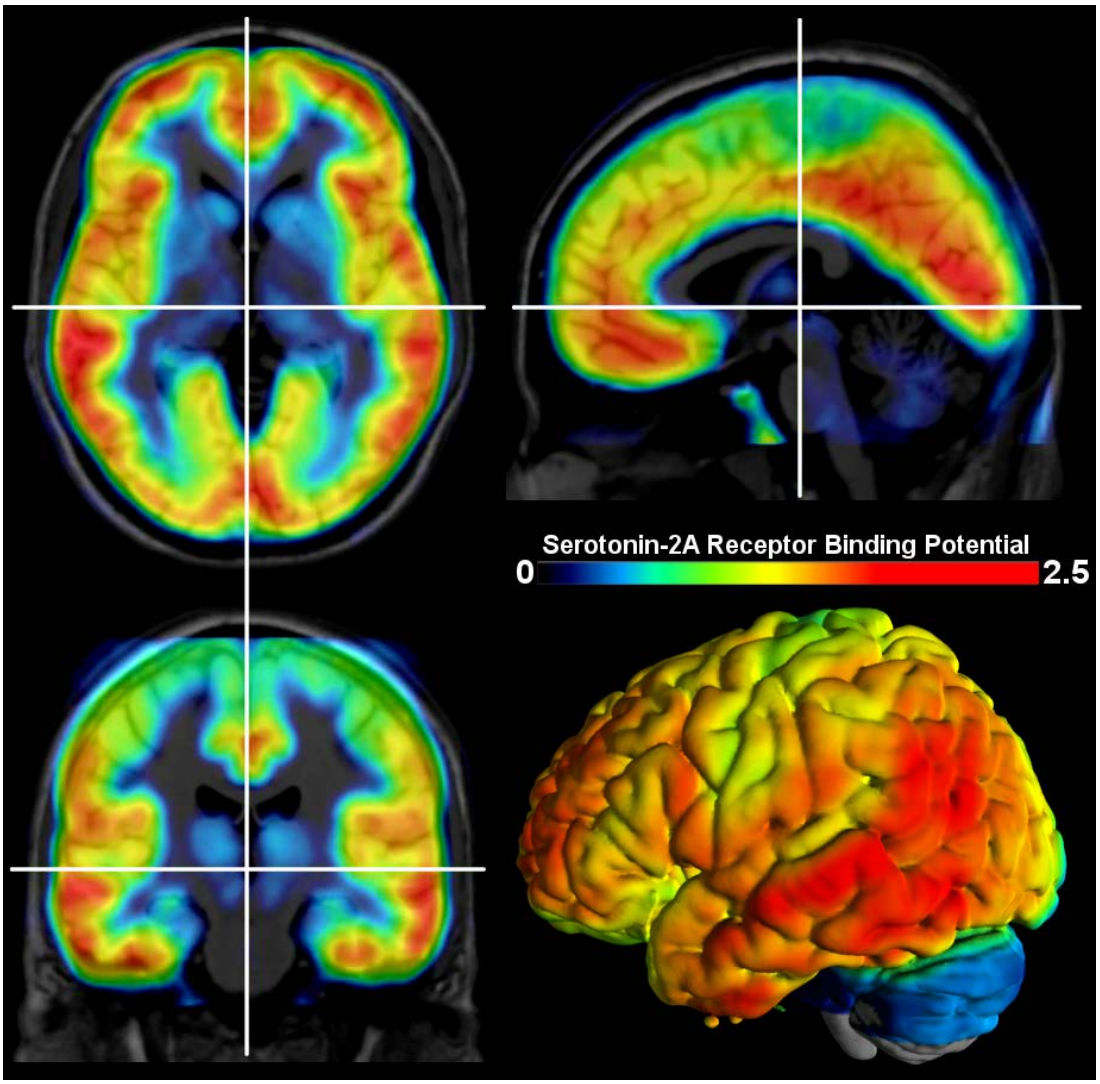

Figure 23: Average **distribution of the serotonin 2A (5-HT_{2A}) receptor** in the human brain measured with PET and the radioligand [^{18}F]altanserin. The color table indicates receptor binding potentials. Reproduced from (Saulin et al., 2012); created by Savli.

1.2.4 The serotonin transporter

The serotonin transporter (SERT or 5-HTT) is a monoamine integral membrane transporter protein. Because of its role in the regulation of serotonergic concentration and signal activation it has received considerable attention. The concentration of synaptic serotonin is directly controlled by its reuptake, thus it became a molecular target for drugs (e.g. selective serotonin reuptake inhibitors) that alter 5-HTT function. The most promising PET ligands applied in the studies involving 5-HTT are [^{11}C]DASB (Houle et al., 2000a) and [^{11}C]MADAM (Lundberg et al., 2005).

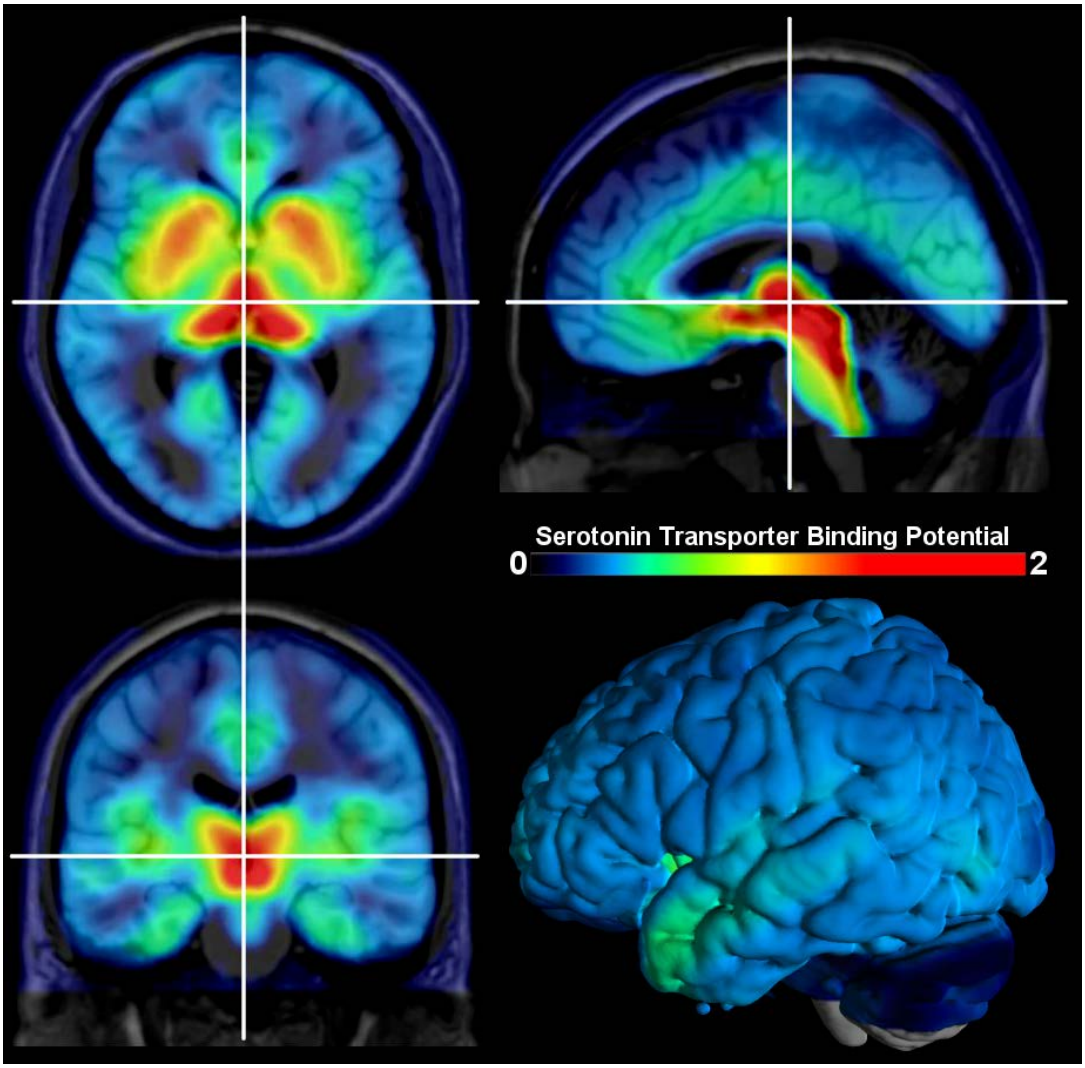

Figure 24: Average distribution of the serotonin transporter (5-HTT, SERT) in the human brain measured with PET and the radioligand [^{11}C]DASB. The color table indicates receptor binding potentials. Reproduced from (Saulin et al., 2012); created by Savli.

1.3 Brain receptor imaging

Receptors are specific structures (usually proteins) on membranes that play a pivotal role in brain function exerting regulatory roles on neurotransmission (Heiss and Herholz, 2006). On the presynaptic site they control transmitter release and reuptake. Postsynaptically, monoamine induced signals lead to defined response cascades either by G-protein coupled receptors (second messenger) or ligand-gated ion channels. The large number of receptors and transporters tremendously vary in their distribution throughout the brain. PET is a molecular imaging tool for the *in vivo* measurement and characterization of these biomolecules (Weissleder and Mahmood, 2001). For this purpose radiotracers are required. These are radioactive labeled molecules that follow or trace the desired target (Price, 2003). Most essential for the quantification are appropriate radiotracers to visualize targets such as receptors, transporters and enzymes (Laruelle et al., 2003). Ideally they are analogues of systemic substances and profess identical behaviour similarly to the biological organism (Cherry et al., 2003). The development of adequate candidates is a challenging undertaking since they need to meet a number of pharmacological criteria to be suitable radioligands. First, when the tracer is applied to the organism, it ought not to perturb the biological system, hence a small amount of substance with sufficient sensitivity is required (Price, 2003). Second, it should not be toxic, but it should cross the blood-brain barrier (BBB). The latter limits its lipophilicity (logP value) to approximately 1.5-4, and its molecular weight below 450. Third, the tracer should selectively bind with a high affinity to the respective binding site (high selectivity and affinity), while the affinity on the one hand needs to be high enough to result in an acceptable signal-to-noise ratio, on the other hand not too high lest it fails to reach the binding equilibrium within the given scan time. Fourth, during metabolism its radiolabelled metabolites should not enter the brain (Laruelle et al., 2003). Additionally, some qualities required from potential tracers stand in direct conflict with each other, e.g. a higher lipophilicity facilities easier brain penetration, which is desirable, but at the same time

promotes nonspecific binding, a less favourable property. Furthermore, the translation of chemical compounds from rodents to non-human primates and finally to humans remains another complex task, since the successful parameters in one species often cannot be linearly translated to another.

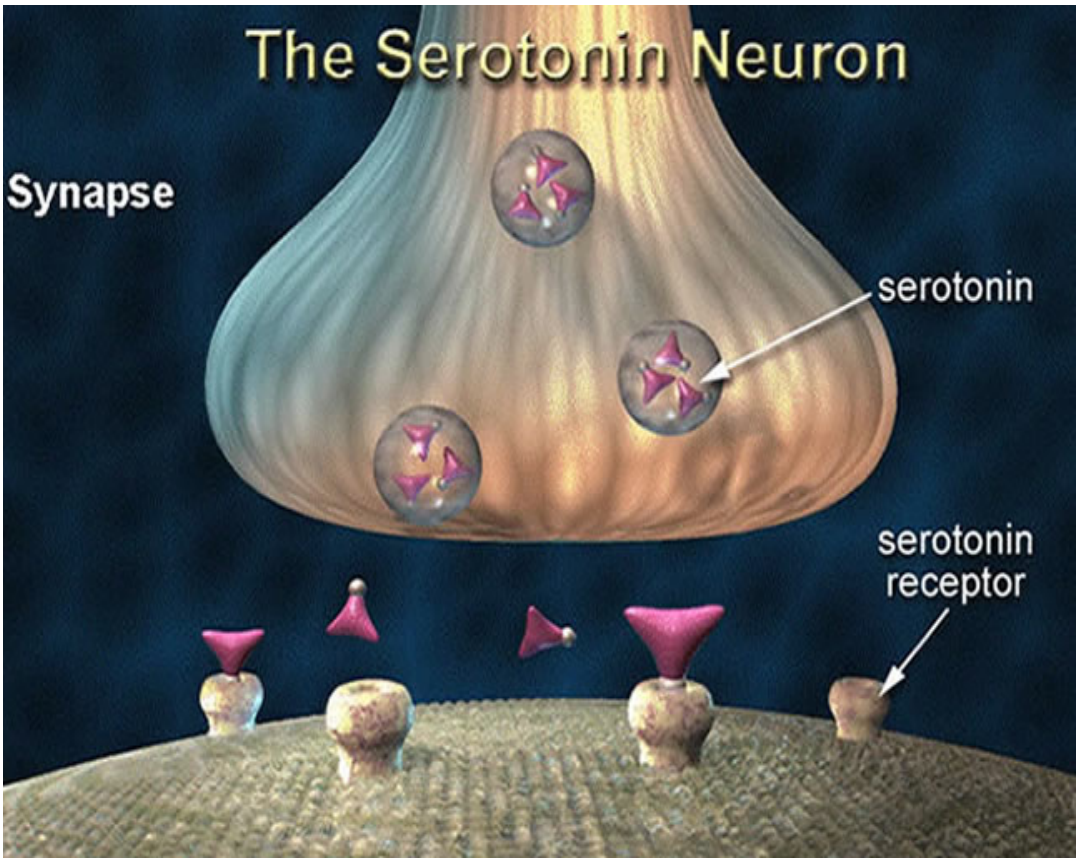

Figure 25: The serotonin neuron. Serotonin is released presynaptically from vesicles into the synaptic cleft and bind to receptors located on both pre- and postsynaptic target sites. Reproduced from unibe.ch.

1.3.1 Receptor Quantification

The fundamental concept of the quantification of molecular targets such as receptors, has been preceded by decades of research and originates from *in vitro* radioligand binding assays (Ichise et al., 2001). *In vitro*, the absolute number of binding sites (B_{max}) and the affinity (K_D) is determined using a radiotracer together with the unlabelled radioligand at different concentrations. In humans, the same *in vivo* experiments cannot be performed due the high amount of unlabeled drugs required (Frankle et al., 2005). Therefore the 'Binding Potential' (BP) has been introduced for PET imaging which constitutes the main outcome measure in neuroreceptor quantification (Mintun et al., 1984). The BP (ml/g) equals to the ratio of receptor density (B_{max} nM or fmol per gram of tissue) and radioligand equilibrium dissociation constant (K_D), which is the inverse of the ligand affinity ($1/K_D$, nM, or fmol per mL of brain water).

$$\mathrm{BP} = \frac{\mathrm{B_{max}}}{\mathrm{K_D}} = \mathrm{B_{max}} \cdot \frac{1}{\mathrm{K_D}} = \mathrm{B_{max}} \cdot \text{affinity} \tag{13}$$

In a reversible receptor model (see Figure 26), where the ligand [L] and the receptor [R] are freely mixed, the biomolecular association and unimolecular dissociation are assumed to form a complex [RL] (Laruelle et al., 2003). This interaction has been described by (Michaelis and Menten, 1913):

$$[\mathrm{L}] + [\mathrm{R}] \overset{\mathrm{k_{on}/k_{off}}}{\Longleftrightarrow} [\mathrm{R}][\mathrm{L}] \tag{14}$$

where [L] is the concentration of the radioligand, [R] is the unbound receptor, [RL] is the concentration of the receptor-ligand complex, and k_{on} (ligand-receptor association rate) and k_{off} (ligand-receptor complex dissociation rate) are the kinetic rate constants (Ichise et al., 2001).

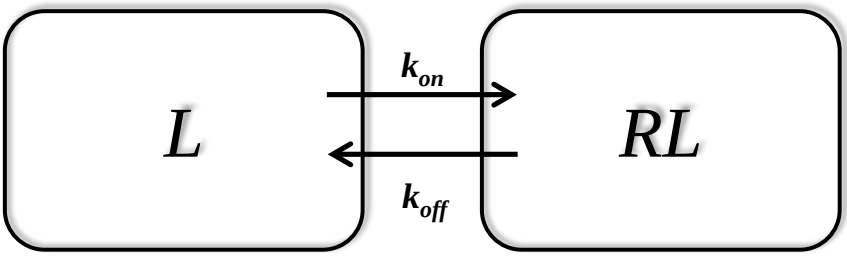

Figure 26: Receptor-Ligand model

The concentration of the receptor-ligand complex [LR] will change over time proportionally to the free concentration of the ligand [L]. In contrast, the free concentration of the receptor [R] is decreasing proportionally to [LR] (Frankle et al., 2005):

$$\frac{\mathrm{d([RL])}}{\mathrm{dt}} = \mathrm{k_{on}[L][R] - k_{off}[RL]} \tag{15}$$

where $\frac{d([RL])}{dt}$ is the change in the concentration of the receptor-ligand complex over time. When the system reaches equilibrium, i.e. $\frac{d([RL])}{dt} = 0$, then

$$\mathrm{k_{on}[L][R] = k_{off}[RL]} \tag{16}$$

and

$$\frac{\mathrm{[L][R]}}{\mathrm{[LR]}} = \frac{\mathrm{k_{on}}}{\mathrm{k_{off}}} = \mathrm{K_D} \tag{17}$$

where K_D is the equilibrium dissociation constant. Equilibrium is the condition in which association and dissociation of the ligand-receptor complex equal per unit time (Laruelle et al., 2003). Since the unit of k_{off} is time^{-1} and the units of k_{on} (concentration · time)$^{-1}$, the equilibrium dissociation constant has the units of concentration (Slifstein and Laruelle, 2001).

1.4 Neuroanatomy

The cerebral cortex has been subdivided into numerous distinct areas characterized by structural, functional and cytoarchitectonic features (Zilles et al., 2002). Among several segregations of the human cortex, the “Brodmann areas” (BA) introduced in 1909 became the most popular ones (Zilles and Amunts, 2010). It describes the cytoarchitectonic segregation of the cortex. Even current neuroimaging study results are frequently reported based on the Brodmann areas. Another more recent somatotopically ordered representational map is the anatomical parcellation by Tzourio-Mazoyer (Tzourio-Mazoyer et al., 2002). In this method the spatially normalized single-subject high-resolution T1-weighted volume provided by the Montreal Neurological Institute (MNI) has been categorized into 3D definitions of various volumes of interest in each hemisphere.

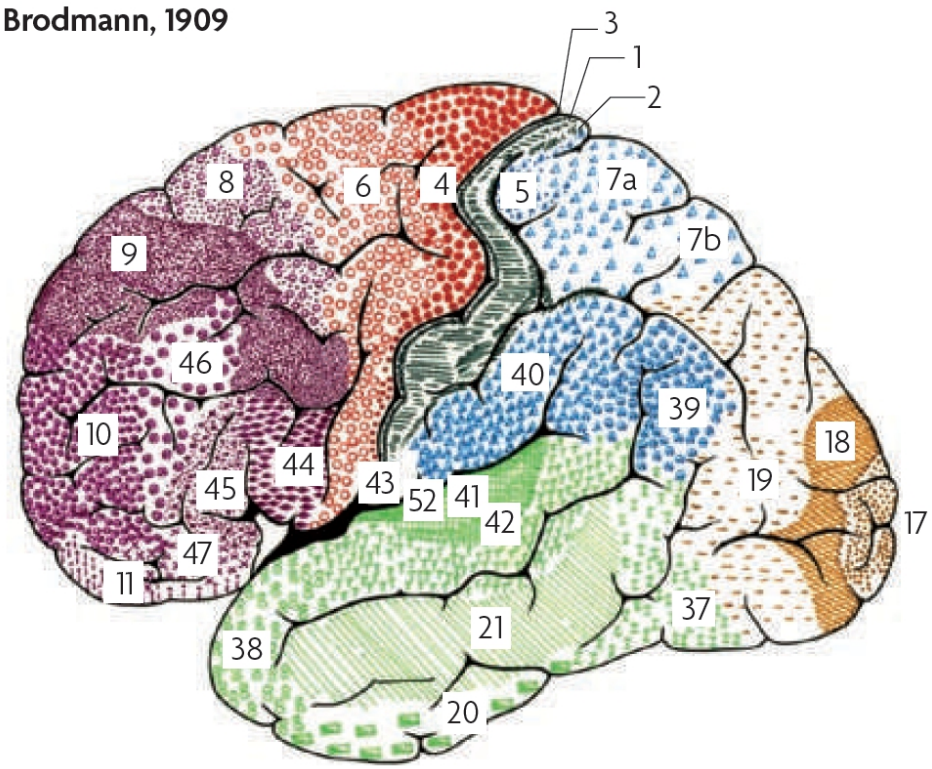

Figure 27: Brodmann Areas. Reproduced from (Zilles and Amunts, 2010)

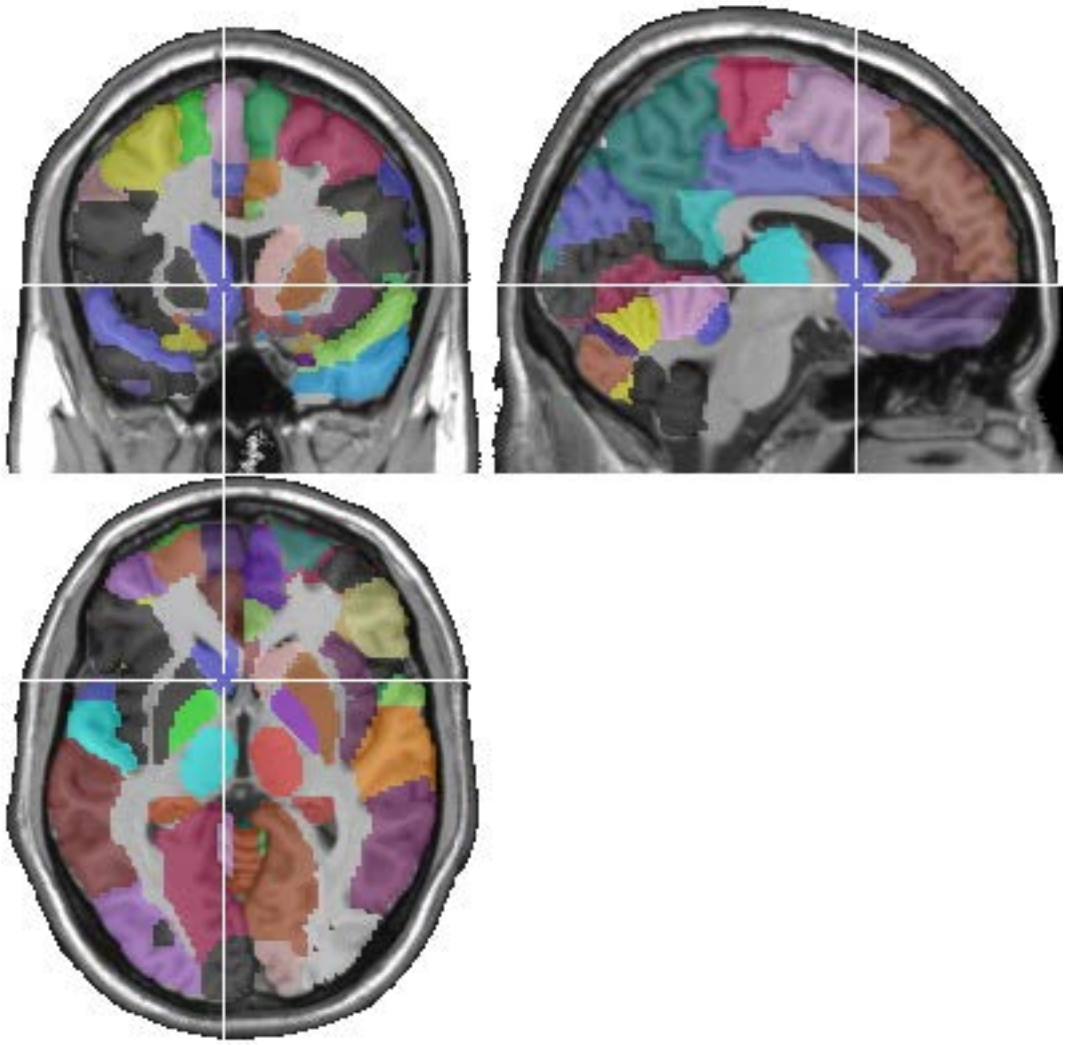

Figure 28: Macroscopic anatomic parcellation of the MNI MRI single subject brain (AAL Regions) according to (Tzourio-Mazoyer et al., 2002)

1.5 Databases

Databases from post-mortem and also *in vivo* human studies that quantified the abovementioned receptors are readily available. These databases, however, have provided the data of selected regions of interest only, thus the availability of a comprehensive dataset with a thorough coverage of the entire brain is desirable. Besides, existing datasets of serotonergic protein binding potentials are quantified on the basis of individually delineated ROIs which make the measurements dependent on the investigator's abilities. Furthermore, multiple receptor subsystems are usually not quantified within one specific study and methodologies of data collection and analysis vary often considerably in different studies. In other words, the manner of treating data of various serotonergic proteins is not identical and correspondingly the data of various subsystems obtained by different studies impedes direct comparisons. Data sharing in neuroimaging research is seemingly of great value. Making neuroimaging data suitable for sharing and comparable across multiple centers is challenging, but it would encourage data pooling and meta-analysis and researchers without an access to neuroimaging modalities would benefit from the opportunity of conducting studies using existing data.

2 Experimental Setup and Methods

2.1 Participants

A total of 95 healthy subjects (mean age = 28.0±6.9 years, range= 18-54, 59% males) were included in this multicenter PET study. For demographic details see Table 3. All subjects were recruited via advertisement and had participated in previous studies as healthy control subjects (Gallezot et al., 2010; Hurlemann et al., 2008; Lanzenberger et al., 2007; Stein et al., 2008). Prior to inclusion, all subjects underwent a medical examination including general physical, neurological and mental health status, and were excluded if they had any previous substance or alcohol abuse. All subjects were physically healthy and life-time naïve for psychotropic drugs. Furthermore, female participants were tested for pregnancy prior to PET-measurement. All participants gave written informed consent according to the procedures approved by the local Ethics Committees at the Medical University of Vienna, the Medical Faculty of the University of Düsseldorf and the Yale School of Medicine Human Investigation Committee.

Table 3: Demographic data

Binding protein	**5-HT$_{1A}$**	**5-HT$_{2A}$**	**5-HT$_{1B}$**	**5-HTT**	
Radioligand	[*carbonyl*-^{11}C] WAY-100635	[^{18}F]altanserin	[^{11}C]P943	[^{11}C]DASB	
n	35	19	23	18	
proportion males	51%	58%	65%	67%	χ^2=1.64, p=0.65 [a]
age (mean±SD)	26.3±5.2	28.2±5.7	28.7±7.0	30.5±9.5	$F_{(3,91)}$=1.64, p=0.19 [b]
age range (min - max)	21 - 47	21 - 40	18 - 44	19 - 54	

[a] χ^2-test, [b] one-way ANOVA

2.2 Radiosynthesis and data acquisition

2.2.1 [*carbonyl*-^{11}C]WAY-100635

[*carbonyl*-^{11}C]WAY-100635 (N-(2-(1-(4-(2-Methoxyphenyl)-piperazinyl)ethyl)-N-pyridinyl)cyclohexane-[*carbonyl*-^{11}C]carboxamide) binds with high affinity and selectivity to the 5-HT_{1A} receptor (Farde et al., 1997; Pike et al., 1996). It is furthermore a 5-HT_{1A} receptor antagonist (Pike et al., 1996). [*carbonyl*-^{11}C]WAY-100635 was synthesized according to an optimized procedure (Wadsak et al., 2007) at the Radiochemistry Unit of the PET center at the Department of Nuclear Medicine at the Medical University of Vienna. PET scans were conducted with a GE Advance PET scanner (General Electric Medical Systems, Milwaukee, Wisconsin) at the Department of Nuclear Medicine, Medical University of Vienna as described previously (Fink et al., 2009; Lanzenberger et al., 2007; Spindelegger et al., 2009)). Briefly, the head of each subject was placed in the scanner parallel to the orbitomeatal line using a laser beam system. Correct positioning was carried out with a scout scan in order to cover the cerebellum in the field of view (FOV). A polyurethane cushion and straps covering forehead and chin were used to ensure a stable head position during scan time. Subjects were also instructed not to speak or move during the measurement. Tissue attenuation was measured in a five-minute transmission scan in 2D mode with a retractable ^{68}Ge ring source. The 3D dynamic acquisition started simultaneously with intravenous bolus injection of [*carbonyl*-^{11}C]WAY-100635 solved in phosphate buffered saline (pH 7.4). The mean injected activity of the radioligand was 5.65±0.8 (mean ± SD) MBq/kg body weight, with a mean specific radioactivity at the time of injection of 153±117 GBq/µmol, and a radiochemical purity of 97.5±1.3%. Thirty time frames covering the total acquisition time of 90 min were acquired, 15 frames of 1 min and 15 frames of 5 min duration. Scatter and attenuation correction were applied and PET data were reconstructed by means of an iterative filtered back-projection algorithm (FORE-ITER) re-

sulting in 35 contiguous slices (matrix 128×128) with a spatial resolution of 4.36 mm full-width at half maximum (FWHM) at the center of the FOV.

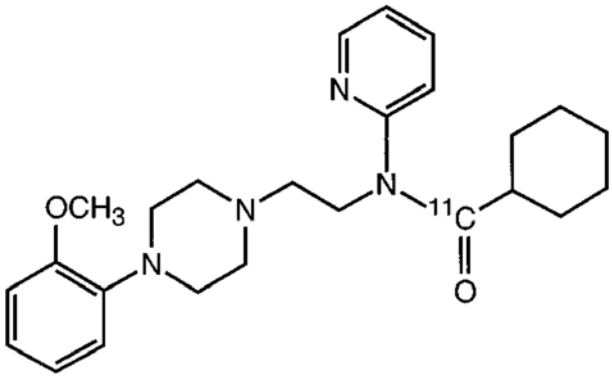

Figure 29: Structural formula of [*carbonyl*-^{11}C]WAY-100635. Reproduced from (Farde et al., 1997).

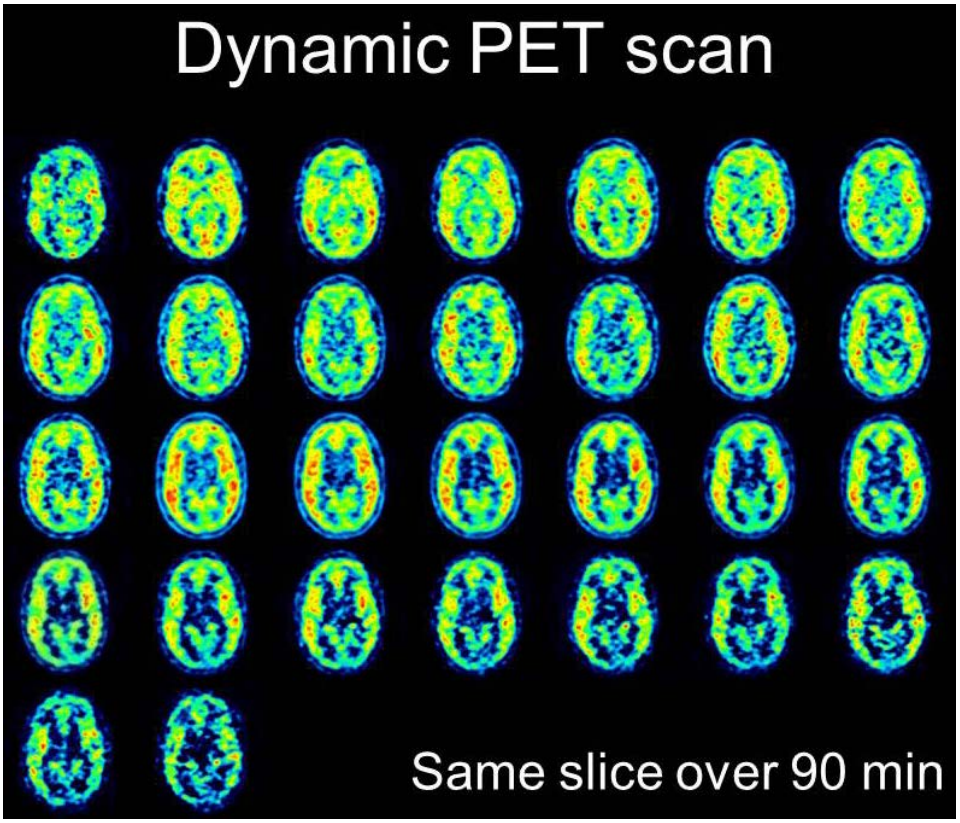

Figure 30: Dynamic PET scan of the 5-HT_{1A} antagonist [*carbonyl*-^{11}C]WAY-100635. Each image represents one time frame of the same slice through the course of 90min and demonstrates accumulation of the radiotracer as well as wash out phase and tracer decay. Colour codes indicate radiotracer concentration given in Bq/cc.

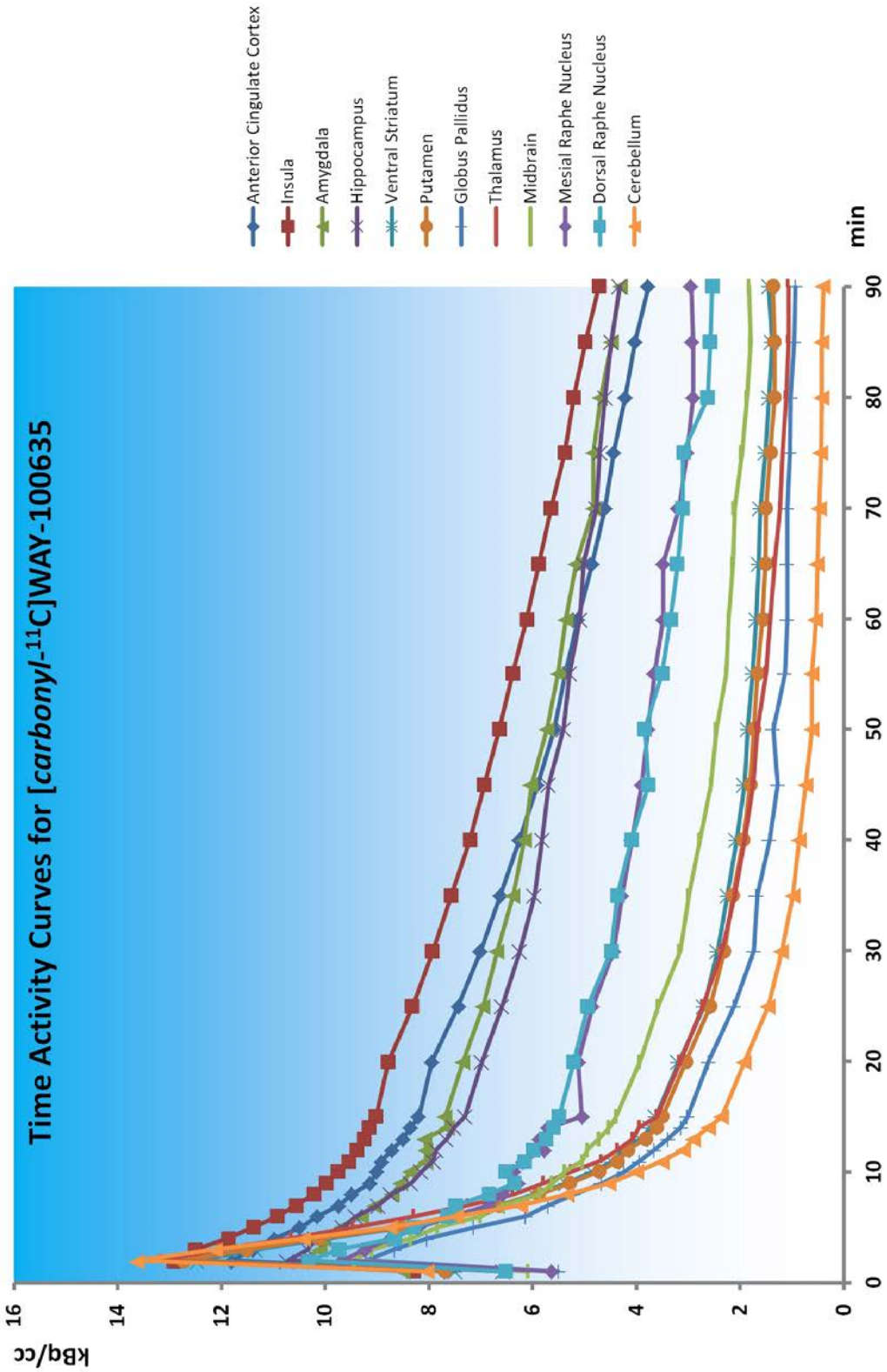

Figure 31: Average time activity curves (TACs) for [*carbonyl*-^{11}C]WAY-100635 binding of 12 representative regions of interest (ROIs) through the course of 90 min. High peaks in the beginning indicate a rapid influx of the ligand, however it soon reaches binding equilibrium.

2.2.2 [^{11}C]P943

[^{11}C]P943 (R-1-[4-(2-methoxy-isopropyl)-phenyl]-3-[2-(4-methyl-piperazin-1-yl)benzyl]-pyrrolidin-2-one) is a potent 5-HT$_{1B}$ antagonist, which binds with high affinity to the 5-HT$_{1B}$ receptors (Gallezot et al., 2010; Nabulsi et al., 2010). It is a highly selective ligand, since the *in vitro* affinity of P943 is at least 100-fold lower for other 5-HT and non-5-HT receptors. Behaving as an *in vitro* antagonist, P943 blocks the reduction in adenylate cyclase activity elicited in isolated guinea pig substantia nigra by a 5-HT$_{1B}$ agonist (Gallezot et al., 2010). [^{11}C]P943 was prepared at the Department of Diagnostic Radiology, Yale University, New Haven. PET image acquisition and image reconstruction were performed as described previously (Gallezot et al., 2010; Nabulsi et al., 2010). Briefly, reagents and solvents were purchased from Sigma-Aldrich, Fisher Scientific, Merck or J. T. Baker. Both the P943 standard and the *N*-desmethyl-precursor were provided by Pfizer, Inc. Synthesis of [^{11}C]P943 was carried out primarily with the GE's TRACERLab^{TM} FXC automated synthesizer. Radioisotope C-11 carbon dioxide ([^{11}C]CO_2) was produced by the $^{14}N(p,\alpha)^{11}C$ nuclear reaction with the PETtrace cyclotron (GE Medical Systems) using 16.5±0.1 MeV proton irradiation (40 min, 55 µA) of nitrogen gas (6.0) mixed with 0.5% oxygen (6.0). C-11 methyl iodide ([^{11}C]CH_3I) was synthesized from [^{11}C]CO_2 using the GE's MeI Microlab® module. Briefly, [^{11}C]CO_2 was catalytically reduced with H_2 to C-11 methane ([^{11}C]CH_4) followed by solid phase reaction with iodine to form [^{11}C]CH_3I (Larsen et al., 1997). Then [^{11}C]CH_3I was delivered to the FXC module, where it was swept through the silver triflate column ((Jewett, 1992)) at 190° C, and the resulting [^{11}C]methyl triflate was bubbled into a solution of desmethyl P943 (1 mg) in 400 µL of anhydrous dimethylformamide (DMF) cooled at -30° C until activity peaked. The resulting solution was then heated at 100° C for 4 minutes. The reaction mixture was cooled down to 80° C, then diluted with 1 mL of de-ionized water and purified by preparative RP-HPLC. A Phenomenex's Luna 10μ C18(2) 250 x 10 mm semi preparative reverse-phase column was used, and eluted under isocratic conditions with a mobile

phase composed of 40:60 (v/v) acetonitrile/0.1 M ammonium acetate buffer of pH 5.5 (adjusted with glacial acetic acid) and a flow rate of 5 mL/min. The radio-fraction eluting between 11-13 min was collected in the round-bottom flask containing 50 mL of de-ionized water, and loaded onto a Waters Classic C18 Sep-Pak cartridge. The Sep-Pak was washed with 10 mL of 1 mM HCl, and then eluted with 1 mL ethanol into the FXC's product vessel which contained a mixture of 7 mL saline and 40 µL of 4.2% sodium bicarbonate (sterile, preservative and pyrogen free). The Sep-Pak was further eluted with saline (3 mL), and the combined product mixture was passed through a sterile 0.2 µm membrane filter (13 mm, Millipores MILLEX GV) into a sterile assembly comprising of a QC vial connected to a vented dose vial. Identity of the tracer was confirmed by a co-injection with the standard. On the average, the total synthesis time (n=100) was about 38 min from end of beam (EOB), with a radiochemical yield of 10% (decay uncorrected) at end of synthesis (EOS). The average radiochemical activity (non-decay corrected and based on trapped [^{11}C]methyl triflate) has been 2405 ± 962 MBq, with an average specific activity of 351.5 ± 133.2 GBq/µmol calculated at EOS. The average chemical and radiochemical purities were ≥95%.

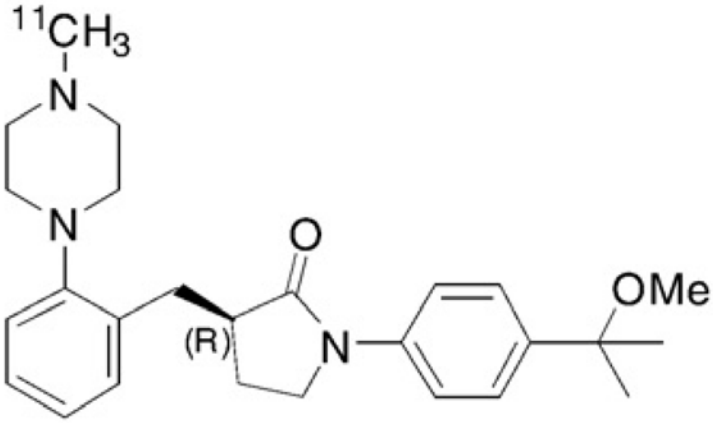

Figure 32: Structural formula of [^{11}C]P943. Reproduced from (Nabulsi et al., 2010).

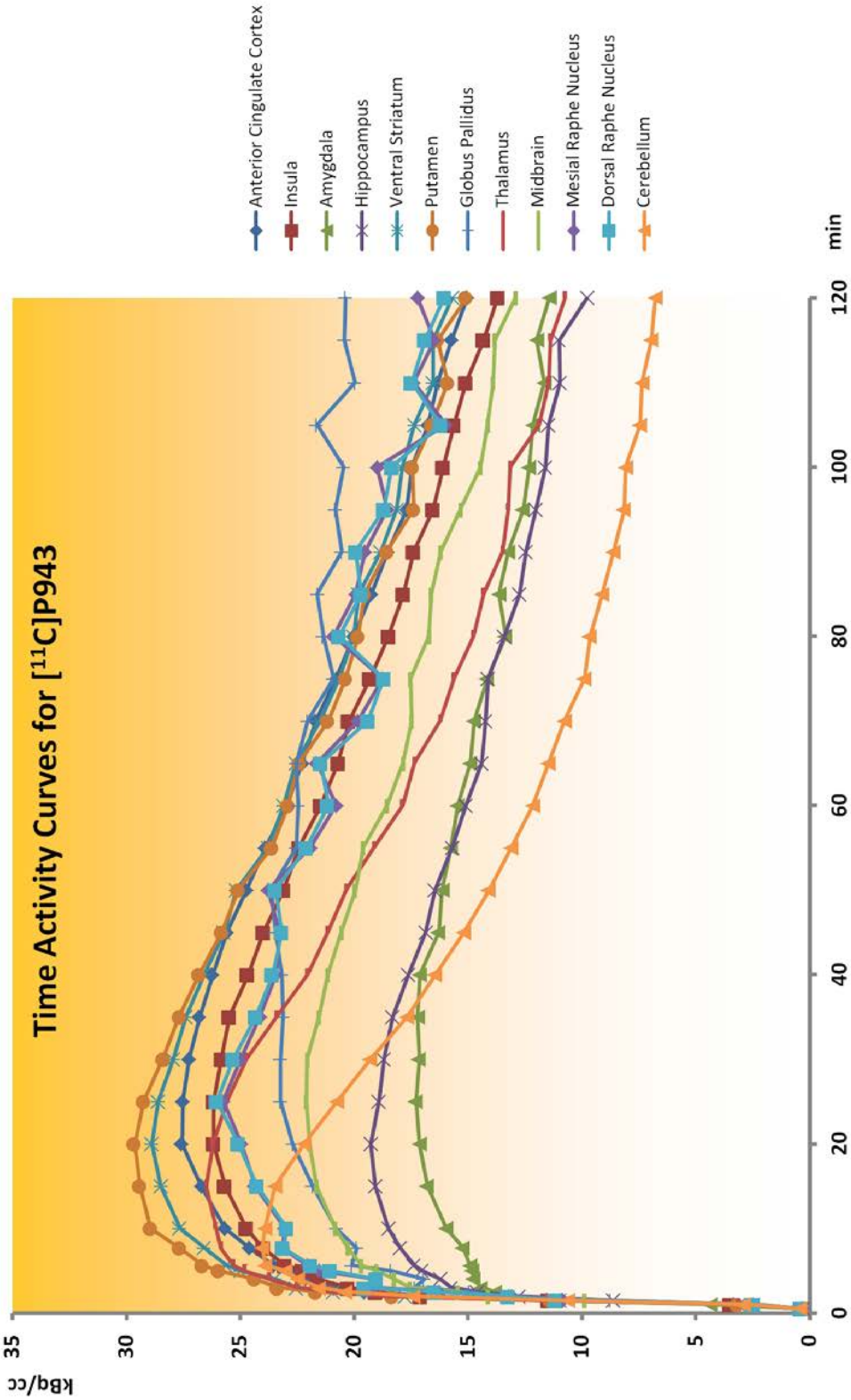

Figure 33: Average time activity curves (TACs) for [^{11}C]P943 binding of 12 representative regions of interest (ROIs) through the course of 120 min.

2.2.3 [^{18}F]altanserin

[^{18}F]altanserin (3-[2-[4-(4-[^{18}F]Fluorobenzoyl)-1-piperidyl]ethyl]-2-sulfanyl-3H-quinazolin-4-one) is a highly selective radioligand for the 5-HT_{2A} receptor. Radiosynthesis was performed at the Institute of Nuclear Chemistry, Research Center Jülich as published previously (Hurlemann et al., 2005; Hurlemann et al., 2008). Briefly, [^{18}F]altanserin was synthetized according to (Lemaire et al., 1991) followed by high performance liquid chromatography (HPLC) (Hamacher, 1995). The radiochemical yield was ≈30% and the radiochemical purity >99%. Mean specific radioactivity was 177±104GBq/µmol at the time of injection. PET scans were performed with a Siemens ECAT EXACT HR+ scanner (Siemens-CTI, Knoxville, TN, USA) in 3 dimensional mode. A lead ring was inserted into the scanner gantry to reduce scatter from outside the FOV. Attenuation correction was obtained by a 10min transmission scan (with three ^{68}Ge/^{68}Ga line sources).

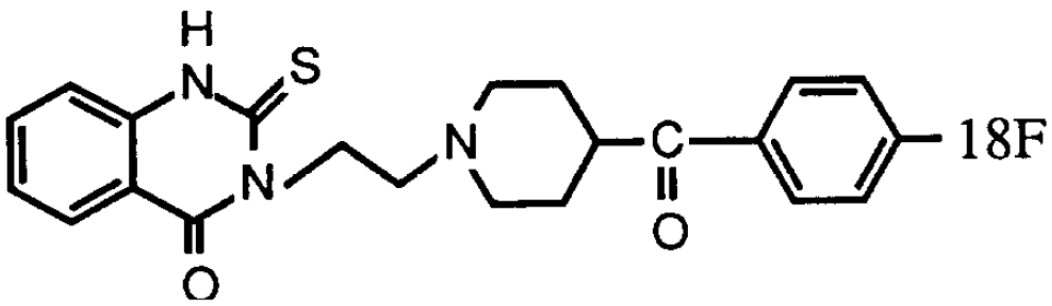

Figure 34: Structural formula of [^{18}F]altanserin. Reproduced from (Biver et al., 1997).

[^{18}F]altanserin was injected as a slow bolus over 2min followed by continuous infusion with a bolus/infusion ratio of K_{Bol}=2.1h. Mean injected radioactivity was 230±11MBq solved in 10ml saline. Dynamic PET data were recorded in six time frames of 10min length starting from 120min after the intra-

venous application of [^{18}F]altanserin. Venous blood samples were drawn at 2, 5, 10, 20, 30, 45, 60, 120, 130, 140, 150, 160, 170, and 180 min post-injection. Selective liquid extraction with quantitation of the recovery of total radioactivity was applied to determine the fraction of radioactive parent compound in plasma, followed by thin-layer chromatography (Matusch et al., 2007). Decay, scatter and attenuation correction, and correction for randoms were applied before rebinning into 2D sinograms (FORE). PET data were reconstructed by filtered backprojection (Shepp filter, filter width = 2.5mm) resulting in a voxel size of 2×2×2.43mm³ (63 slices; FWHM 5.8×5.8×6.6mm³ at 10cm from the central axis).

2.2.4 [^{11}C]DASB

[^{11}C]DASB ([^{11}C]N,N-Dimethyl-2-(2-amino-4-cyanophenylthio)benzylamine) is a highly selective radioligand for the *in vivo* quantification of the serotonin transporter (Ginovart et al., 2001; Houle et al., 2000b; Wilson et al., 2002; Wilson et al., 2000). [^{11}C]DASB was synthesized in the Department of Nuclear Medicine of the Medical University of Vienna (for details see (Haeusler et al., 2009)). Briefly, [^{11}C]DASB was prepared in a fully-automated C11-methylation synthesizer (GE Medical Systems, Uppsala, Sweden). Freshly prepared [^{11}C]methyl iodide was trapped online in the reaction mixture containing 1 mg of precursor (MASB; desmethyl-DASB; obtained from ABX, Radeberg, Germany) in 500 µL of DMSO (dimethylsulfoxide). The reaction mixture was heated at 100°C for 2 min, diluted with 1 mL of mobile phase and subsequently transferred to the semi-preparative HPLC system (column: Supelco ABZ+ 5 µm, 250 x 10 mm). Purification was achieved using RP-HPLC with a mobile phase consisting of 40% acetonitrile and 60% 0.1 mol/L ammonium acetate at a flow rate of 8mL/min. The product fraction was then diluted and subjected to solid phase extraction (Waters, C18 Sep-Pak) to reduce contents of residual solvents. After washing with water the purified product was eluted with ethanol. Finally, the ethanolic product solution was formulated with saline and phosphate buffer and sterile filtrated under aseptic conditions (laminar air flow hot cell). Typically, 2-9 GBq of [^{11}C]DASB were prepared within 35±3 min (n=66). Subsequently, quality control was assessed measuring radiochemical and chemical purity (using analytical HPLC), pH, isotonicity, radionuclidic purity and residual solvents (using gas chromatography). Sterility and endotoxines were controlled after the release of the product, in accordance with the regulations for radiopharmaceutical preparations laid down in the European Pharmacopoiea (2005). The injected radioactivity (mean = 344.5 MBq, SD = 57) was of high radiochemical purity (>95%, mean 98.5%, SD=1.3) and of high specific activity (mean = 40.4 GBq/µmol, SD = 20.8) at the time of injection.

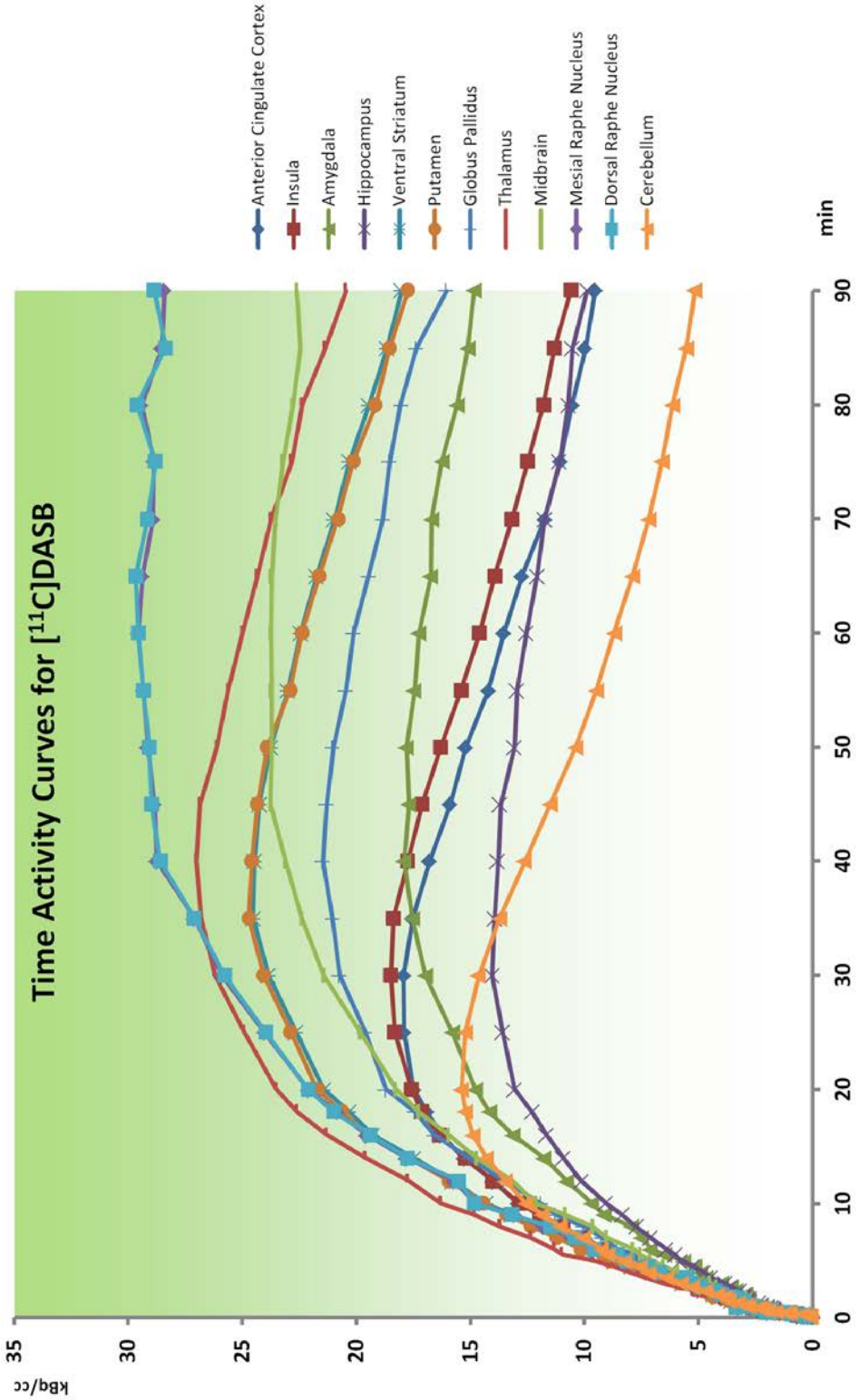

Figure 35: Average time activity curves (TACs) for [^{11}C]DASB binding of 12 representative regions of interest (ROIs) through the course of 90 min. Tracer shows slow kinetics and reaches binding equilibrium at late time points.

PET scans were conducted with a GE Advance PET scanner (General Electric Medical Systems, Milwaukee, Wisconsin) at the Department of Nuclear Medicine, Medical University of Vienna. The 3D dynamic acquisition started simultaneously with intravenous bolus injection of [^{11}C]DASB.

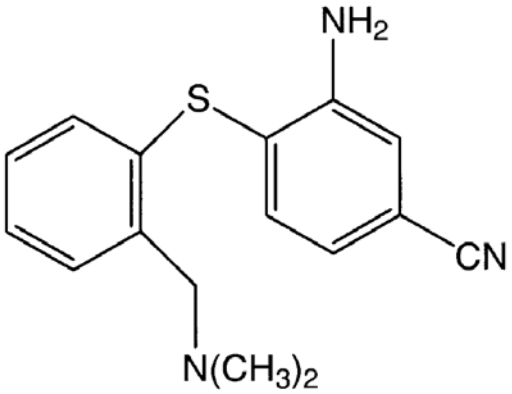

Figure 36: Structural formula of [^{11}C]DASB. Reproduced from (Houle et al., 2000b).

Figure 37: Hot cell for radioligand production.

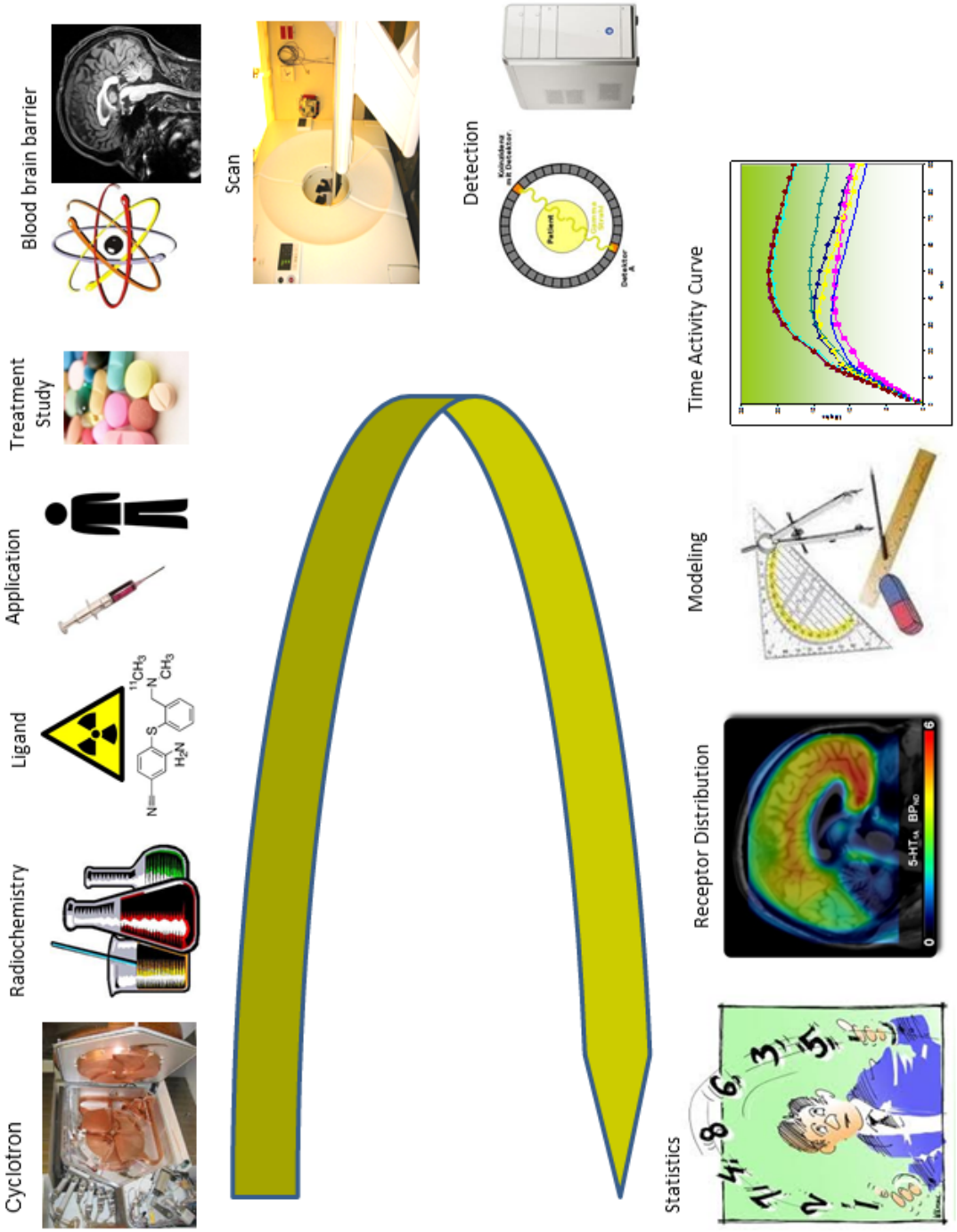

Figure 38: Schematic illustration of an exemplary brain receptor PET study from synthesis to receptor distribution.

2.3 Image preprocessing

Raw PET scans were inspected visually and motion correction using SPM8 (http://www.fil.ion.ucl.ac.uk/spm/software/spm8/) was carried out by co-registration of each frame to the mean of the subjects' motion-free frames. Dynamic PET scans were normalized onto tracer-specific templates in MNI stereotactic space by computing the transformation matrices of individual PET_{ADD} (sum over all time frames) and subsequent application to dynamic scans. Preprocessing of 5-HT_{2A} scans were performed at the Research Centre Jülich using SPM2 (Hurlemann et al., 2008). Ligand-specific templates were created following the approach introduced by Meyer and colleagues (Meyer et al., 1999) and provided mean values for each voxel. Furthermore, an isotropic 8mm Gaussian kernel was chosen for smoothing the original PET images. Finally, the quality of each spatial normalization was visually inspected again and adapted if necessary.

2.4 Region of interest definition

In order to avoid the bias introduced by manual region of interest (ROI) delineation a standardized ROI template was generated comprising numerous brain areas. The ROI template (see Figures 39 and 40) follows two popular parcellation schemes: 1) Brodmann Areas comprising 41 ROIs and 2) the automated anatomical labeling (AAL) brain atlas (Tzourio-Mazoyer et al., 2002) based on the MNI T1-weighted brain covering cortical as well as subcortical regions (Fink et al., 2009; Stein et al., 2008). Furthermore, the template was completed by midbrain and raphe ROIs, thus constituting a total of 52 ROIs. A detailed list of ROI names can be found in Tables 4 and 5.

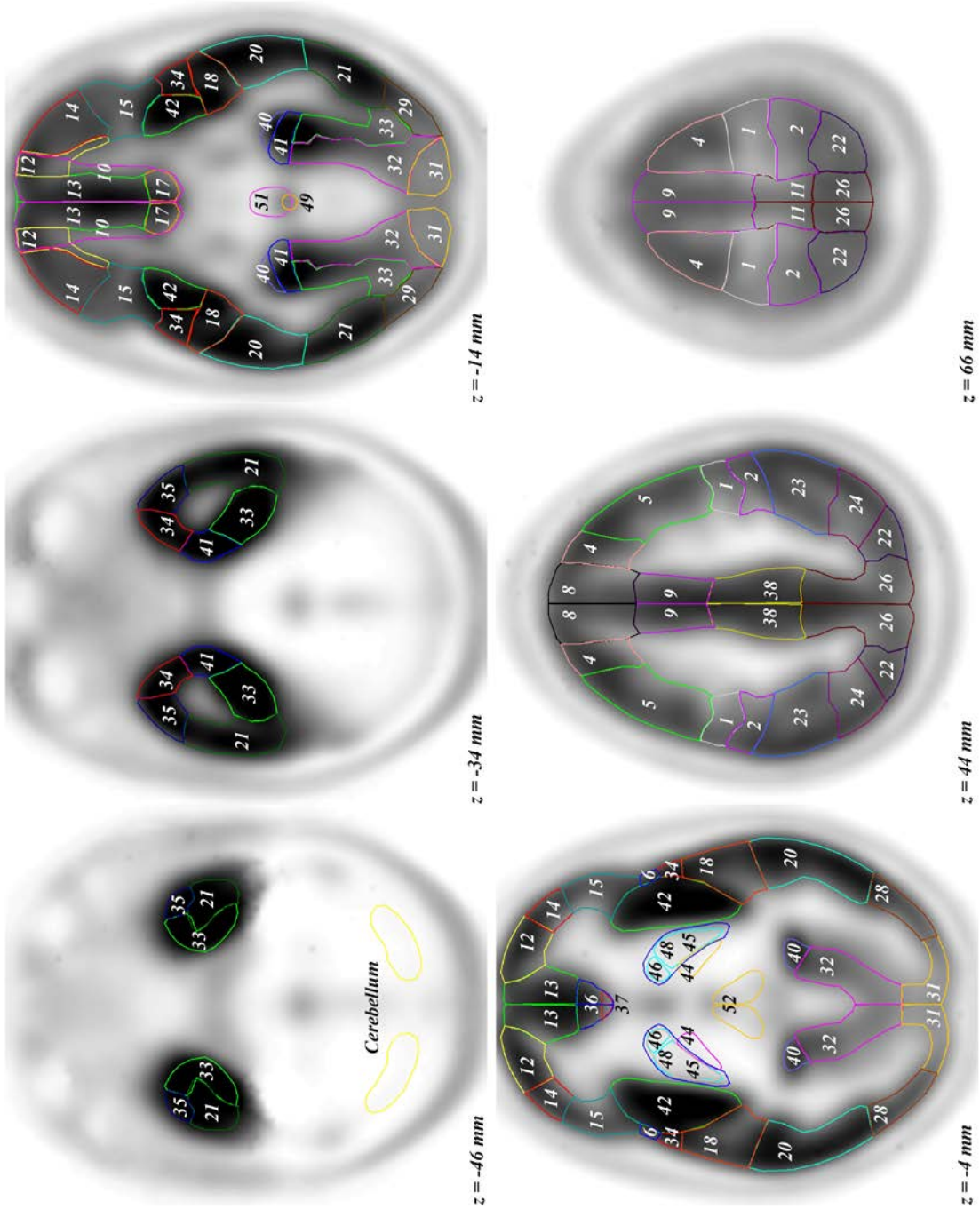

Figure 39 depicts the regions of interest (ROI) template according to the **automated anatomic labeling (AAL)** parcellation scheme (Tzourio-Mazoyer et al., 2002) superimposed on a mean [*carbonyl*-^{11}C]WAY-100635 PET image. This template comprises 52 ROIs on both hemispheres. A detailed list of ROI names can be found in Table 4. The PET image reflects the distribution of 5-HT_{1A} receptors. Selected transaxial views at z = -46, -34, -14, -4, 44, and 66 mm are parallel to the anterior commissure and posterior commisure (AC-PC) plane. Reproduced from (Savli et al., 2012).

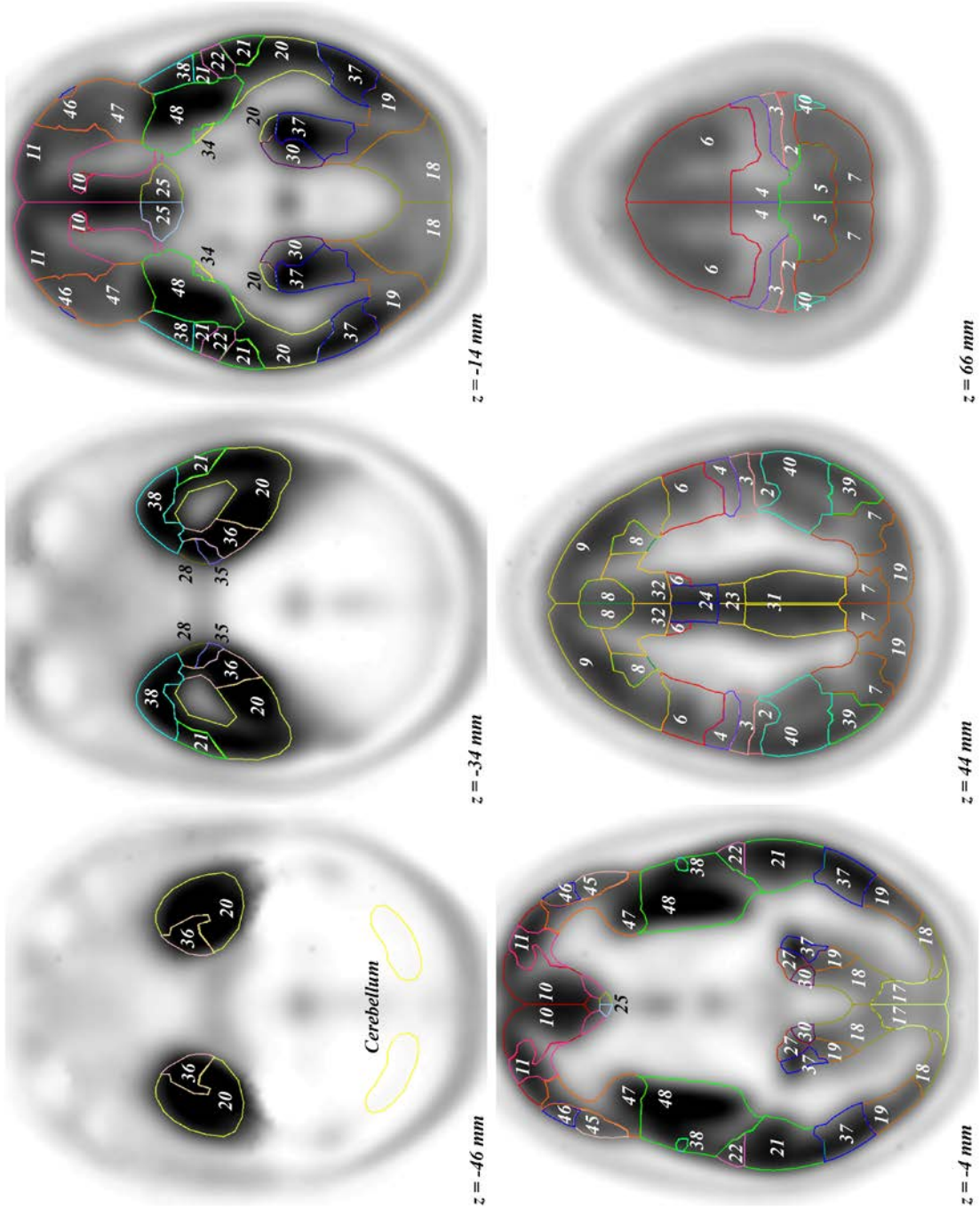

Figure 40 depicts the regions of interest (ROI) template according to the **Brodmann Areas** organizational scheme superimposed on mean [*carbonyl*-^{11}C]WAY-100635 PET image. This template comprises 41 ROIs on both hemispheres. A detailed list of ROI names can be found in Table 4. The PET image reflects the distribution of 5-HT_{1A} receptors. Selected transaxial views at z = -46, -34, -14, -4, 44, and 66 mm are parallel to the anterior commissure and posterior commisure (AC-PC) plane. Reproduced from (Savli et al., 2012).

2.5 Data quantification

An in-house MATLAB program computed time activity curves from normalized PET scans applying the ROI template to each scan. The outcome parameter from the PET studies, the binding potential (BP, (Innis et al., 2007)), which serves as an index for receptor density, was calculated using the kinetic modeling tool PKIN as implemented in PMOD (PMOD Technologies Ltd, Zürich, Switzerland). For quantification of [*carbonyl*-^{11}C]WAY-100635, [^{11}C]P943 and [^{11}C]DASB binding the "multilinear reference tissue model" (MRTM/MRTM2) was used as described previously by Ichise et al. (Ichise et al., 2003). The clearance rate k_2' was calculated individually for insula (5-HT_{1A}), calcarine fissure (5-HT_{1B}) and thalamus (5-HTT) ROIs, respectively, using MRTM and subsequently inserted into MRTM2. Since the cerebellum has been reported either devoid of or containing negligible receptor densities, it is a suitable reference region (Ginovart et al., 2001; Kish et al., 2005; Parsey et al., 2005). Cerebellar ROIs were drawn symmetrically on three contiguous slices representing grey matter excluding vermis and venous sinus (Parsey et al., 2006). BP_{ND} was calculated using the cerebellum as reference region. [^{18}F]altanserin scans were parameterized on the basis of the cerebellum as a reference region ($C_{Reference}$) and the plasma activity concentration attributable to parent compound (C_{Plasma}) according to the following equation: $BP_P = (C_{ROI} - C_{Reference}) / C_{PPC}$ with radioactivity concentrations averaged from 120 to 180 min p.i. (Pinborg et al., 2003). [^{18}F]altanserin binding potentials were read out from parameterized maps. Additionally to the ROI analysis mean tracer-specific whole-brain voxel-wise maps were computed. This was accomplished by first calculating binding potential values for each voxel and subsequently averaging individual maps (see Figure 41).

2.6 Statistical analysis

Quantitative data analysis consisted of descriptive statistics (arithmetic mean, standard deviation, and range) and of correlation analysis. All calculations were computed using the software package R 2.14.2. To assess the quality of the ROI template regarding outcome parameters, binding potentials with results from 10 representative *in vivo* PET databases were compared (Adams et al., 2004; Bose et al., 2011; Cannon et al., 2006; Gallezot et al., 2010; Hurlemann et al., 2008; Ito et al., 1999; Meltzer et al., 2001; Rabiner et al., 2002; Takano et al., 2010; Tauscher et al., 2001) compiled from manual delineation procedures. To this end, data from corresponding ROIs was collected and correlation coefficients were calculated for each subset. Both, Pearson and Spearman coefficients were computed since some studies involved only few ROIs.

Moreover, *in vivo* binding potentials were compared with post-mortem binding as given in the autoradiography study of Varnäs *et al.* (Varnäs et al., 2004). Here, the 17 matching ROIs were anterior cingulate cortex, posterior cingulate cortex, insular cortex, frontal cortex, temporal polar cortex, temporal cortex, occipital cortex, hippocampus, parahippocampal gyrus, amygdala, globus pallidus, caudate nucleus, putamen, striatum, thalamus, brainstem, and dorsal raphe nucleus. For comparison with *in vivo* PET data, the post-mortem values were averaged for different cortical layers for each region. Finally, linear equations were computed to establish direct associations from binding potentials to tissue binding but excluding extreme outliers caused by e.g. partial volume effects.

Applying average ROI BPs, partial correlation coefficients between receptor pairs were calculated to scrutinize associations within serotonergic binding proteins. The arrangement of these pairs was 5-HT_{1A} versus 5-HT_{2A} controlled for 5-HT_{1B} and 5-HTT, 5-HT_{1B} versus 5-HT_{2A} controlled for 5-HT_{1B} and

5-HTT, 5-HT_{1A} versus 5-HT_{1B} controlled for 5-HT_{2A} and 5-HTT. Both atlases (BA and AAL ROIs) were examined separately.

3 Results

The distribution patterns of the four proteins measured with the radioligands [*carbonyl*-^{11}C]WAY-100635, [^{11}C]P943, [^{18}F]altanserin, and [^{11}C]DASB were diverse from each other. Average voxel-wise maps are illustrated in Figure 41. Regional binding potential values are reported as mean, SD values and range in Tables 4 and 5. ROI volumes ranged from 0.05cm³ in dorsal and median raphe nucleus to 58.3cm³ in middle frontal gyrus and 0.7cm³ in BA26 to 101.46cm³ in BA48. Moreover, mean binding potential values displayed as polar coordinate plots resulted in distinct topological patterns for each protein (see Figures 42 and 43).

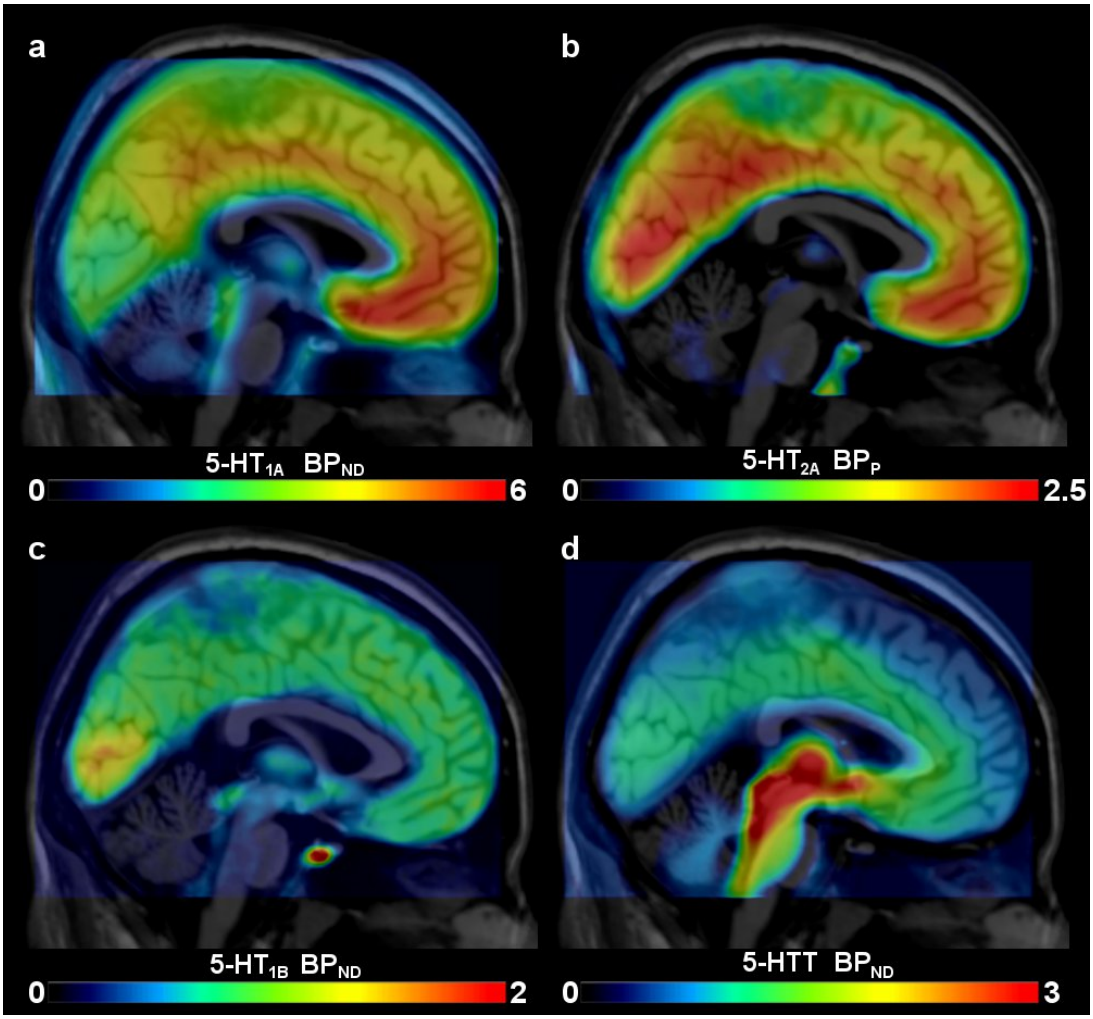

Figure 41: Distribution of the serotonin 1A receptor (5-HT_{1A}) (**a**), the serotonin 2A receptor (5-HT_{2A}) (**b**), serotonin 1B (5-HT_{1B}) receptor (**c**) and the serotonin transporter (5-HTT) (**d**) in the human brain measured with PET using the selective radioligands [*carbonyl*-^{11}C]WAY-100635, [^{18}F]altanserin, [^{11}C]P943 and [^{11}C]DASB, respectively. Color tables indicate receptor binding potentials. Maps are mean PET images based on healthy controls superimposed on a T1-weighted MRI in MNI space. Sagittal view at x=-1mm. Reproduced from (Savli et al., 2012).

3.1 PET Binding Potential

Binding potential values were quantified for both cortical parcellation schemes (AAL and Brodmann Areas; see Tables 4 and 5). Briefly, the ROI analysis yielded high 5-HT_{1A} binding in frontal and temporal regions as well as in the insula and the amygdala. Highest values were found in the temporal pole and parahippocampal gyrus. Parietal areas, regions around central gyrus and subcortical ROI except the dorsal raphe nucleus showed only low specific tracer binding. Contrary to 5-HT_{1A}, 5-HT_{1B} mostly displayed balanced BP_{ND} with the exception of calcarine fissure, pallidum and nucleus accumbens, where the highest values were obtained. Lowest BP_{ND} were found in the hippocampus, parahippocampal gyrus, but also in the thalamus, midbrain, and amygdala. Similarly, 5-HT_{2A} binding was relatively homogenous throughout the cortex. Highest binding potentials were observed in middle frontal gyrus, middle temporal gyrus, angular gyrus and calcarine fissure, lowest in all subcortical ROIs, including the hippocampus and parahippocampal gyrus. Inversely to receptor binding, 5-HTT was predominantly high in subcortical regions with peak values in dorsal raphe nucleus, midbrain, and thalamus, whereas cortical binding was generally low. Moderate binding was observed in the limbic lobe.

Brain Area and Region of Interest		Volume (cm^3)	Binding Potential (mean ± SD)				Range			
			5-HT_{1A}	5-HT_{2A}	5-HT_{1B}	5-HTT	5-HT_{1A}	5-HT_{2A}	5-HT_{1B}	5-HTT
Central region										
1	Precentral gyrus	37.01	2.45 ± 0.43	1.15 ± 0.29	0.74 ± 0.15	0.21 ± 0.10	1.74 - 3.40	0.44 - 1.54	0.39 - 0.98	0.02 - 0.42
2	Postcentral gyrus	40.73	2.68 ± 0.47	1.33 ± 0.36	0.70 ± 0.16	0.25 ± 0.10	1.76 - 3.76	0.50 - 1.93	0.37 - 1.00	0.07 - 0.42
3	Rolandic operculum	13.70	4.18 ± 0.69	1.86 ± 0.45	0.87 ± 0.18	0.40 ± 0.10	2.76 - 5.69	0.90 - 2.59	0.56 - 1.33	0.23 - 0.54
Frontal lobe, Lateral surface										
4	Superior frontal gyrus, dorsolateral	54.88	3.25 ± 0.56	1.46 ± 0.42	0.81 ± 0.17	0.20 ± 0.09	2.15 - 4.66	0.37 - 2.12	0.51 - 1.25	0.06 - 0.36
5	Middle frontal gyrus	58.30	3.41 ± 0.61	1.76 ± 0.46	1.00 ± 0.17	0.22 ± 0.08	2.40 - 5.20	0.67 - 2.49	0.62 - 1.29	0.09 - 0.36
6	Inferior frontal gyrus, opercular part	15.49	3.50 ± 0.58	1.68 ± 0.44	0.93 ± 0.18	0.23 ± 0.09	2.34 - 5.08	0.65 - 2.38	0.55 - 1.33	0.10 - 0.40
7	Inferior frontal gyrus, triangular part	15.28	3.12 ± 0.51	1.62 ± 0.44	0.97 ± 0.19	0.24 ± 0.08	2.09 - 4.33	0.64 - 2.36	0.51 - 1.36	0.12 - 0.38
Frontal lobe, Medial surface										
8	Superior frontal gyrus, medial	42.06	3.54 ± 0.62	1.58 ± 0.47	0.84 ± 0.20	0.22 ± 0.09	2.32 - 5.17	0.42 - 2.22	0.63 - 1.51	0.05 - 0.40
9	Supplementary motor area	36.68	3.04 ± 0.52	1.32 ± 0.43	0.75 ± 0.17	0.29 ± 0.11	2.06 - 4.23	0.19 - 1.93	0.50 - 1.12	0.12 - 0.50
10	ventromedial prefrontal cortex	32.11	4.04 ± 0.70	1.56 ± 0.40	0.73 ± 0.13	0.43 ± 0.08	2.55 - 6.10	0.66 - 2.30	0.56 - 1.17	0.30 - 0.56
11	Paracentral lobule	12.87	2.81 ± 0.49	1.26 ± 0.41	0.63 ± 0.17	0.34 ± 0.12	1.91 - 3.84	0.12 - 1.77	0.29 - 0.96	0.15 - 0.57
Frontal lobe, Orbital surface										
12	Superior frontal gyrus, orbital part	14.28	4.15 ± 0.72	1.70 ± 0.47	0.81 ± 0.19	0.39 ± 0.08	2.71 - 6.05	0.61 - 2.52	0.62 - 1.51	0.24 - 0.51
13	Superior frontal gyrus, medial orbital	15.38	3.70 ± 0.62	1.53 ± 0.38	0.80 ± 0.15	0.30 ± 0.07	2.40 - 5.36	0.75 - 2.22	0.57 - 1.30	0.18 - 0.41
14	Middle frontal gyrus, orbital part	13.38	3.54 ± 0.64	1.80 ± 0.44	0.93 ± 0.14	0.27 ± 0.07	2.39 - 5.17	0.83 - 2.46	0.72 - 1.31	0.14 - 0.40
15	Inferior frontal gyrus, orbital part	19.58	3.55 ± 0.61	1.67 ± 0.44	0.81 ± 0.16	0.37 ± 0.10	2.39 - 5.28	0.59 - 2.30	0.59 - 1.33	0.22 - 0.59
16	Gyrus rectus	8.85	4.69 ± 0.88	1.77 ± 0.50	0.78 ± 0.18	0.44 ± 0.08	2.86 - 7.31	0.69 - 2.67	0.51 - 1.39	0.34 - 0.60
17	Olfactory cortex	3.58	4.32 ± 0.84	1.35 ± 0.42	0.65 ± 0.10	1.08 ± 0.21	2.46 - 6.80	0.45 - 1.91	0.53 - 0.92	0.79 - 1.59
Temporal lobe, Lateral surface										
18	Superior temporal gyrus	31.20	4.02 ± 0.67	1.82 ± 0.42	0.73 ± 0.17	0.36 ± 0.10	2.50 - 5.53	0.85 - 2.44	0.42 - 1.14	0.21 - 0.49
19	Heschl gyrus	3.23	4.02 ± 0.62	1.71 ± 0.42	0.83 ± 0.15	0.55 ± 0.14	2.71 - 5.36	0.89 - 2.40	0.58 - 1.05	0.31 - 0.74
20	Middle temporal gyrus	47.92	4.43 ± 0.78	1.99 ± 0.46	0.78 ± 0.16	0.28 ± 0.07	2.72 - 6.34	1.07 - 2.72	0.47 - 1.22	0.12 - 0.39
21	Inferior temporal gyrus	39.13	5.02 ± 0.90	1.97 ± 0.47	0.63 ± 0.14	0.25 ± 0.06	2.78 - 6.90	0.96 - 2.75	0.34 - 1.05	0.13 - 0.35
Parietal lobe, Lateral surface										
22	Superior parietal gyrus	33.27	2.95 ± 0.55	1.53 ± 0.38	0.76 ± 0.19	0.16 ± 0.09	1.81 - 4.25	0.72 - 2.23	0.48 - 1.15	-0.02 - 0.29
23	Inferior parietal, but supramarginal and angular gyri	26.42	3.41 ± 0.60	1.69 ± 0.45	0.79 ± 0.17	0.17 ± 0.07	2.29 - 4.88	0.62 - 2.38	0.43 - 1.08	0.04 - 0.27
24	Angular gyrus	19.78	3.53 ± 0.60	1.93 ± 0.47	0.84 ± 0.16	0.17 ± 0.06	2.25 - 4.99	0.87 - 2.63	0.57 - 1.12	0.04 - 0.26
25	Supramarginal gyrus	13.50	3.76 ± 0.63	1.82 ± 0.47	0.87 ± 0.18	0.27 ± 0.09	2.54 - 5.03	0.88 - 2.64	0.48 - 1.22	0.12 - 0.41
Parietal lobe, Medial surface										
26	Precuneus	48.86	3.11 ± 0.51	1.70 ± 0.42	0.73 ± 0.16	0.28 ± 0.10	2.13 - 4.33	0.78 - 2.40	0.41 - 1.06	0.07 - 0.44
Occipital lobe, Lateral surface										
27	Superior occipital gyrus	13.06	2.65 ± 0.48	1.53 ± 0.34	0.92 ± 0.20	0.26 ± 0.10	1.51 - 3.64	0.75 - 2.14	0.48 - 1.32	0.01 - 0.41
28	Middle occipital gyrus	22.45	3.38 ± 0.59	1.78 ± 0.40	0.86 ± 0.19	0.20 ± 0.07	2.04 - 4.69	1.01 - 2.48	0.57 - 1.33	0.01 - 0.27
29	Inferior occipital gyrus	9.47	3.40 ± 0.57	1.77 ± 0.41	0.66 ± 0.20	0.23 ± 0.08	2.14 - 4.56	0.99 - 2.44	0.25 - 1.24	0.04 - 0.34
Occipital lobe, Medial and inferior surfaces										
30	Cuneus	14.73	2.52 ± 0.42	1.77 ± 0.40	0.87 ± 0.23	0.35 ± 0.13	1.41 - 3.28	1.03 - 2.42	0.53 - 1.41	0.02 - 0.60
31	Calcarine fissure and surrounding cortex	13.66	2.05 ± 0.35	1.97 ± 0.39	1.32 ± 0.26	0.37 ± 0.13	1.30 - 2.76	1.13 - 2.62	0.95 - 2.16	0.00 - 0.54
32	Lingual gyrus	25.55	2.80 ± 0.43	1.46 ± 0.36	0.72 ± 0.16	0.37 ± 0.12	1.71 - 3.73	0.61 - 2.05	0.48 - 1.07	0.08 - 0.64
33	Fusiform gyrus	35.94	4.99 ± 0.83	1.67 ± 0.40	0.49 ± 0.11	0.40 ± 0.08	3.29 - 6.66	0.74 - 2.27	0.29 - 0.75	0.22 - 0.53
Limbic lobe										
34	Temporal pole: superior temporal gyrus	18.78	5.22 ± 1.03	1.49 ± 0.41	0.38 ± 0.17	0.56 ± 0.10	2.90 - 7.69	0.43 - 2.00	0.17 - 0.87	0.40 - 0.73
35	Temporal pole: middle temporal gyrus	10.05	5.64 ± 1.18	1.74 ± 0.43	0.45 ± 0.13	0.51 ± 0.10	2.86 - 8.33	0.75 - 2.41	0.13 - 0.67	0.33 - 0.72
36	Anterior cingulate and paracingulate gyri	13.51	3.90 ± 0.71	1.64 ± 0.46	0.89 ± 0.18	0.48 ± 0.09	2.57 - 5.70	0.59 - 2.36	0.62 - 1.43	0.31 - 0.61
37	Subgenual cingulate cortex	1.42	3.78 ± 0.67	1.39 ± 0.47	0.54 ± 0.18	0.84 ± 0.19	2.63 - 5.24	0.49 - 2.31	0.28 - 1.15	0.58 - 1.41
38	Median cingulate and paracingulate gyri	15.91	3.28 ± 0.58	1.43 ± 0.46	0.79 ± 0.12	0.47 ± 0.10	2.19 - 4.81	0.44 - 2.08	0.59 - 0.98	0.34 - 0.64
39	Posterior cingulate gyrus	2.75	2.52 ± 0.49	1.15 ± 0.45	0.49 ± 0.18	0.37 ± 0.11	1.29 - 3.48	0.32 - 1.98	0.16 - 0.80	0.20 - 0.57
40	Hippocampus	5.30	3.76 ± 0.69	0.50 ± 0.24	0.25 ± 0.08	0.48 ± 0.11	2.43 - 5.13	-0.07 - 0.94	0.09 - 0.45	0.29 - 0.64
41	Parahippocampal gyrus	12.99	5.98 ± 1.19	0.74 ± 0.28	0.17 ± 0.07	0.66 ± 0.10	3.69 - 8.63	0.09 - 1.14	0.04 - 0.32	0.50 - 0.81
Insula										
42	Insula	32.77	4.86 ± 0.78	1.67 ± 0.41	0.79 ± 0.16	0.68 ± 0.10	3.32 - 7.10	0.67 - 2.22	0.49 - 1.20	0.51 - 0.82
Subcortical										
43	Amygdala	3.56	4.12 ± 0.87	0.49 ± 0.28	0.32 ± 0.11	1.54 ± 0.25	2.62 - 6.19	-0.19 - 0.92	0.12 - 0.50	1.03 - 2.17
44	Pallidum	1.46	0.20 ± 0.10	0.19 ± 0.16	1.30 ± 0.49	1.69 ± 0.22	0.01 - 0.42	-0.19 - 0.42	0.79 - 3.22	1.35 - 2.19
45	Putamen	5.90	0.51 ± 0.11	0.43 ± 0.16	0.89 ± 0.16	1.85 ± 0.19	0.35 - 0.76	0.14 - 0.79	0.60 - 1.36	1.58 - 2.23
46	Caudate nucleus	1.76	0.30 ± 0.11	0.40 ± 0.17	0.88 ± 0.15	1.85 ± 0.22	0.09 - 0.50	0.04 - 0.75	0.64 - 1.29	1.45 - 2.37
47	Nuclues accumbens	0.33	1.15 ± 0.24	0.35 ± 0.26	1.47 ± 0.32	2.31 ± 0.35	0.68 - 1.76	-0.18 - 0.79	1.11 - 2.36	1.77 - 3.08
48	Striatum	9.86	0.58 ± 0.12	0.45 ± 0.16	0.93 ± 0.16	1.89 ± 0.19	0.42 - 0.86	0.09 - 0.76	0.66 - 1.39	1.61 - 2.25
49	Dorsal raphe nucleus	0.05	2.11 ± 0.50	0.05 ± 0.27	0.86 ± 0.20	5.03 ± 1.06	1.08 - 3.36	-0.40 - 0.59	0.50 - 1.40	3.70 - 7.81
50	Median raphe nucleus	0.05	2.06 ± 0.51	< 0 [a]	0.34 ± 0.16	4.26 ± 1.22	1.11 - 3.24	-0.74 - 0.46	0.03 - 0.74	2.91 - 6.77
51	Midbrain	0.70	1.22 ± 0.29	< 0 [a]	0.56 ± 0.10	3.28 ± 0.50	0.63 - 1.87	-0.76 - 0.30	0.35 - 0.73	2.59 - 4.20
52	Thalamus	4.60	0.54 ± 0.15	0.23 ± 0.22	0.42 ± 0.07	2.18 ± 0.27	0.25 - 0.87	-0.30 - 0.62	0.33 - 0.63	1.79 - 2.75

[a] Regions devoid of protein binding resulted in values below zero.

Table 4: Average binding potential, standard deviation and range according to the AAL (automated anatomic labeling) organizational scheme including 52 regions of interest for the serotonin 1A (5-HT_{1A}), the serotonin 2A (5-HT_{2A}), and serotonin 1B (5-HT_{1B}) receptors, and the serotonin transporter (5-HTT) in the human brain measured with PET. Values are averaged for left and right hemisphere. ROIs are aggregated by lobes and related areas. The sequence and grey-scale correspond to Figure 42.

Functional attribution	Brodmann Area	Volume (cm^2)	Binding Potential (mean ± SD)				Range			
			5-HT_{1A}	5-HT_{2A}	5-HT_{1B}	5-HTT	5-HT_{1A}	5-HT_{2A}	5-HT_{1B}	5-HTT
Somatosensory	BA 1	2.37	2.37 ± 0.46	1.19 ± 0.39	0.65 ± 0.22	0.24 ± 0.12	1.50 - 3.36	0.30 - 1.62	0.23 - 1.07	0.01 - 0.41
Somatosensory	BA 2	11.47	2.86 ± 0.51	1.42 ± 0.40	0.67 ± 0.16	0.23 ± 0.09	1.77 - 3.90	0.55 - 1.99	0.36 - 0.89	0.05 - 0.36
Somatosensory	BA 3	17.11	2.38 ± 0.42	1.21 ± 0.32	0.72 ± 0.16	0.26 ± 0.11	1.53 - 3.41	0.46 - 1.79	0.39 - 1.03	0.06 - 0.44
Motor	BA 4	30.31	2.29 ± 0.41	1.03 ± 0.31	0.69 ± 0.16	0.25 ± 0.11	1.53 - 3.16	0.26 - 1.57	0.35 - 0.94	0.03 - 0.50
Somatosensory	BA 5	18.84	2.72 ± 0.49	1.19 ± 0.40	0.54 ± 0.17	0.25 ± 0.11	1.91 - 3.94	0.11 - 1.79	0.20 - 0.86	0.08 - 0.44
Motor	BA 6	76.66	2.86 ± 0.51	1.29 ± 0.37	0.76 ± 0.15	0.18 ± 0.09	1.94 - 4.09	0.31 - 1.75	0.44 - 1.03	0.03 - 0.36
Visual - Parietal	BA 7	51.33	2.88 ± 0.51	1.52 ± 0.39	0.72 ± 0.17	0.16 ± 0.09	1.87 - 4.13	0.65 - 2.14	0.47 - 1.07	-0.02 - 0.29
Motor - Frontal Eye Fields	BA 8	25.80	3.16 ± 0.56	1.53 ± 0.44	0.85 ± 0.17	0.15 ± 0.09	2.09 - 4.53	0.28 - 2.12	0.60 - 1.16	0.00 - 0.34
Cognition	BA 9	35.93	3.51 ± 0.63	1.66 ± 0.48	0.89 ± 0.17	0.19 ± 0.09	2.34 - 5.17	0.46 - 2.45	0.60 - 1.31	0.03 - 0.34
Cognition	BA 10	39.82	3.88 ± 0.68	1.70 ± 0.48	0.92 ± 0.22	0.31 ± 0.09	2.58 - 5.71	0.61 - 2.43	0.67 - 1.71	0.15 - 0.46
Cognition	BA 11	40.90	3.86 ± 0.66	1.60 ± 0.40	0.76 ± 0.14	0.36 ± 0.07	2.52 - 5.68	0.71 - 2.29	0.58 - 1.23	0.23 - 0.47
Visual	BA 17	21.55	2.28 ± 0.37	1.93 ± 0.40	1.22 ± 0.26	0.39 ± 0.14	1.37 - 2.97	1.06 - 2.63	0.83 - 1.98	0.03 - 0.63
Visual	BA 18	52.74	2.55 ± 0.41	1.57 ± 0.34	0.82 ± 0.18	0.30 ± 0.11	1.52 - 3.27	0.82 - 2.09	0.54 - 1.30	0.03 - 0.48
Visual	BA 19	49.54	3.09 ± 0.51	1.59 ± 0.36	0.71 ± 0.16	0.22 ± 0.08	1.92 - 4.19	0.86 - 2.14	0.41 - 1.06	0.01 - 0.31
Visual - Temporal	BA 20	59.91	5.29 ± 0.98	1.78 ± 0.44	0.52 ± 0.11	0.30 ± 0.07	2.97 - 7.41	0.85 - 2.47	0.33 - 0.80	0.14 - 0.42
Visual - Temporal	BA 21	28.41	4.53 ± 0.86	1.98 ± 0.47	0.74 ± 0.16	0.31 ± 0.07	2.64 - 6.72	1.02 - 2.78	0.46 - 1.13	0.17 - 0.44
Audition - Wernicke's	BA 22	14.25	3.98 ± 0.72	1.97 ± 0.46	0.77 ± 0.17	0.29 ± 0.08	2.32 - 5.68	0.96 - 2.81	0.45 - 1.19	0.15 - 0.42
Cognition	BA 23	11.07	3.15 ± 0.54	1.65 ± 0.42	0.74 ± 0.14	0.45 ± 0.10	2.06 - 4.48	0.81 - 2.34	0.47 - 0.96	0.25 - 0.62
Cognition	BA 24	9.46	3.40 ± 0.67	1.28 ± 0.47	0.81 ± 0.15	0.60 ± 0.10	2.11 - 5.01	0.23 - 1.83	0.52 - 1.16	0.40 - 0.77
Cognition	BA 25	5.53	3.87 ± 0.74	1.26 ± 0.42	0.60 ± 0.10	0.93 ± 0.19	2.18 - 5.91	0.40 - 1.79	0.43 - 0.83	0.67 - 1.48
Cognition	BA 26	0.70	2.05 ± 0.58	0.81 ± 0.56	0.52 ± 0.22	0.37 ± 0.13	0.54 - 3.09	0.01 - 1.94	0.00 - 0.81	0.13 - 0.56
Visual - Temporal	BA 27	1.89	2.58 ± 0.55	0.45 ± 0.37	0.03 ± 0.08	0.32 ± 0.10	1.50 - 4.03	-0.47 - 1.10	-0.17 - 0.19	0.10 - 0.46
Cognition	BA 28	3.66	5.41 ± 1.32	0.51 ± 0.29	0.21 ± 0.12	1.09 ± 0.19	3.06 - 9.08	-0.26 - 0.86	0.03 - 0.48	0.74 - 1.53
Visual - Temporal	BA 30	11.57	3.44 ± 0.53	0.96 ± 0.37	0.23 ± 0.10	0.43 ± 0.08	2.29 - 4.47	0.17 - 1.48	0.06 - 0.42	0.26 - 0.59
Somatosensory	BA 31	18.08	3.58 ± 0.58	1.87 ± 0.46	0.80 ± 0.15	0.38 ± 0.10	2.40 - 5.10	0.88 - 2.62	0.52 - 1.05	0.18 - 0.54
Motor	BA 32	28.60	3.35 ± 0.57	1.49 ± 0.43	0.82 ± 0.16	0.34 ± 0.09	2.20 - 4.69	0.50 - 2.05	0.60 - 1.37	0.19 - 0.47
Olfaction	BA 34	3.42	3.19 ± 0.55	0.47 ± 0.27	0.37 ± 0.12	1.58 ± 0.26	2.21 - 4.55	-0.21 - 0.87	0.14 - 0.56	1.09 - 2.22
Cognition	BA 35	4.10	5.36 ± 1.09	0.38 ± 0.25	0.22 ± 0.09	0.81 ± 0.14	3.39 - 7.73	-0.18 - 0.75	0.04 - 0.45	0.58 - 1.03
Cognition	BA 36	12.02	6.34 ± 1.30	1.23 ± 0.37	0.28 ± 0.10	0.65 ± 0.09	3.62 - 9.97	0.26 - 1.73	0.12 - 0.47	0.47 - 0.81
Visual - Temporal	BA 37	47.74	4.20 ± 0.68	1.76 ± 0.41	0.60 ± 0.14	0.28 ± 0.07	2.76 - 5.55	0.91 - 2.40	0.29 - 0.97	0.09 - 0.37
Emotion	BA 38	20.47	4.92 ± 1.03	1.51 ± 0.42	0.37 ± 0.15	0.50 ± 0.10	2.59 - 7.58	0.45 - 1.99	0.12 - 0.82	0.36 - 0.69
Visual - Parietal	BA 39	25.18	3.62 ± 0.63	1.92 ± 0.46	0.81 ± 0.16	0.16 ± 0.06	2.27 - 5.13	0.96 - 2.55	0.51 - 1.06	0.02 - 0.25
Somatosensory	BA 40	28.95	3.31 ± 0.58	1.67 ± 0.47	0.78 ± 0.17	0.16 ± 0.08	2.12 - 4.68	0.60 - 2.36	0.41 - 1.05	0.02 - 0.26
Audition	BA 41	2.88	3.05 ± 0.52	1.44 ± 0.41	0.67 ± 0.13	0.32 ± 0.10	2.06 - 4.35	0.59 - 2.06	0.48 - 1.03	0.19 - 0.50
Audition	BA 42	6.10	4.28 ± 0.76	1.92 ± 0.47	0.89 ± 0.20	0.32 ± 0.08	2.81 - 6.05	0.76 - 2.63	0.53 - 1.32	0.18 - 0.44
Gustatory	BA 43	4.55	3.06 ± 0.58	1.52 ± 0.37	0.97 ± 0.17	0.25 ± 0.09	1.99 - 4.46	0.67 - 2.03	0.64 - 1.30	0.07 - 0.42
Language - Broca's	BA 44	14.90	3.36 ± 0.60	1.74 ± 0.48	0.96 ± 0.18	0.20 ± 0.09	2.25 - 5.00	0.68 - 2.42	0.60 - 1.27	0.06 - 0.38
Language - Broca's	BA 45	19.29	3.34 ± 0.57	1.76 ± 0.47	1.01 ± 0.18	0.25 ± 0.08	2.28 - 4.85	0.71 - 2.57	0.63 - 1.34	0.14 - 0.38
Cognition	BA 46	24.18	3.47 ± 0.64	1.82 ± 0.48	0.99 ± 0.17	0.25 ± 0.08	2.41 - 5.50	0.74 - 2.62	0.62 - 1.39	0.15 - 0.39
Cognition	BA 47	23.03	3.54 ± 0.60	1.72 ± 0.45	0.88 ± 0.18	0.36 ± 0.09	2.43 - 5.20	0.66 - 2.36	0.65 - 1.45	0.22 - 0.57
no distinct function	BA 48	101.46	3.95 ± 0.61	1.57 ± 0.39	0.75 ± 0.15	0.49 ± 0.09	2.72 - 5.47	0.70 - 2.15	0.43 - 1.11	0.34 - 0.64

Table 5: Average binding potential, standard deviation and range according to the Brodmann Area (BA) organizational scheme including 41 regions of interest for the serotonin 1A (5-HT_{1A}), the serotonin 2A (5-HT_{2A}), serotonin 1B (5-HT_{1B}) receptors, and the serotonin transporter (5-HTT) in the human brain measured with PET. Values are averaged for left and right hemisphere. Brodmann Areas of similar functional attributions are illustrated in Figure 43.

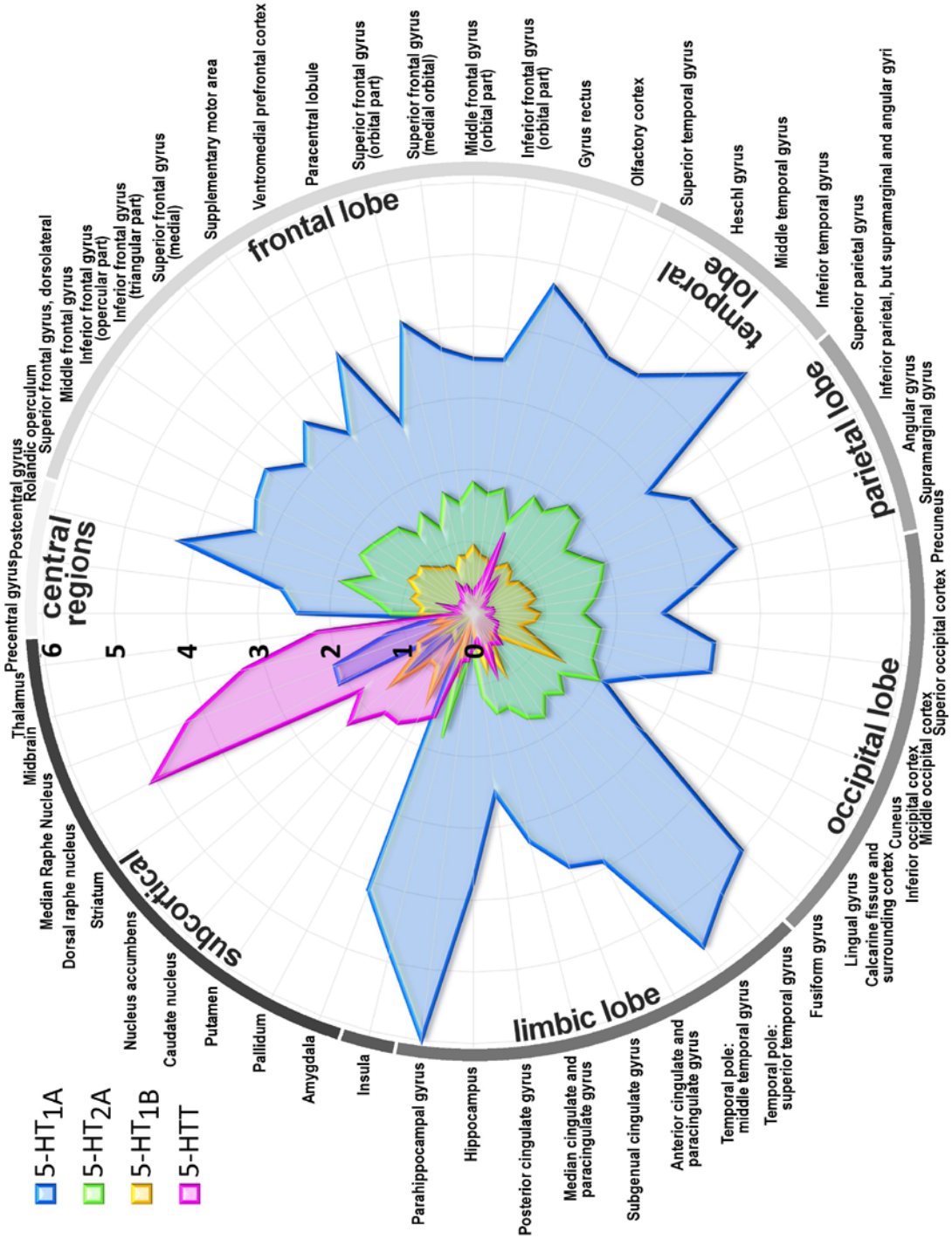

Figure 42 shows the distinct topological pattern of the serotonin 1A ($5\text{-}HT_{1A}$, blue), serotonin 2A ($5\text{-}HT_{2A}$, green), and serotonin 1B ($5\text{-}HT_{1B}$, yellow) receptors, and the serotonin transporter (5-HTT, red) across the human brain listed according to the **AAL (automated anatomic labeling)** organizational scheme including 52 regions of interest (ROI). The radial axis indicates bind-

ing potential (BP) values measured by PET. BP values are averaged for left and right hemisphere regions. ROIs are aggregated by lobes and related areas. The sequence and grey-scale arcs correspond to Table 4. Reproduced from (Savli et al., 2012).

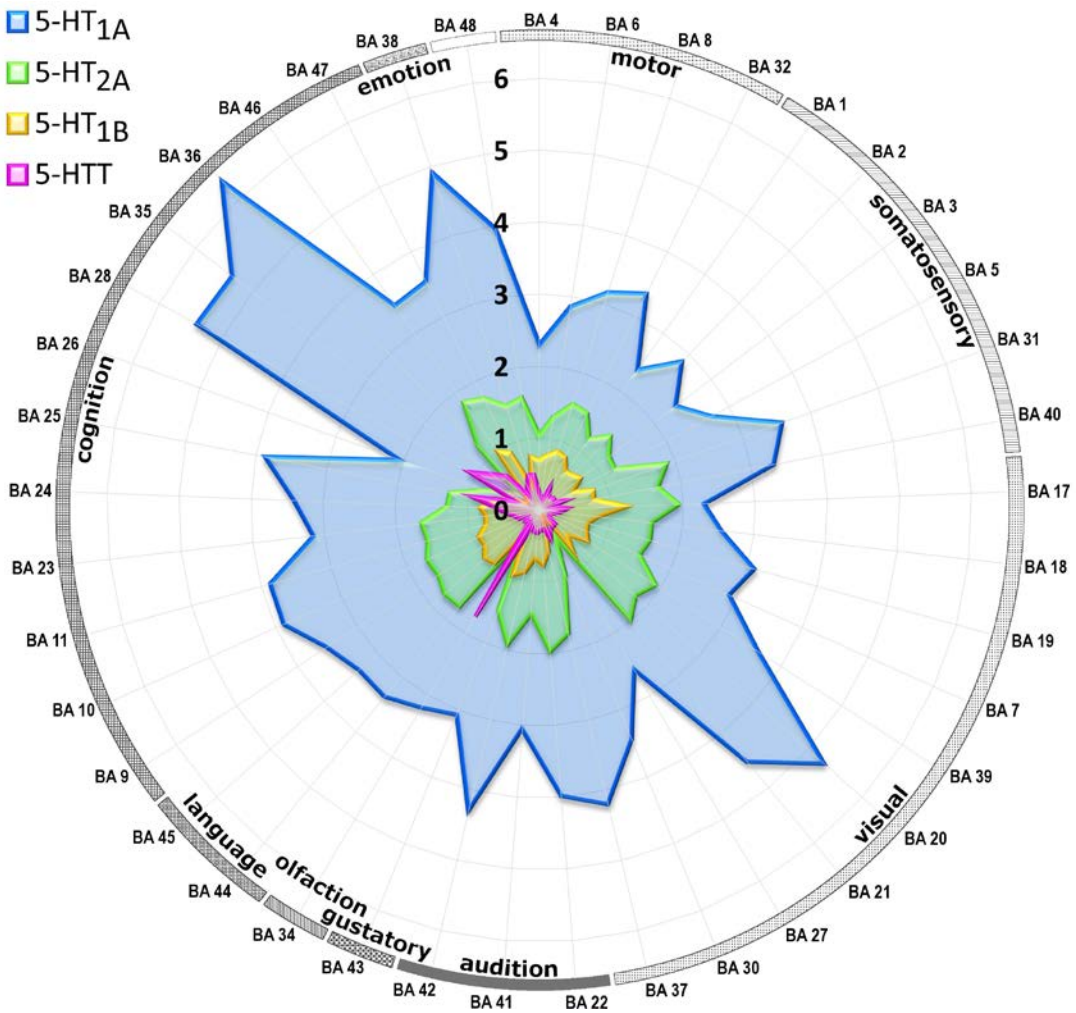

Figure 43 shows the distinct topological pattern of the serotonin 1A ($5\text{-}HT_{1A}$, blue), serotonin 2A ($5\text{-}HT_{2A}$, green), and serotonin 1B ($5\text{-}HT_{1B}$, yellow) receptors, and the serotonin transporter (5-HTT, red) across the human brain listed according to the **Brodmann Area (BA)** organizational scheme including 41 regions of interest (ROI). The radial axis indicates binding potential (BP) values measured by PET. BP values are averaged for left and right hemisphere regions. Brodmann Areas are aggregated by areas of similar functional attributions as indicated by arcs. See Table 5 for ordinal sequence. Reproduced from (Savli et al., 2012).

3.2 Comparison with *in vivo* data

Averaged BP values quantified by the automated template method presented in this article were in good agreement with outcomes from manual delineation procedures (R-values 0.73-0.99). Table 6 summarizes the correlation coefficients between BP estimates obtained from the present study and corresponding findings from previously published *in vivo* databases.

	Study in comparison			Present study		ROIs	Correlations			
							Pearson		Spearman	
	Study	HC	Age [a]	HC	Age		r	p	ρ	p
5-HT_{1A}	Ito et al. 1999	6 (m)	20-42	35 (18m/17f)	26.3±5.2 (21-47)	24	0.910	< 0.001	0.874	< 0.001
	Tauscher et al. 2001	19 (11m/8f)	34 (22-53)	35 (18m/17f)	26.3±5.2 (21-47)	8	0.945	< 0.001	0.994	< 0.001
	Meltzer et al. 2001	21 (10m/11f)	52 (21-80)	35 (18m/17f)	26.3±5.2 (21-47)	8	0.859	0.006	0.905	0.002
	Rabiner et al. 2002	61 (m)	35.5±7.7 (24-53)	35 (18m/17f)	26.3±5.2 (21-47)	17	0.750	< 0.001	0.747	< 0.001
	Takano et al. 2011	17 (m)	24.4±5.9 (20-40)	35 (18m/17f)	26.3±5.2 (21-47)	14	0.940	< 0.001	0.930	< 0.001
	Bose et al. 2011	42 (m)	38±11 (25-60)	35 (18m/17f)	26.3±5.2 (21-47)	12	0.726	< 0.001	0.580	< 0.001
5-HT_{2A}	Adams et al. 2004	52 (30m/22f)	46 (21-79)	19 (11m/8f)	28.2±5.7 (21-40)	15	0.901	< 0.001	0.584	0.022
	Hurlemann et al. 2008	21 (13m/8f)	26.8±3.7 (21-33)	19 (11m/8f)	28.2±5.7 (21-40) [b]	9	0.967	< 0.001	0.767	0.016
5-HT_{1B}	Gallezot et al. 2010	6 (2m/6f)	26.5±5.9 (18-35)	11 (5m/6f)	27.0±6.3 (19-43) [b]	8	0.803	0.054	0.886	0.019
5-HTT	Cannon et al. 2006	37 (13m/24f)	32±9 (18-55)	18 (12m/6f)	30.5±9.5 (19-54)	5	0.891	0.042	0.900	0.037
	Takano et al. 2011	17 (m)	24.4±5.9 (20-40)	18 (12m/6f)	30.5±9.5 (19-54)	14	0.987	< 0.001	0.969	< 0.001
	Bose et al. 2011	42 (m)	38±11 (25-60)	18 (12m/6f)	30.5±9.5 (19-54)	15	0.977	< 0.001	0.841	< 0.001

[a] age information are provided as published in the respective article

[b] data partly identical to study in comparison

Table 6 summarizes the correlation coefficients between average binding potential (BP) estimates obtained from the present PET study and corre-

sponding findings from other database results. For this comparison selected regions of interest were included according to the data availability of the respective study. Overall, BP values from the presented automated delineation method significantly correlated with 10 comparable PET studies. HC columns (healthy controls) indicate the number of subjects (male/female) included.

3.3 Comparison with post-mortem data

As illustrated in Figure 44 high concordance with post-mortem data obtained from the autoradiography study of Varnäs et al (Varnäs et al., 2004) was observed. Correlation coefficients for 5-HT_{1A} were: r=0.44, p=0.076 (Pearson), and ρ=0.76, p<0.001 (Spearman). Excluding the two outliers hippocampus and dorsal raphe nucleus, with their remarkably high concentration, the correlation coefficient increased to r=0.89, p<0.001 (Pearson). The translation from *in vivo* BP_{ND} to post-mortem receptor density (given in pmol/g) was established by means of the linear equation:

$$[^3\mathrm{H}]\mathrm{WAY\text{-}100635\ binding} = 9.04 \times [\mathrm{carbonyl\text{-}}\ ^{11}\mathrm{C}]\mathrm{WAY\text{-}100635}\ \mathrm{BP_{ND}} - 3.15 \quad (18)$$

Thus, a BP_{ND} of 1 is equivalent to 5.89 pmol/g 5-HT_{1A} density in tissue.

The 5-HT_{1B} correlation coefficients were r=0.63, p=0.006 (Pearson) and ρ=0.64, p=0.006 (Spearman). The linear equation

$$[^3\mathrm{H}]\mathrm{GR\ 125743\ binding} = 18.46 \times [^{11}\mathrm{C}]\mathrm{P943}\ \mathrm{BP_{ND}} + 5.04 \quad (19)$$

resulted in 23.5 pmol/g 5-HT_{1B} receptor density in tissue corresponding to a BP_{ND} of 1.

The best accordance was observed in the 5-HT_{2A} pair, with exceptionally high correlation coefficients of r=0.93, p<0.001 (Pearson) and ρ=0.94, p<0.001 (Spearman). Derived from the linear equation

$$[^3\mathrm{H}]\mathrm{MDL100907\ binding} = 25.28 \times [^{18}\mathrm{F}]\mathrm{altanserin}\ \mathrm{BP_P} + 6.16 \quad (20)$$

the BP_P of 1 equals 31.44 pmol/g 5-HT_{2A} receptor density in tissue.

Finally, for 5-HTT correlation coefficients were r=0.87, p<0.001 (Pearson) and ρ=0.72, p=0.001 (Spearman). Excluding dorsal raphe ROI, the correlation was r=0.71, p=0.002. Furthermore, the linear equation

$$[^3\mathrm{H}]\mathrm{Citalopram\ binding} = 9.92 \times \left[^{11}\mathrm{C}\right]\mathrm{DASB\ BP_{ND}} + 1.41 \qquad (21)$$

yielded 11.33 pmol/g 5-HTT tissue density for a BP_{ND} of 1.

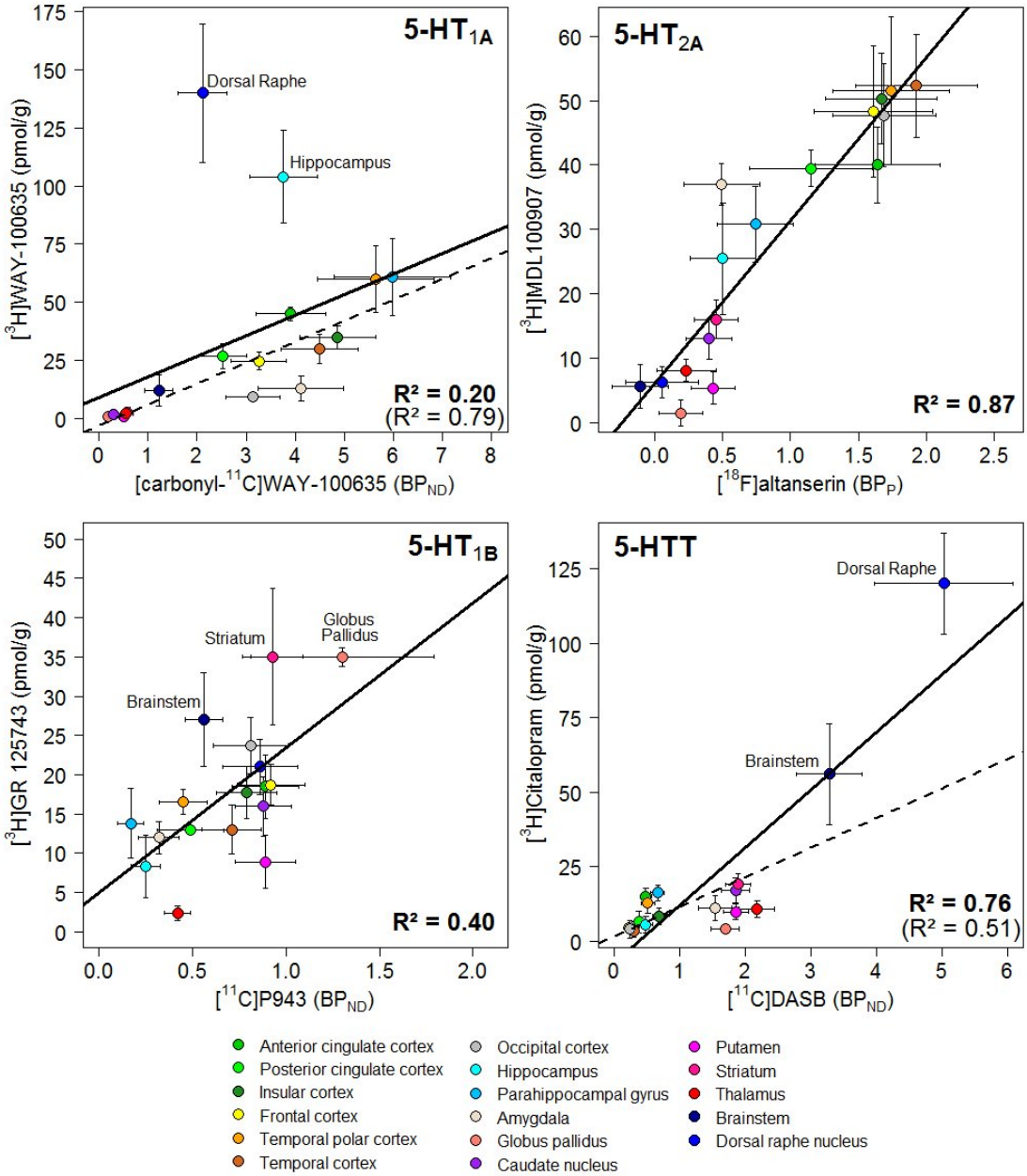

Figure 44 illustrates the linear relationship between receptor/transporter in vivo binding potentials (BP) measured by PET and post-mortem binding from autoradiography (Varnäs et al., 2004). 17 matching regions of interest were included to compare with PET data. Linear equations established the translation between in vivo BP to post-mortem receptor density (given in pmol/g): [^{3}H]WAY-100635 binding = 9.04 × [*carbonyl*-^{11}C]WAY-100635 BP_{ND} - 3.15 (5-HT_{1A}), [^{3}H]GR125743 binding = 18.46 × [^{11}C]P943 BP_{ND} + 5.04 (5-HT_{1B}), [^{3}H]MDL100907 binding = 25.28 × [^{18}F]altanserin BP_{P} + 6.16

(5-HT_{2A}), [^{3}H]Citalopram binding = 9.92 × [^{11}C]DASB BP_{ND} + 1.41 (5-HTT), respectively. Dashed lines and R^2-values (Pearson) in brackets denote associations excluding outliers (see results section). Error bars indicate standard deviations of the mean value. Reproduced from (Savli et al., 2012).

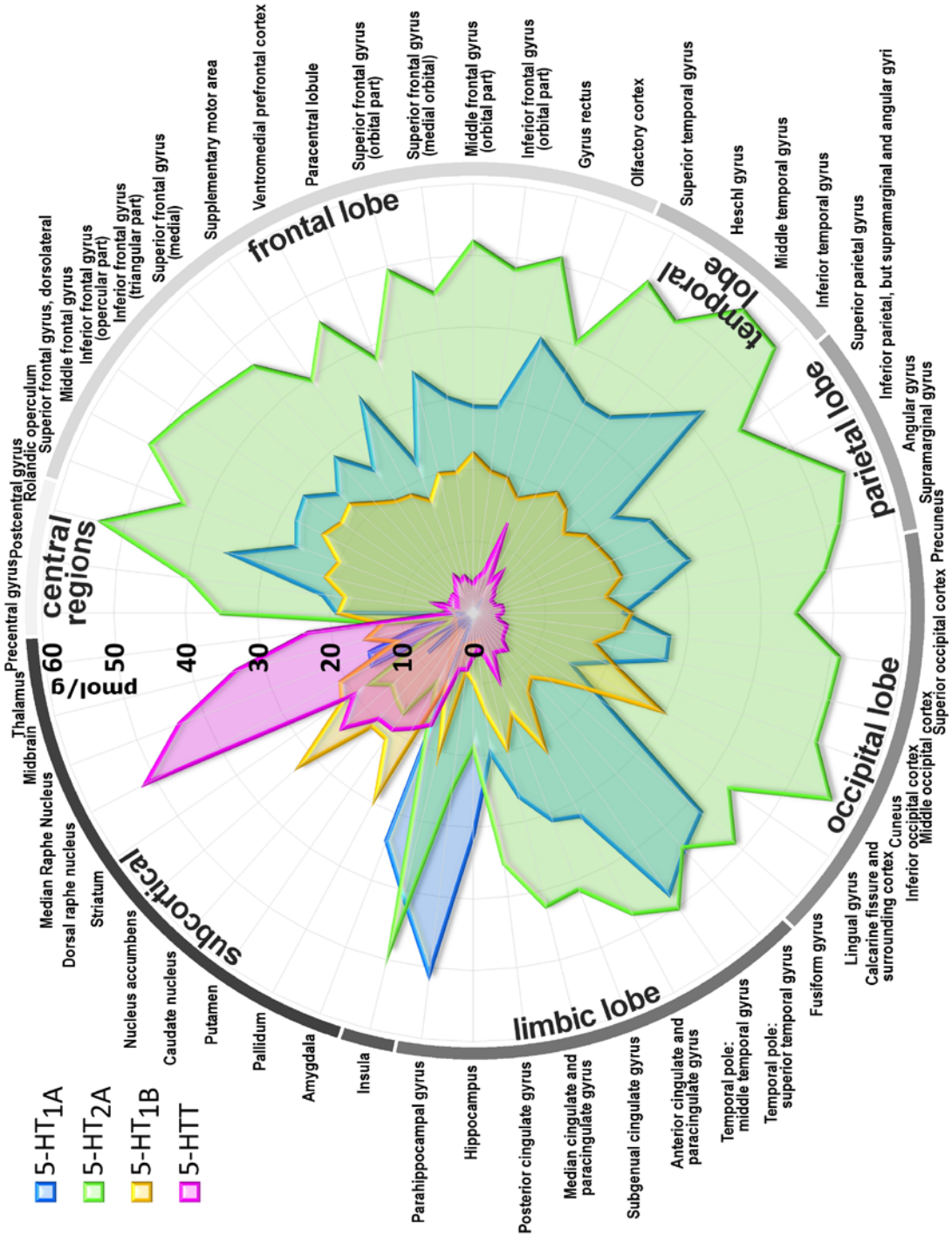

Figure 45 shows the distinct topological pattern of the serotonin 1A ($5\text{-}HT_{1A}$, blue), serotonin 2A ($5\text{-}HT_{2A}$, green), and serotonin 1B ($5\text{-}HT_{1B}$, yellow) receptors, and the serotonin transporter (5-HTT, red) across the human brain listed according to the **AAL (automated anatomic labeling)** organizational scheme including 52 regions of interest (ROI). The radial axis indicates receptor densities given in pmol/mg. BP values are averaged for left and right

hemisphere regions. ROIs are aggregated by lobes and related areas. The sequence and grey-scale arcs correspond to Table 4.

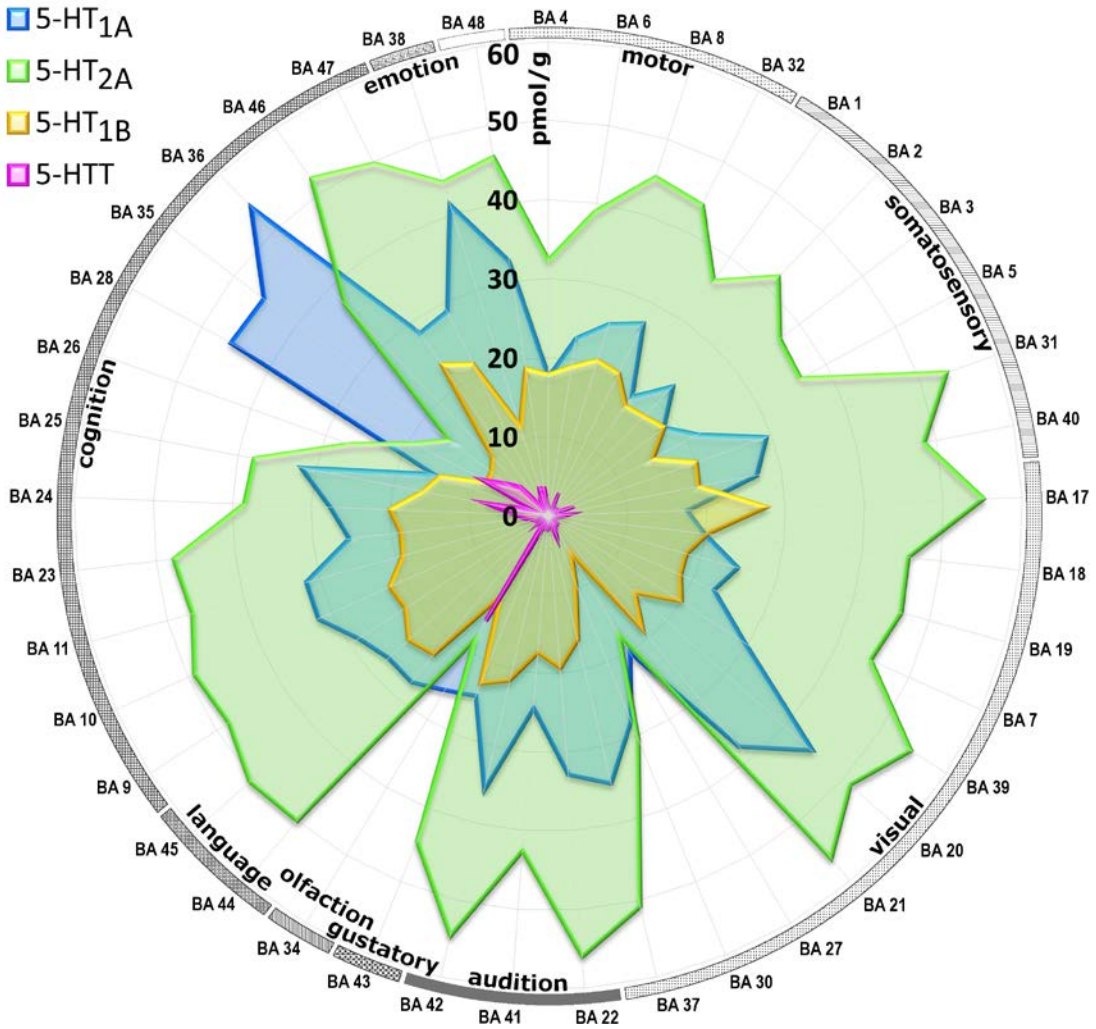

Figure 46 shows the distinct topological pattern of the serotonin 1A ($5\text{-}HT_{1A}$, blue), serotonin 2A ($5\text{-}HT_{2A}$, green), and serotonin 1B ($5\text{-}HT_{1B}$, yellow) receptors, and the serotonin transporter (5-HTT, red) across the human brain listed according to the Brodmann Area (BA) organizational scheme including 41 regions of interest (ROI). The radial axis indicates receptor densities given in pmol/mg. BP values are averaged for left and right hemisphere regions. Brodmann Areas are aggregated by areas of similar functional attributions as indicated by arcs. See Table 5 for ordinal sequence.

3.4 Interaction between binding proteins

Examining BA, significant partial correlations were found between 5-HT_{1A} and 5-HT_{2A} binding potentials controlled for 5-HT_{1B} and 5-HTT ($r=0.68$, $p<0.001$), 5-HT_{1A} and 5-HT_{1B} controlled for 5-HT_{2A} and 5-HTT ($r=-0.66$, $p<0.001$), and 5-HT_{1B} and 5-HT_{2A} controlled for 5-HT_{1A} and 5-HTT ($r=0.83$, $p<0.001$), respectively (see Figures 47-49). Considering AAL ROIs, the partial correlation coefficient between 5-HT_{1A} and 5-HT_{2A} binding potentials controlled for 5-HT_{1B} and 5-HTT was $r=0.67$, between 5-HT_{1A} and 5-HT_{1B} controlled for 5-HT_{2A} and 5-HTT was $r=-0.72$, and between 5-HT_{1B} and 5-HT_{2A} controlled for 5-HT_{1A} and 5-HTT was $r=0.60$, respectively (see Figures 50-52). Again, all p-values were $p<0.001$.

3.4.1 Brodmann Areas

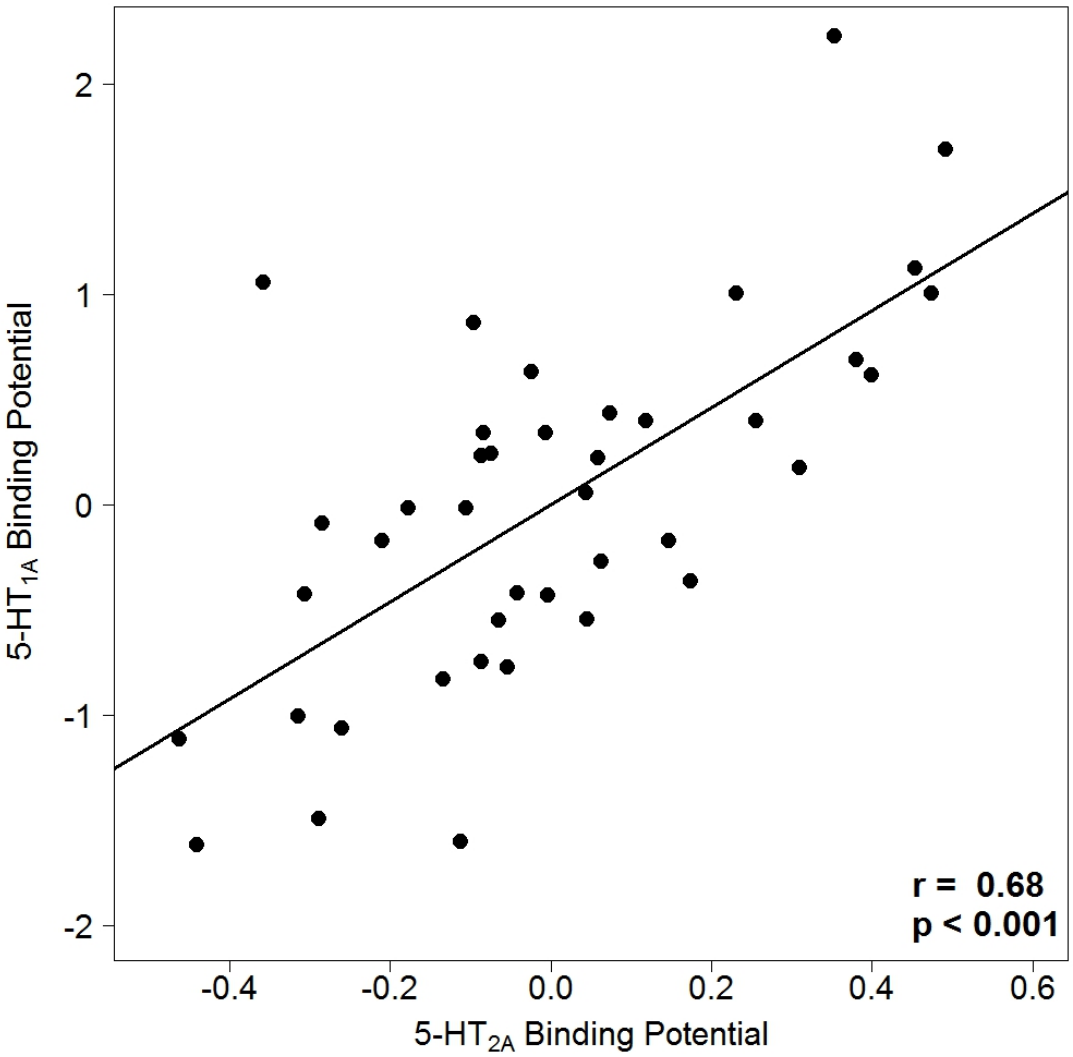

Figure 47: Partial regression plot between 5-HT_{1A} and 5-HT_{2A} binding potentials controlled for 5-HT_{1B} and 5-HTT (r=0.68, p<0.001). Partial regression plots adjust simple scatter plots for variables of noninterest. Notably, this adjustment implies that plotted values may yield positive as well as negative values (mean centered). Data points are **Brodmann Areas** binding potentials, averaged for both hemispheres.

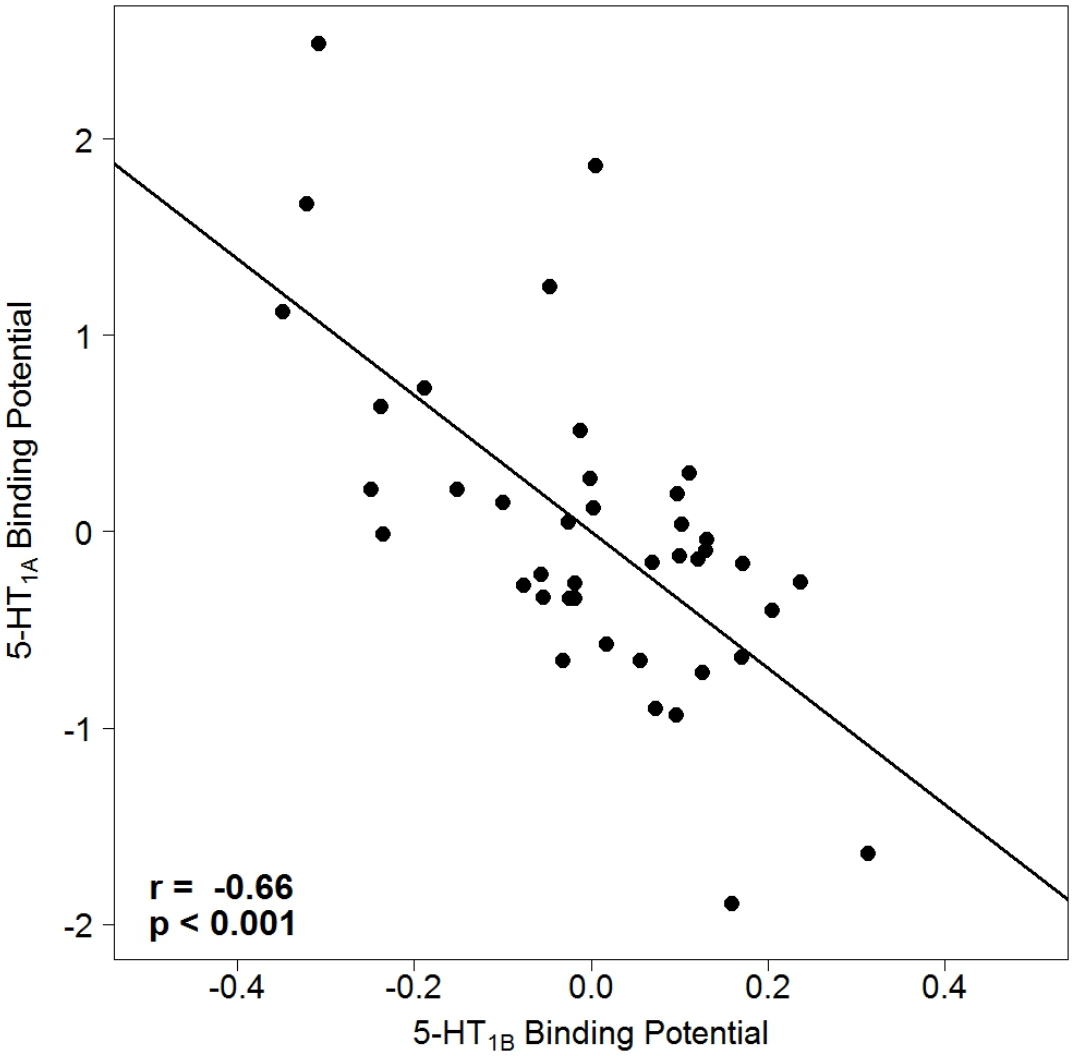

***Figure 48*:** Partial regression plot between 5-HT_{1A} and 5-HT_{1B} binding potentials controlled for 5-HT_{2A} and 5-HTT (r=-0.66, p<0.001). Partial regression plots adjust simple scatter plots for variables of noninterest. Notably, this adjustment implies that plotted values may yield positive as well as negative values (mean centered). Data points are **Brodmann Areas** binding potentials, averaged for both hemispheres.

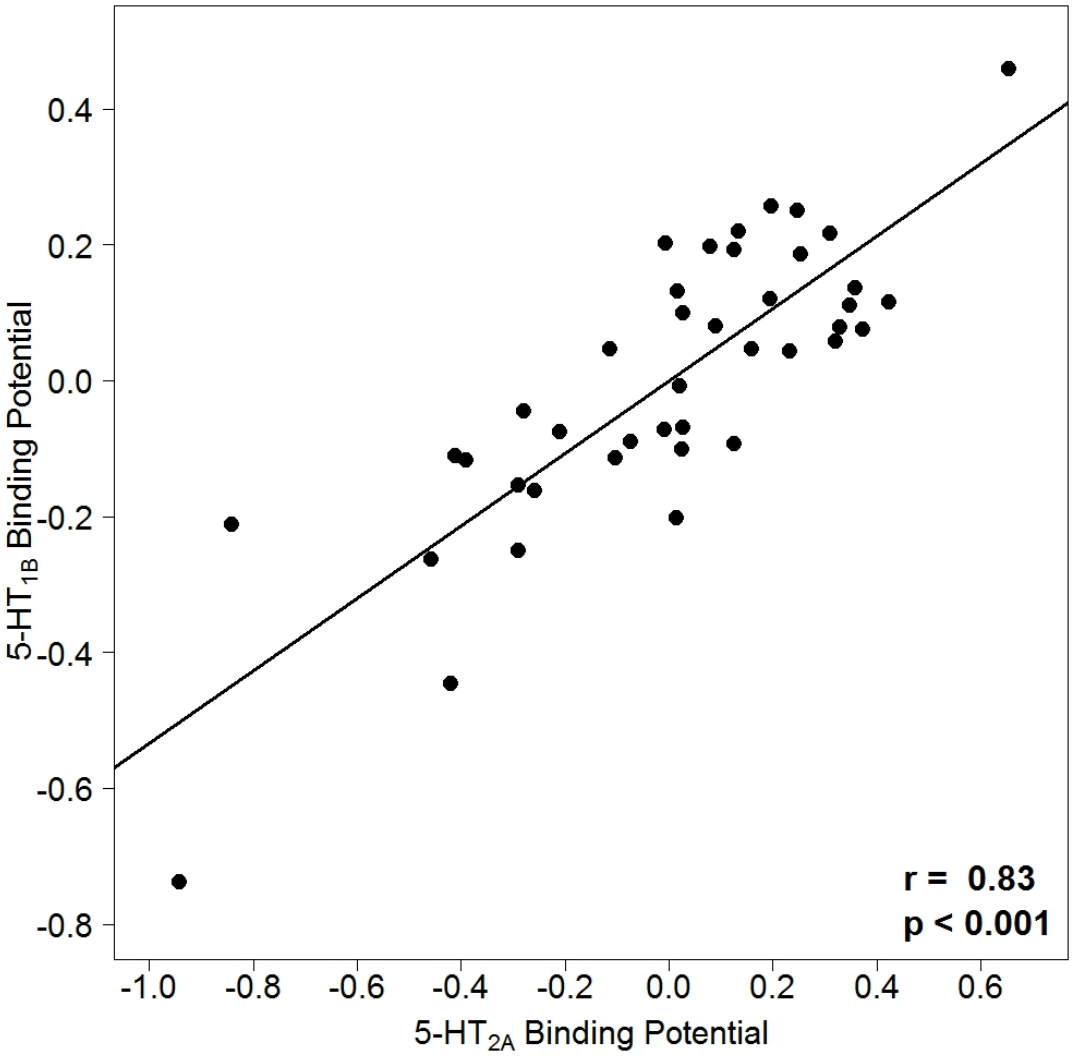

Figure 49: Partial regression plot between 5-HT_{1B} and 5-HT_{2A} binding potentials controlled for 5-HT_{1A} and 5-HTT ($r=0.83$, $p<0.001$). Partial regression plots adjust simple scatter plots for variables of noninterest. Notably, this adjustment implies that plotted values may yield positive as well as negative values (mean centered). Data points are **Brodmann Areas** binding potentials, averaged for both hemispheres.

3.4.2 AAL Regions

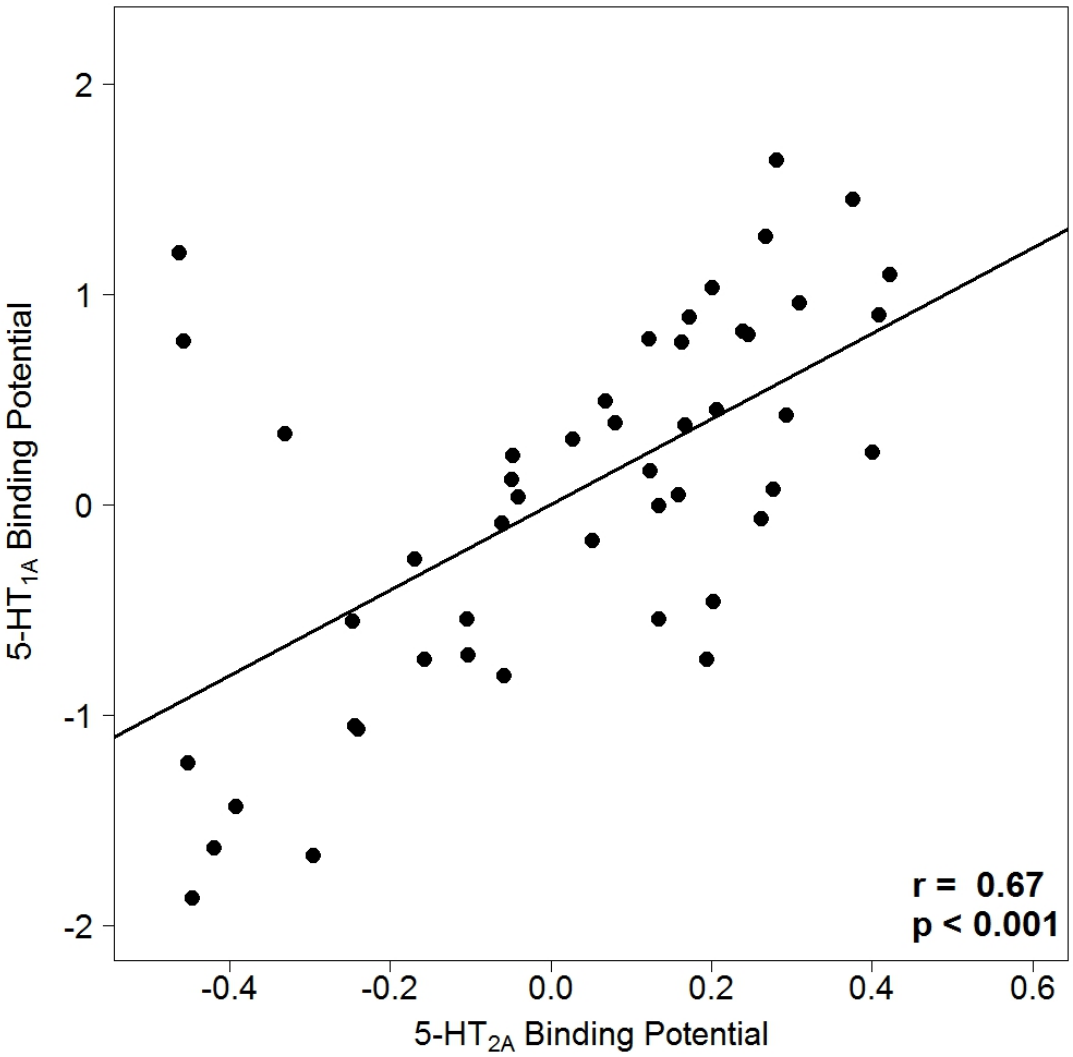

Figure 50: Partial regression plot between 5-HT_{1A} and 5-HT_{2A} binding potentials controlled for 5-HT_{1B} and 5-HTT (r=0.67, p<0.001). Partial regression plots adjust simple scatter plots for variables of noninterest. Notably, this adjustment implies that plotted values may yield positive as well as negative values (mean centered). Data points are **AAL** binding potentials, averaged for both hemispheres.

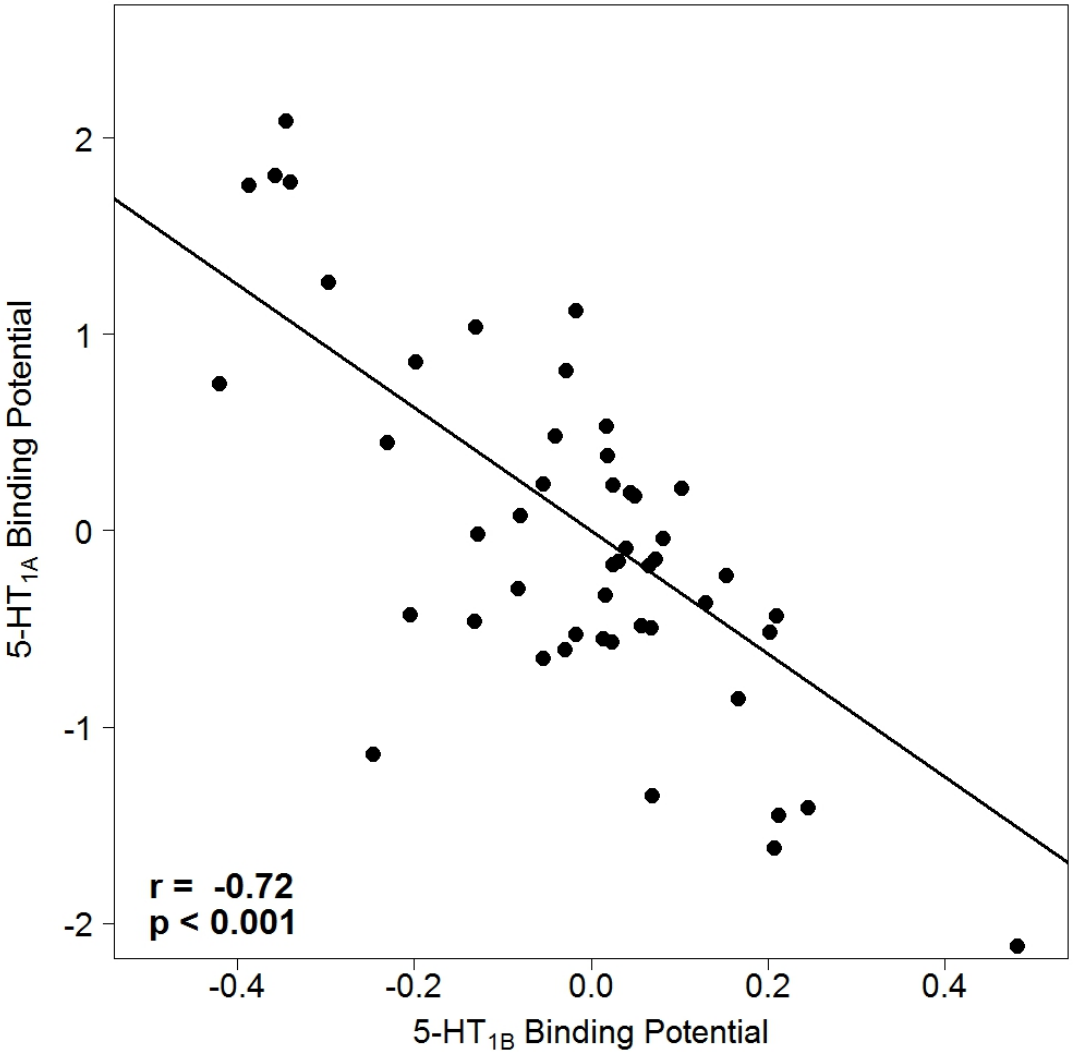

***Figure 51*:** Partial regression plot between 5-HT_{1A} and 5-HT_{1B} binding potentials controlled for 5-HT_{2A} and 5-HTT (r=-0.72, p<0.001). Partial regression plots adjust simple scatter plots for variables of noninterest. Notably, this adjustment implies that plotted values may yield positive as well as negative values (mean centered). Data points are **AAL** binding potentials, averaged for both hemispheres.

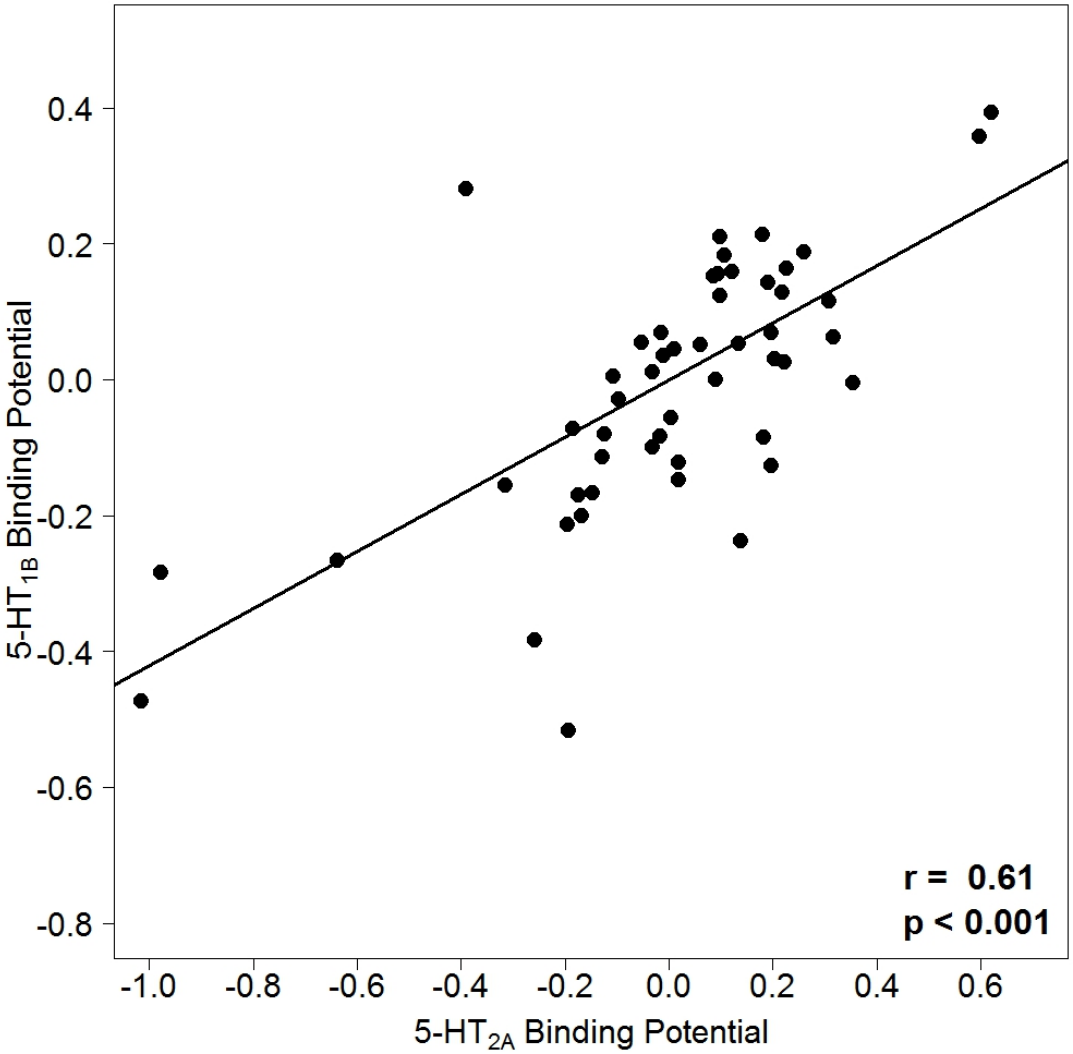

***Figure 52*:** Partial regression plot between 5-HT_{1B} and 5-HT_{2A} binding potentials controlled for 5-HT_{1A} and 5-HTT ($r=0.61$, $p<0.001$). Partial regression plots adjust simple scatter plots for variables of noninterest. Notably, this adjustment implies that plotted values may yield positive as well as negative values (mean centered). Data points are **AAL** binding potentials, averaged for both hemispheres.

4 Discussion

The main serotonergic neuroreceptors – the major inhibitory receptors (5-HT_{1A}, 5-HT_{1B}), the major excitatory receptor (5-HT_{2A}) and the serotonin transporter (5-HTT or SERT) – were quantified in healthy subjects using PET and the selective radioligands [*carbonyl*-^{11}C]WAY-100635, [^{11}C]P943, [^{18}F]altanserin, and [^{11}C]DASB, respectively. A comprehensive database of the average receptor distribution in different ROIs was prepared. In contrast to the previously published results, a database comparing 4 major target proteins of the entire brain including a total of 93 ROIs was provided. The binding potentials of cortical and subcortical regions as the mean, standard deviation and range using automated anatomical labeling (AAL, 52 regions) (Tzourio-Mazoyer et al., 2002) and the parcellation according to the cytoarchitectural organization of the human cortex of Brodmann (41 regions) are included in the presented PET dataset (see Table 4 and 5). Parametric images illustrate the distinct local distributions of each binding protein (see Figure 41). Furthermore, by means of linear equations, *in vivo* BP values were translated to post-mortem tissue densities. Finally, partial correlations provided evidence of local interaction among the major serotonergic neuroreceptors.

4.1 Database of standard values

Yielding comparable PET data from different centers is often challenging as a result of the differences between scanners, imaging equipment and analyzing methods. To generate representative datasets to be used as a standard, a uniform pipeline of operations as data processing pathway was applied for all subjects. Data sets were normalized to a tracer-specific template into a standard space. Then binding potential values were quantified from each map applying the ROI template which was equal for all maps. Blood-brain barrier passing metabolites (e.g. [^{18}F]altanserinol) impeded the quantification with established reference models (such as MRTM/MRTM2), hence

[^{18}F]altanserin scans were parameterized according to Pinborg et al. (Pinborg et al., 2003). Nevertheless, 5-HT_{2A} binding potential values were obtained applying the same ROI template. Using the ROI template the bias of the manual delineation procedures could be bypassed which is a burdensome undertaking and the precision of the delineation is largely dependent on the individual's knowledge and abilities. Besides, the standard ROI template permits a rater independent and volume unbiased comparison of equal ROI size and location between the tracers (see Figures 39 and 40).

Moreover, the quality of the automated outcome was examined with regard to several previously published *in vivo* datasets and a strong agreement with these results was found. One methodological issue which should be taken into account is that the presented standard ROIs were not delineated manually, which was the case in previous studies. Nonetheless, highly significant correlations (R-values 0.73-0.99) demonstrate the accordance with the current results (see Table 6).

This database can contribute to standard definitions of reference ranges, thus it provides the opportunity to be used as a template. It provides a reference source to aid the design and interpretation of clinical studies and multimodal imaging studies. Through these datasets a broader and more precise understanding of the serotonergic neurotransmission and therefore the neuropsychiatric disorders related to this system would be possible. Also, it can be applied for group comparisons between healthy control subjects and patients. The distribution of receptors may vary dramatically from subject to subject under both, physiological and pathological conditions. In spite of the existence of such widely variant topologies, functions and interactions of the binding proteins, the presented data provide a template which can be used for interpretation of the alterations taking place in the serotonergic system during neuropsychiatric disorders.

One obvious modality that might benefit from this dataset is PET itself, particularly studies including small sample sizes. Interpretation of the data obtained from such PET studies would be facilitated using the presented data for comparison and to examine if the subjects are in the standard range or not. Moreover, neuroimaging centers without access to a PET scanner may apply the database to analyze the findings of other neuroimaging modalities in association to the PET derived data. In case of treatment studies of both healthy subjects and patients, this database may serve for comparison purposes as well.

In the same way, functional MRI studies (fMRI) can benefit from the PET data set. Neuronal activation found in fMRI studies can be investigated and interpreted using serotonergic receptor distributions. Close connection between distribution patterns of neurotransmitter receptors and functional organization in the cerebral cortex is already suggested by numerous studies (Eickhoff et al., 2007; Scheperjans et al., 2005; Wohlschläger et al., 2005; Zilles et al., 2002). Further examples include a link between 5-HT_{1A} receptor distribution and functional fields of the human cortex as examined by Gerstl et al. (Gerstl et al., 2008) and the default mode network (Hahn et al., 2012). Similarly, the database may enable more sophisticated interpretations in structural (Kraus et al., 2012) and pharmacological fMRI studies (Anderson et al., 2011; McKie et al., 2005; Windischberger et al., 2010).

The voxel-wise parametric maps of the receptors' densities provided in standard space can be downloaded from a website (www.meduniwien.ac.at/neuroimaging/downloads.html) and may assist as a template for co-registration/normalization purposes. Using the widespread analyze data format, it comfortably can be integrated into popular neuroimaging software tools (SPM, PMOD, FSL, etc.), thus facilitates other laboratories' first-level analyses of their raw data or similar preprocessing manipulations.

4.2 Comparison with post-mortem data

Similar to a recent 5-HT_{1B} study (Gallezot et al., 2010), the correlation of the current data was examined with a post-mortem dataset (Varnäs et al., 2004). This study is one of the most comprehensive works regarding binding of major serotonergic receptors across the entire brain. Assuming a linear correspondence, conversion equations were computed in order to directly translate *in vivo* PET binding potentials to post-mortem receptor densities (pmol/g), which promotes the interpretation of different receptor distributions. Interestingly, a few outliers were noticed (see Figure 44), which were regions of extremely high *in vitro* binding. Excluding these regions, the correlations became even more pronounced. These outlying data might be caused by differing ROI quantification methodologies. Results of the present *in vivo* study underlie the partial volume effect, which particularly influences small structures with high densities such as dorsal raphe nucleus yielding underestimated BP values.

4.3 Interaction between inhibitory and excitatory receptors

Significant partial correlations were observed in the intra-regional densities of 5-HT_{1A} and 5-HT_{2A} and also 5-HT_{1B} and 5-HT_{2A}, adjusted for the other receptor and serotonin transporter. A strong negative correlation was found between the binding potentials of 5-HT_{1A} and 5-HT_{1B} controlled for 5-HT_{2A} and SERT. Both parcellation schemes, BA and AAL, yielded similar results (see Figures 47-52).

This findings support the hypothesis of the existence of a functional balance between the different receptors of the serotonergic system. A functional interaction between 5-HT_{1A}, 5-HT_{1B} and 5-HT_{2A} receptors (Chojnacka-Wojcik, 1992) and 5-HT_{1A} and 5-HT_{2A} receptors (Fox et al., 2010; Salmi and Ahlenius, 1998) in rodents have been previously reported. The behavioral and biochemical effects of 5-HT_{2A} receptor activation are modulated by activ-

ity of the 5-HT_{1A} receptor subtype (Eison and Mullins, 1996). Positive correlations were observed between the two pairs of inhibitory and excitatory subtypes (1A and 2A, 1B and 2A) and a negative relationship between the two inhibitory subtypes (1A and 1B). These correlations were observed only when controlling for the 5-HTT and the other receptor. That means standard correlation coefficients between the mean BP values of any two receptor sub-type did not show significance except for 5-HT_{2A} and 5-HT_{1B} which were observed to be linearly correlated. Examining the data for partial correlation controlling just for the third receptor sub type resulted weak but significant correlations and finally partial correlations controlling for both the third receptor and the transporter led to the quite high R values. This emphasizes a systemically organized mechanisms regarding local receptor expression.
The correlations observed between mean BP values of each subsystem in Brodmann area based ROIs, were equally strong as correlations between the BP values of the same subtypes but in ROIs delineated according to AAL scheme. The consistency in the results in spite of serving two different delineation templates highlights the fact that the serotonergic system interconnection is an actual property of this system and the present results are not dependent on the served processing methods. This fact was proved even more clearly after obtaining as strong partial correlations between the mean voxel-wised BP values of the same receptor sub types.

The inhibitory receptors are negatively correlated, which means the inhibitory activity of the serotonergic system is balanced; i.e. when the density of one major inhibitory component is high, the other major inhibitory component would show lower densities.

The serotonergic system responds appropriately to relevant biological signals, but at the same time it functions to maintain the homeostasis in the system; i.e. modification of biological alterations in inputs, expression and firing rates. This is attained through the interaction of several homeostatic mechanisms which includes the inherent properties of the serotonin subsys-

tems (Best et al., 2010). Various neurotransmitter systems including the serotonergic system show adaptive characteristics. Multiple feed-back and feed-forward mechanisms have been explained inside this system and between serotonergic and other neurotransmitter systems.

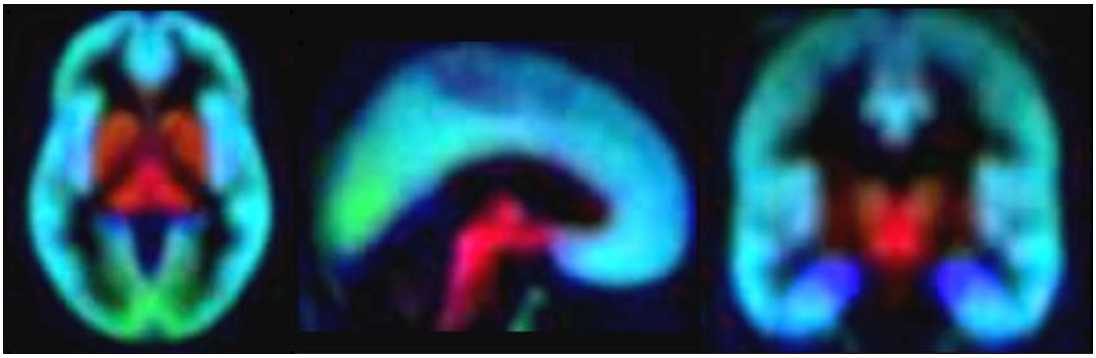

Figure 53: Triplanar sections of a computed RGB map of superimposed receptor and transporter quantities. Red indicates serotonin transporter dominance, blue 5-HT_{1A} dominance and green 5-HT_{2A} dominance, respectively.

This global cortical interrelationship between serotonergic functional subsystems might be a result of the modulation of the genetic expression of neuroreceptors during different stages of brain development (Beste et al., 2010). Furthermore, a variety of mechanisms regulating the expression of receptor and transporter proteins on the surface of serotonergic cell membranes might modulate this balanced relationship too (Chang et al., 2012; Zimmer et al., 2004). However, the variety of biological processes which underlie brain plasticity of the serotonergic neurons are not restricted to the early stages of neurodevelopment and the change continues through life (Azmitia et al., 1990; Azmitia and Whitaker-Azmitia, 1991).

To the best of my knowledge it is the first time that the integrated function which was hypothesized on the basis of *ex vivo* studies, could be observed *in vivo*. The higher order correlations of the serotonergic system throughout the entire brain provide direct *in vivo* evidence for a balanced serotonergic interconnectivity on a local level.

4.4 Limitations and outlook

Binding potentials acquired by PET, to a large extent depend on the specificity and sensitivity of the applied radioligands. Hence, the obtained quantities are an approximation to the actual receptor density values and are valid for the respective radioligand only and may vary when using another tracer for the same receptor subtype. Nonetheless, the relationship formulated here allows novel conclusions of PET data.

Another limitation of this study was the fact that it was impossible to determine the binding potentials of all the different receptor subtypes in the same subjects to avert the radiation exposure according to the permitted radiation dose limits in each of the subjects. In spite of this unavoidable constraint the subject groups (matched for sex and age) were carefully selected. The database, nonetheless, reflects the average receptor/transporter distribution of the healthy human brain.

Beyond further serotonergic receptor subtypes (Saulin et al., 2012), the approaches presented here are applicable to examine the distribution of other neurotransmitter systems, e.g. the dopaminergic and norepinephrenergic system including receptors, transporters and enzymes (e.g., MAOA, COMT) in case of suitable radioligands.

In conclusion, the database provides quantitative information considering the major inhibitory (5-HT_{1A}, 5-HT_{1B}) and excitatory (5-HT_{2A}) serotonin receptor subtypes and the 5-HT transporter in healthy subjects. This knowledge might improve our understanding of the alterations taking place in the serotonergic system during neuropsychiatric disorders. Moreover, the translation from *in vivo* to postmortem data computed in this study permits novel interpretations of PET binding potentials.

As the serotonergic system is a substantial target of various neuropsychoactive drugs, the findings of interconnections within the system may

have relevance for a better understanding of the mechanisms associated with antidepressant, antianxiety, antipsychotic, etc. of the developed serotonergic pharmaceuticals and might contribute to the introduction of more optimized drugs and treatment regimens. Future investigations about the impact of SSRIs, as the commonly used antidepressants and anxiolytics may shed light on some other aspects of this efficacious drug category.

5 References

2005. Radiopharmaceutical Preparations (Radiopharmaceutica, 5.0/0125). European Pharmacopoeia (Europäisches Arzneibuch). 5th Edition (5. Ausgabe Grundwerk), Official Austrian Version. Verlag Österreich GmbH, Vienna, pp. 823-831.

Abi-Dargham, A., 2007. Alterations of serotonin transmission in schizophrenia. Int Rev Neurobiol 78, 133-164.

Adams, K.H., Hansen, E.S., Pinborg, L.H., Hasselbalch, S.G., Svarer, C., Holm, S., Bolwig, T.G., Knudsen, G.M., 2005. Patients with obsessive-compulsive disorder have increased 5-HT2A receptor binding in the caudate nuclei. The international journal of neuropsychopharmacology / official scientific journal of the Collegium Internationale Neuropsychopharmacologicum 8, 391-401.

Adams, K.H., Pinborg, L.H., Svarer, C., Hasselbalch, S.G., Holm, S., Haugbol, S., Madsen, K., Frokjaer, V., Martiny, L., Paulson, O.B., Knudsen, G.M., 2004. A database of [(18)F]-altanserin binding to 5-HT(2A) receptors in normal volunteers: normative data and relationship to physiological and demographic variables. Neuroimage 21, 1105-1113.

Aghajanian, G.K., Marek, G.J., 2000. Serotonin model of schizophrenia: emerging role of glutamate mechanisms. Brain research. Brain research reviews 31, 302-312.

Akimova, E., Lanzenberger, R., Kasper, S., 2009. The serotonin-1A receptor in anxiety disorders. Biol Psychiatry 66, 627-635.

Anderson, I.M., Juhasz, G., Thomas, E., Downey, D., McKie, S., Deakin, J.F., Elliott, R., 2011. The effect of acute citalopram on face emotion processing in remitted depression: a pharmacoMRI study. European neuropsychopharmacology : the journal of the European College of Neuropsychopharmacology 21, 140-148.

Assem-Hilger, E., Lanzenberger, R., Savli, M., Wadsak, W., Mitterhauser, M., Mien, L.K., Stogmann, E., Baumgartner, C., Kletter, K., Asenbaum, S., 2010. Central serotonin 1A receptor binding in temporal lobe epilepsy: a [carbonyl-(11)C]WAY-100635 PET study. Epilepsy & behavior : E&B 19, 467-473.

Azmitia, E.C., 2010. Evolution of Serotonin: Sunlight to Suicide. In: Müller, C.P., Jakobs, B.L. (Eds.), Handbook of Behavioral Neurobiology of Serotonin. Elsevier, London, pp. 3-22.

Azmitia, E.C., Frankfurt, M., Davila, M., Whitaker-Azmitia, P.M., Zhou, F.C., 1990. Plasticity of fetal and adult CNS serotonergic neurons: role of growth-regulatory factors. Annals of the New York Academy of Sciences 600, 343-363; discussion 363-345.

Azmitia, E.C., Whitaker-Azmitia, P.M., 1991. Awakening the sleeping giant: anatomy and plasticity of the brain serotonergic system. The Journal of clinical psychiatry 52 Suppl, 4-16.

Bailer, U.F., Frank, G.K., Henry, S.E., Price, J.C., Meltzer, C.C., Weissfeld, L., Mathis, C.A., Drevets, W.C., Wagner, A., Hoge, J., Ziolko, S.K.,

McConaha, C.W., Kaye, W.H., 2005. Altered brain serotonin 5-HT1A receptor binding after recovery from anorexia nervosa measured by positron emission tomography and [carbonyl11C]WAY-100635. Arch Gen Psychiatry 62, 1032-1041.
Bailey, D.L., 2005. Data Acquisition and Performance Characteriszation in PET. In: Bailey, D.L., Townsend, D.W., Valk, P.E., Maisey, M.N. (Eds.), Positron Emission Tomography
Basic Sciences. Springer, London, pp. 41-62.
Bailey, D.L., Karp, J.S., Surti, S., 2005. Physics and Instrumentation in PET. In: Bailey, D.L., Townsend, D.W., Valk, P.E., Maisey, M.N. (Eds.), Positron Emission Tomography
Basic Sciences. Springer, London, pp. 13-39.
Bailey, D.L., Townsend, D.W., Valk, P.E., Maisey, M.N., 2003. Positron Emission Tomography, 1 ed. Springer.
Basu, S., Kwee, T.C., Surti, S., Akin, E.A., Yoo, D., Alavi, A., 2011. Fundamentals of PET and PET/CT imaging. Annals of the New York Academy of Sciences 1228, 1-18.
Benninghoff, J., Ven, A.V., Schloesser, R.J., Moessner, R., Moller, H.J., Rujescu, D., 2012. The complex role of the serotonin transporter in adult neurogenesis and neuroplasticity. A critical review. The world journal of biological psychiatry : the official journal of the World Federation of Societies of Biological Psychiatry 13, 240-247.
Best, J., Nijhout, H.F., Reed, M., 2010. Serotonin synthesis, release and reuptake in terminals: a mathematical model. Theoretical biology & medical modelling 7, 34.
Beste, C., Domschke, K., Falkenstein, M., Konrad, C., 2010. Differential modulations of response control processes by 5-HT1A gene variation. NeuroImage 50, 764-771.
Boschert, U., Amara, D.A., Segu, L., Hen, R., 1994. The mouse 5-hydroxytryptamine1B receptor is localized predominantly on axon terminals. Neuroscience 58, 167-182.
Bose, S.K., Mehta, M.A., Selvaraj, S., Howes, O.D., Hinz, R., Rabiner, E.A., Grasby, P.M., Turkheimer, F.E., Murthy, V., 2011. Presynaptic 5-HT1A is related to 5-HTT receptor density in the human brain. Neuropsychopharmacology : official publication of the American College of Neuropsychopharmacology 36, 2258-2265.
Bramley, J.R., Sollars, P.J., Pickard, G.E., Dudek, F.E., 2005. 5-HT1B receptor-mediated presynaptic inhibition of GABA release in the suprachiasmatic nucleus. J Neurophysiol 93, 3157-3164.
Briley, M., Chopin, P., Moret, C., 1990. Effect of serotonergic lesion on "anxious" behaviour measured in the elevated plus-maze test in the rat. Psychopharmacology 101, 187-189.
Cannon, D.M., Ichise, M., Fromm, S.J., Nugent, A.C., Rollis, D., Gandhi, S.K., Klaver, J.M., Charney, D.S., Manji, H.K., Drevets, W.C., 2006. Serotonin transporter binding in bipolar disorder assessed using [11C]DASB and positron emission tomography. Biol Psychiatry 60, 207-217.

Carey, R.J., DePalma, G., Damianopoulos, E., Shanahan, A., Muller, C.P., Huston, J.P., 2005. Evidence that the 5-HT1A autoreceptor is an important pharmacological target for the modulation of cocaine behavioral stimulant effects. Brain research 1034, 162-171.
Carson, R.E., Lang, L., Watabe, H., Der, M.G., Adams, H.R., Jagoda, E., Herscovitch, P., Eckelman, W.C., 2000. PET evaluation of [(18)F]FCWAY, an analog of the 5-HT(1A) receptor antagonist, WAY-100635. Nucl Med Biol 27, 493-497.
Chang, J.C., Tomlinson, I.D., Warnement, M.R., Ustione, A., Carneiro, A.M., Piston, D.W., Blakely, R.D., Rosenthal, S.J., 2012. Single molecule analysis of serotonin transporter regulation using antagonist-conjugated quantum dots reveals restricted, p38 MAPK-dependent mobilization underlying uptake activation. The Journal of neuroscience : the official journal of the Society for Neuroscience 32, 8919-8929.
Chee, I.S., Lee, S.W., Kim, J.L., Wang, S.K., Shin, Y.O., Shin, S.C., Lee, Y.H., Hwang, H.M., Lim, M.R., 2001. 5-HT2A receptor gene promoter polymorphism -1438A/G and bipolar disorder. Psychiatric genetics 11, 111-114.
Cherry, S.R., Dahlbom, M., Hoffman, E.J., 1991. 3d Pet Using a Conventional Multislice Tomograph without Septa. Journal of Computer Assisted Tomography 15, 655-668.
Cherry, S.R., Sorenson, J.A., Phelps, M.E., 2003. Physics in Nuclear Medicine, 3 ed. Elsevier, Philadelphia.
Chojnacka-Wojcik, E., 1992. Functional interaction between 5-HT1B and 5-HT1A or 5-HT2 receptors in mice. Polish journal of pharmacology and pharmacy 44, 251-260.
Clark, M.S., Neumaier, J.F., 2001. The 5-HT1B receptor: behavioral implications. Psychopharmacol Bull 35, 170-185.
Colsher, J.G., 1980. Fully 3-Dimensional Positron Emission Tomography. Physics in Medicine and Biology 25, 103-115.
Conti, M., 2011. Focus on time-of-flight PET: the benefits of improved time resolution. Eur J Nucl Med Mol Imaging 38, 1147-1157.
Cormack, A.M., 1973. Reconstruction of densities from their projections, with applications in radiological physics. Phys Med Biol 18, 195-207.
Daube-Witherspoon, M.E., Muehllehner, G., 1987. Treatment of Axial Data in 3-Dimensional Pet. Journal of Nuclear Medicine 28, 1717-1724.
Davis, L.L., Suris, A., Lambert, M.T., Heimberg, C., Petty, F., 1997. Post-traumatic stress disorder and serotonin: new directions for research and treatment. Journal of psychiatry & neuroscience : JPN 22, 318-326.
Defrise, M., 2001. A short reader's guide to 3D tomographic reconstruction. Computerized Medical Imaging and Graphics 25, 113-116.
Defrise, M., Kinahan, P., Michel, C., 2005. Image Reconstruction Algorithms in PET. In: Bailey, D.L., Townsend, D.W., Valk, P.E., Maisey, M.N. (Eds.), Positron Emission Tomography
Basic Sciences. Springer, London, pp. 63-90.

Defrise, M., Kinahan, P.E., Townsend, D.W., Michel, C., Sibomana, M., Newport, D.F., 1997. Exact and approximate rebinning algorithms for 3-D PET data. Ieee Transactions on Medical Imaging 16, 145-158.
Eickhoff, S.B., Schleicher, A., Scheperjans, F., Palomero-Gallagher, N., Zilles, K., 2007. Analysis of neurotransmitter receptor distribution patterns in the cerebral cortex. Neuroimage 34, 1317-1330.
Einstein, A., 1905. Is the inertia of a body dependent on its energy content? Annalen Der Physik 18, 639-641.
Eison, A.S., Mullins, U.L., 1996. Regulation of central 5-HT2A receptors: a review of in vivo studies. Behavioural brain research 73, 177-181.
Evans, A.K., Reinders, N., Ashford, K.A., Christie, I.N., Wakerley, J.B., Lowry, C.A., 2008. Evidence for serotonin synthesis-dependent regulation of in vitro neuronal firing rates in the midbrain raphe complex. European journal of pharmacology 590, 136-149.
Fahey, F.H., 2002. Data acquisition in PET imaging. J Nucl Med Technol 30, 39-49.
Farde, L., Ginovart, N., Ito, H., Lundkvist, C., Pike, V.W., McCarron, J.A., Halldin, C., 1997. PET-characterization of [carbonyl-11C]WAY-100635 binding to 5-HT1A receptors in the primate brain. Psychopharmacology (Berl) 133, 196-202.
Feldberg, W., Myers, R.D., 1964. Effects on Temperature of Amines Injected into the Cerebral Ventricles. A New Concept of Temperature Regulation. The Journal of physiology 173, 226-231.
Fink, K.B., Gothert, M., 2007. 5-HT receptor regulation of neurotransmitter release. Pharmacol Rev 59, 360-417.
Fink, M., Wadsak, W., Savli, M., Stein, P., Moser, U., Hahn, A., Mien, L.K., Kletter, K., Mitterhauser, M., Kasper, S., Lanzenberger, R., 2009. Lateralization of the serotonin-1A receptor distribution in language areas revealed by PET. Neuroimage 45, 598-605.
Fox, M.A., Stein, A.R., French, H.T., Murphy, D.L., 2010. Functional interactions between 5-HT2A and presynaptic 5-HT1A receptor-based responses in mice genetically deficient in the serotonin 5-HT transporter (SERT). British journal of pharmacology 159, 879-887.
Frankle, W.G., Slifstein, M., Talbot, P.S., Laruelle, M., 2005. Neuroreceptor imaging in psychiatry: theory and applications. Int Rev Neurobiol 67, 385-440.
Gallezot, J.D., Nabulsi, N., Neumeister, A., Planeta-Wilson, B., Williams, W.A., Singhal, T., Kim, S., Maguire, R.P., McCarthy, T., Frost, J.J., Huang, Y., Ding, Y.S., Carson, R.E., 2010. Kinetic modeling of the serotonin 5-HT(1B) receptor radioligand [(11)C]P943 in humans. J Cereb Blood Flow Metab 30, 196-210.
Gerstl, F., Windischberger, C., Mitterhauser, M., Wadsak, W., Holik, A., Kletter, K., Moser, E., Kasper, S., Lanzenberger, R., 2008. Multimodal imaging of human early visual cortex by combining functional and molecular measurements with fMRI and PET. Neuroimage 41, 204-211.

Ginovart, N., Wilson, A.A., Meyer, J.H., Hussey, D., Houle, S., 2001. Positron emission tomography quantification of [(11)C]-DASB binding to the human serotonin transporter: modeling strategies. J Cereb Blood Flow Metab 21, 1342-1353.
Gorzalka, B.B., Mendelson, S.D., Watson, N.V., 1990. Serotonin receptor subtypes and sexual behavior. Annals of the New York Academy of Sciences 600, 435-444; discussion 445-436.
Haeusler, D., Mien, L.K., Nics, L., Ungersboeck, J., Philippe, C., Lanzenberger, R.R., Kletter, K., Dudczak, R., Mitterhauser, M., Wadsak, W., 2009. Simple and rapid preparation of [(11)C]DASB with high quality and reliability for routine applications. Appl Radiat Isot 67, 1654-1660.
Hahn, A., Wadsak, W., Windischberger, C., Baldinger, P., Hoflich, A.S., Losak, J., Nics, L., Philippe, C., Kranz, G.S., Kraus, C., Mitterhauser, M., Karanikas, G., Kasper, S., Lanzenberger, R., 2012. Differential modulation of the default mode network via serotonin-1A receptors. Proceedings of the National Academy of Sciences of the United States of America 109, 2619-2624.
Hajos, M., Hoffmann, W.E., Tetko, I.V., Hyland, B., Sharp, T., Villa, A.E., 2001. Different tonic regulation of neuronal activity in the rat dorsal raphe and medial prefrontal cortex via 5-HT(1A) receptors. Neuroscience letters 304, 129-132.
Haleem, D.J., 1993. Serotonergic neurotransmission in the regulation of appetite: a receptor approach. Pakistan journal of pharmaceutical sciences 6, 89-96.
Hamacher, H., 1995. [Standardization of complex natural substances--official goals and their realization]. Pharm Unserer Zeit 24, 130-136.
Heiss, W.D., Herholz, K., 2006. Brain receptor imaging. J Nucl Med 47, 302-312.
Herold, C., Palomero-Gallagher, N., Gunturkun, O., Zilles, K., 2012. Serotonin 5-HT(1A) receptor binding sites in the brain of the pigeon (Columba livia). Neuroscience 200, 1-12.
Hornung, J.P., 2003. The human raphe nuclei and the serotonergic system. Journal of chemical neuroanatomy 26, 331-343.
Houle, S., Ginovart, N., Hussey, D., Meyer, J.H., Wilson, A.A., 2000a. Imaging the serotonin transporter with positron emission tomography: initial human studies with [11C]DAPP and [11C]DASB. European journal of nuclear medicine 27, 1719-1722.
Houle, S., Ginovart, N., Hussey, D., Meyer, J.H., Wilson, A.A., 2000b. Imaging the serotonin transporter with positron emission tomography: initial human studies with [11C]DAPP and [11C]DASB. European journal of nuclear medicine 27, 1719-1722.
Hounsfield, G.N., 1973. Computerized transverse axial scanning (tomography). 1. Description of system. Br J Radiol 46, 1016-1022.
Hounsfield, G.N., 1977. The E.M.I. scanner. Proc R Soc Lond B Biol Sci 195, 281-289.

Hounsfield, G.N., 1980. Computed medical imaging. Nobel lecture, Decemberr 8, 1979. J Comput Assist Tomogr 4, 665-674.
Hoyer, D., Hannon, J.P., Martin, G.R., 2002. Molecular, pharmacological and functional diversity of 5-HT receptors. Pharmacology, biochemistry, and behavior 71, 533-554.
Hoyer, D., Schoeffter, P., Waeber, C., Palacios, J.M., 1990. Serotonin 5-HT1D receptors. Annals of the New York Academy of Sciences 600, 168-181; discussion 181-162.
Hudson, H.M., Larkin, R.S., 1994. Accelerated image reconstruction using ordered subsets of projection data. IEEE Trans Med Imaging 13, 601-609.
Humm, J.L., Rosenfeld, A., Del Guerra, A., 2003. From PET detectors to PET scanners. Eur J Nucl Med Mol Imaging 30, 1574-1597.
Hurlemann, R., Boy, C., Meyer, P.T., Scherk, H., Wagner, M., Herzog, H., Coenen, H.H., Vogeley, K., Falkai, P., Zilles, K., Maier, W., Bauer, A., 2005. Decreased prefrontal 5-HT2A receptor binding in subjects at enhanced risk for schizophrenia. Anatomy and embryology 210, 519-523.
Hurlemann, R., Matusch, A., Kuhn, K.-U., Berning, J., Elmenhorst, D., Winz, O., Kolsch, H., Zilles, K., Wagner, M., Maier, W., Bauer, A., 2008. 5-HT2A receptor density is decreased in the at-risk mental state. Psychopharmacology 195, 579-590.
Ichise, M., Liow, J.S., Lu, J.Q., Takano, A., Model, K., Toyama, H., Suhara, T., Suzuki, K., Innis, R.B., Carson, R.E., 2003. Linearized reference tissue parametric imaging methods: application to [11C]DASB positron emission tomography studies of the serotonin transporter in human brain. J Cereb Blood Flow Metab 23, 1096-1112.
Ichise, M., Meyer, J.H., Yonekura, Y., 2001. An introduction to PET and SPECT neuroreceptor quantification models. J Nucl Med 42, 755-763.
Innis, R.B., Cunningham, V.J., Delforge, J., Fujita, M., Gjedde, A., Gunn, R.N., Holden, J., Houle, S., Huang, S.C., Ichise, M., Iida, H., Ito, H., Kimura, Y., Koeppe, R.A., Knudsen, G.M., Knuuti, J., Lammertsma, A.A., Laruelle, M., Logan, J., Maguire, R.P., Mintun, M.A., Morris, E.D., Parsey, R., Price, J.C., Slifstein, M., Sossi, V., Suhara, T., Votaw, J.R., Wong, D.F., Carson, R.E., 2007. Consensus nomenclature for in vivo imaging of reversibly binding radioligands. J Cereb Blood Flow Metab 27, 1533-1539.
Ito, H., Halldin, C., Farde, L., 1999. Localization of 5-HT1A receptors in the living human brain using [carbonyl-11C]WAY-100635: PET with anatomic standardization technique. J Nucl Med 40, 102-109.
Jacobs, B.L., 1991. Serotonin and behavior: emphasis on motor control. The Journal of clinical psychiatry 52 Suppl, 17-23.
Jewett, D.M., 1992. A simple synthesis of [11C]methyl triflate. Int J Rad Appl Instrum A 43, 1383-1385.
Johnson, C.A., Seidel, J., Carson, R.E., Gandler, W.R., Sofer, A., Green, M.V., DaubeWitherspoon, M.E., 1997. Evaluation of 3D

reconstruction algorithms for a small animal PET camera. Ieee Transactions on Nuclear Science 44, 1303-1308.
Jones, T., Rabiner, E.A., 2012. The development, past achievements, and future directions of brain PET. J Cereb Blood Flow Metab 32, 1426-1454.
Jouvet, M., 1967. Mechanisms of the states of sleep: a neuropharmacological approach. Research publications - Association for Research in Nervous and Mental Disease 45, 86-126.
Kalman, S., 2002. Introduction to PET Instrumentation. J Nucl Med Technol 30, 63; author reply 63.
Kimble, T., Chou, M., Chai, B.H.T., 2003. Scintillation properties of LYSO crystals. 2002 Ieee Nuclear Science Symposium, Conference Record, Vols 1-3, 1434-1437.
Kinahan, P.E., Michel, C., Defrise, M., Townsend, D.W., Sibomana, M., Lonneux, M., Newport, D.F., Luketich, J.D., 1997. Fast iterative image reconstruction of 3D PET data. 1996 Ieee Nuclear Science Symposium - Conference Record, Vols 1-3, 1918-1922.
Kinahan, P.E., Rogers, J.G., 1989. Analytic 3d Image-Reconstruction Using All Detected Events. Ieee Transactions on Nuclear Science 36, 964-968.
Kish, S.J., Furukawa, Y., Chang, L.-J., Tong, J., Ginovart, N., Wilson, A., Houle, S., Meyer, J.H., 2005. Regional distribution of serotonin transporter protein in postmortem human brain: Is the cerebellum a SERT-free brain region? Nuclear Medicine and Biology 32, 123-128.
Kranz, G.S., Kasper, S., Lanzenberger, R., 2010. Reward and the serotonergic system. Neuroscience 166, 1023-1035.
Kraus, C., Hahn, A., Savli, M., Kranz, G.S., Baldinger, P., Hoflich, A., Spindelegger, C., Ungersboeck, J., Haeusler, D., Mitterhauser, M., Windischberger, C., Wadsak, W., Kasper, S., Lanzenberger, R., 2012. Serotonin-1A receptor binding is positively associated with gray matter volume - A multimodal neuroimaging study combining PET and structural MRI. Neuroimage.
Lanzenberger, R., Mitterhauser, M., Kranz, G.S., Spindelegger, C., Wadsak, W., Stein, P., Moser, U., Savli, M., Kletter, K., Kasper, S., 2011. Progesterone level predicts serotonin-1a receptor binding in the male human brain. Neuroendocrinology 94, 84-88.
Lanzenberger, R., Wadsak, W., Spindelegger, C., Mitterhauser, M., Akimova, E., Mien, L.K., Fink, M., Moser, U., Savli, M., Kranz, G.S., Hahn, A., Kletter, K., Kasper, S., 2010. Cortisol plasma levels in social anxiety disorder patients correlate with serotonin-1A receptor binding in limbic brain regions. The international journal of neuropsychopharmacology / official scientific journal of the Collegium Internationale Neuropsychopharmacologicum 13, 1129-1143.
Lanzenberger, R.R., Mitterhauser, M., Spindelegger, C., Wadsak, W., Klein, N., Mien, L.K., Holik, A., Attarbaschi, T., Mossaheb, N., Sacher, J., Geiss-Granadia, T., Kletter, K., Kasper, S., Tauscher, J., 2007.

Reduced serotonin-1A receptor binding in social anxiety disorder. Biol Psychiatry 61, 1081-1089.
Laruelle, M., Slifstein, M., Huang, Y., 2003. Relationships between radiotracer properties and image quality in molecular imaging of the brain with positron emission tomography. Mol Imaging Biol 5, 363-375.
Lauder, J.M., Wallace, J.A., Wilkie, M.B., DiNome, A., Krebs, H., 1983. Roles for serotonin in neurogenesis. Monographs in neural sciences 9, 3-10.
Lecomte, R., 2009. Novel detector technology for clinical PET. Eur J Nucl Med Mol Imaging 36 Suppl 1, S69-85.
Lemaire, C., Cantineau, R., Guillaume, M., Plenevaux, A., Christiaens, L., 1991. Fluorine-18-altanserin: a radioligand for the study of serotonin receptors with PET: radiolabeling and in vivo biologic behavior in rats. Journal of nuclear medicine : official publication, Society of Nuclear Medicine 32, 2266-2272.
Lewellen, T.K., 2008. Recent developments in PET detector technology. Phys Med Biol 53, R287-317.
Lewitt, R.M., 1983. Reconstruction Algorithms - Transform Methods. Proceedings of the Ieee 71, 390-408.
Lokitz, S.J., Coleman, R.E., Yoshizumi, T.T., Toncheva, G.I., Daigle, L.T., Colsher, J.G., Turkington, T.G., 2006. CT Based Attenuation Correction for PET Brain Imaging. 2006 Ieee Nuclear Science Symposium Conference Record, Vol 1-6, 3320-3325.
Lundberg, J., Odano, I., Olsson, H., Halldin, C., Farde, L., 2005. Quantification of 11C-MADAM binding to the serotonin transporter in the human brain. J Nucl Med 46, 1505-1515.
Mann, J.J., 1999. Role of the serotonergic system in the pathogenesis of major depression and suicidal behavior. Neuropsychopharmacology : official publication of the American College of Neuropsychopharmacology 21, 99S-105S.
Manuck, S.B., Flory, J.D., McCaffery, J.M., Matthews, K.A., Mann, J.J., Muldoon, M.F., 1998. Aggression, impulsivity, and central nervous system serotonergic responsivity in a nonpatient sample. Neuropsychopharmacology : official publication of the American College of Neuropsychopharmacology 19, 287-299.
Martin, K.F., Hannon, S., Phillips, I., Heal, D.J., 1992. Opposing roles for 5-HT1B and 5-HT3 receptors in the control of 5-HT release in rat hippocampus in vivo. British journal of pharmacology 106, 139-142.
Matusch, A., Hurlemann, R., Rota Kops, E., Winz, O.H., Elmenhorst, D., Herzog, H., Zilles, K., Bauer, A., 2007. Acute S-ketamine application does not alter cerebral [18F]altanserin binding: a pilot PET study in humans. J Neural Transm 114, 1433-1442.
Maura, G., Raiteri, M., 1986. Cholinergic terminals in rat hippocampus possess 5-HT1B receptors mediating inhibition of acetylcholine release. European journal of pharmacology 129, 333-337.

Mayer, L.E., Walsh, B.T., 1998. The use of selective serotonin reuptake inhibitors in eating disorders. The Journal of clinical psychiatry 59 Suppl 15, 28-34.
McKie, S., Del-Ben, C., Elliott, R., Williams, S., del Vai, N., Anderson, I., Deakin, J.F., 2005. Neuronal effects of acute citalopram detected by pharmacoMRI. Psychopharmacology 180, 680-686.
Melke, J., Westberg, L., Nilsson, S., Landen, M., Soderstrom, H., Baghaei, F., Rosmond, R., Holm, G., Bjorntorp, P., Nilsson, L.G., Adolfsson, R., Eriksson, E., 2003. A polymorphism in the serotonin receptor 3A (HTR3A) gene and its association with harm avoidance in women. Arch Gen Psychiatry 60, 1017-1023.
Meltzer, C.C., Drevets, W.C., Price, J.C., Mathis, C.A., Lopresti, B., Greer, P.J., Villemagne, V.L., Holt, D., Mason, N.S., Houck, P.R., Reynolds, C.F., 3rd, DeKosky, S.T., 2001. Gender-specific aging effects on the serotonin 1A receptor. Brain Res 895, 9-17.
Meyer, J.H., Gunn, R.N., Myers, R., Grasby, P.M., 1999. Assessment of Spatial Normalization of PET Ligand Images Using Ligand-Specific Templates. Neuroimage 9, 545-553.
Michaelis, L., Menten, M.L., 1913. The kenetics of the inversion effect. Biochemische Zeitschrift 49, 333-369.
Milak, M.S., Severance, A.J., Ogden, R.T., Prabhakaran, J., Kumar, J.S., Majo, V.J., Mann, J.J., Parsey, R.V., 2008. Modeling considerations for 11C-CUMI-101, an agonist radiotracer for imaging serotonin 1A receptor in vivo with PET. J Nucl Med 49, 587-596.
Mintun, M.A., Raichle, M.E., Kilbourn, M.R., Wooten, G.F., Welch, M.J., 1984. A quantitative model for the in vivo assessment of drug binding sites with positron emission tomography. Ann Neurol 15, 217-227.
Miyazaki, K., Miyazaki, K.W., Doya, K., 2012. The Role of Serotonin in the Regulation of Patience and Impulsivity. Molecular neurobiology 45, 213-224.
Moser, U., Wadsak, W., Spindelegger, C., Mitterhauser, M., Mien, L.K., Bieglmayer, C., Kletter, K., Kasper, S., Lanzenberger, R., 2010. Hypothalamic serotonin-1A receptor binding measured by PET predicts the plasma level of dehydroepiandrosterone sulfate in healthy women. Neuroscience letters 476, 161-165.
Moses, W.W., 2007. Recent Advances and Future Advances in Time-of-Flight PET. Nucl Instrum Methods Phys Res A 580, 919-924.
Moses, W.W., Derenzo, S.E., 1999. Prospects for time-of-flight PET using LSO scintillator. Ieee Transactions on Nuclear Science 46, 474-478.
Muller, C.P., Carey, R.J., Huston, J.P., De Souza Silva, M.A., 2007. Serotonin and psychostimulant addiction: focus on 5-HT1A-receptors. Progress in neurobiology 81, 133-178.
Muramatsu, M., Lapiz, M.D., Tanaka, E., Grenhoff, J., 1998. Serotonin inhibits synaptic glutamate currents in rat nucleus accumbens neurons via presynaptic 5-HT1B receptors. The European journal of neuroscience 10, 2371-2379.

Murrough, J.W., Czermak, C., Henry, S., Nabulsi, N., Gallezot, J.D., Gueorguieva, R., Planeta-Wilson, B., Krystal, J.H., Neumaier, J.F., Huang, Y., Ding, Y.S., Carson, R.E., Neumeister, A., 2011a. The effect of early trauma exposure on serotonin type 1B receptor expression revealed by reduced selective radioligand binding. Arch Gen Psychiatry 68, 892-900.

Murrough, J.W., Huang, Y., Hu, J., Henry, S., Williams, W., Gallezot, J.D., Bailey, C.R., Krystal, J.H., Carson, R.E., Neumeister, A., 2011b. Reduced amygdala serotonin transporter binding in posttraumatic stress disorder. Biol Psychiatry 70, 1033-1038.

Nabulsi, N., Huang, Y., Weinzimmer, D., Ropchan, J., Frost, J.J., McCarthy, T., Carson, R.E., Ding, Y.S., 2010. High-resolution imaging of brain 5-HT 1B receptors in the rhesus monkey using [11C]P943. Nucl Med Biol 37, 205-214.

Nichols, D.E., Nichols, C.D., 2008. Serotonin receptors. Chem Rev 108, 1614-1641.

Olivier, B., van Oorschot, R., Waldinger, M.D., 1998. Serotonin, serotonergic receptors, selective serotonin reuptake inhibitors and sexual behaviour. International clinical psychopharmacology 13 Suppl 6, S9-14.

Ouchi, Y., Yoshikawa, E., Futatsubashi, M., Yagi, S., Ueki, T., Nakamura, K., 2009. Altered brain serotonin transporter and associated glucose metabolism in Alzheimer disease. Journal of nuclear medicine : official publication, Society of Nuclear Medicine 50, 1260-1266.

Palkovits, M., Brownstein, M., Saavedra, J.M., 1974. Serotonin content of the brain stem nuclei in the rat. Brain Res 80, 237-249.

Panconesi, A., 2008. Serotonin and migraine: a reconsideration of the central theory. The journal of headache and pain 9, 267-276.

Parsey, R.V., Arango, V., Olvet, D.M., Oquendo, M.A., Van Heertum, R.L., John Mann, J., 2005. Regional heterogeneity of 5-HT1A receptors in human cerebellum as assessed by positron emission tomography. J Cereb Blood Flow Metab 25, 785-793.

Parsey, R.V., Kent, J.M., Oquendo, M.A., Richards, M.C., Pratap, M., Cooper, T.B., Arango, V., Mann, J.J., 2006. Acute occupancy of brain serotonin transporter by sertraline as measured by [11C]DASB and positron emission tomography. Biol Psychiatry 59, 821-828.

Phelps, M.E., Hoffman, E.J., Mullani, N.A., Ter-Pogossian, M.M., 1975. Application of Annihilation Coincidence Detection to Transaxial Reconstruction Tomography. Journal of Nuclear Medicine 16, 210-224.

Pike, V.W., McCarron, J.A., Lammerstma, A.A., Hume, S.P., Poole, K., Grasby, P.M., Malizia, A., Cliffe, I.A., Fletcher, A., Bench, C.J., 1995. First delineation of 5-HT1A receptors in human brain with PET and [11C]WAY-100635. European journal of pharmacology 283, R1-3.

Pike, V.W., McCarron, J.A., Lammertsma, A.A., Osman, S., Hume, S.P., Sargent, P.A., Bench, C.J., Cliffe, I.A., Fletcher, A., Grasby, P.M., 1996. Exquisite delineation of 5-HT1A receptors in human brain with

PET and [carbonyl-11 C]WAY-100635. European journal of pharmacology 301, R5-7.
Pinborg, L.H., Adams, K.H., Svarer, C., Holm, S., Hasselbalch, S.G., Haugbol, S., Madsen, J., Knudsen, G.M., 2003. Quantification of 5-HT2A receptors in the human brain using [18F]altanserin-PET and the bolus/infusion approach. J Cereb Blood Flow Metab 23, 985-996.
Portas, C.M., Bjorvatn, B., Fagerland, S., Gronli, J., Mundal, V., Sorensen, E., Ursin, R., 1998. On-line detection of extracellular levels of serotonin in dorsal raphe nucleus and frontal cortex over the sleep/wake cycle in the freely moving rat. Neuroscience 83, 807-814.
Price, J.C., 2003. Principles of tracer kinetic analysis. Neuroimaging Clin N Am 13, 689-704.
Quist, J.F., Barr, C.L., Schachar, R., Roberts, W., Malone, M., Tannock, R., Basile, V.S., Beitchman, J., Kennedy, J.L., 2003. The serotonin 5-HT1B receptor gene and attention deficit hyperactivity disorder. Molecular psychiatry 8, 98-102.
Rabiner, E.A., Messa, C., Sargent, P.A., Husted-Kjaer, K., Montgomery, A., Lawrence, A.D., Bench, C.J., Gunn, R.N., Cowen, P., Grasby, P.M., 2002. A database of [(11)C]WAY-100635 binding to 5-HT(1A) receptors in normal male volunteers: normative data and relationship to methodological, demographic, physiological, and behavioral variables. Neuroimage 15, 620-632.
Radon, J., 1986. On the Determination of Functions from Their Integral Values along Certain Manifolds. IEEE Trans Med Imaging 5, 170-176.
Rapport, M.M., 1997. The discovery of serotonin. Perspectives in biology and medicine 40, 260-273.
Rapport, M.M., Green, A.A., Page, I.H., 1948. Serum vasoconstrictor, serotonin; isolation and characterization. The Journal of biological chemistry 176, 1243-1251.
Rohren, E.M., Turkington, T.G., Coleman, R.E., 2004. Clinical applications of PET in oncology. Radiology 231, 305-332.
Salmi, P., Ahlenius, S., 1998. Evidence for functional interactions between 5-HT1A and 5-HT2A receptors in rat thermoregulatory mechanisms. Pharmacology & toxicology 82, 122-127.
Sarhan, H., Cloez-Tayarani, I., Massot, O., Fillion, M.P., Fillion, G., 1999. 5-HT1B receptors modulate release of [3H]dopamine from rat striatal synaptosomes. Naunyn-Schmiedeberg's archives of pharmacology 359, 40-47.
Sari, Y., Miquel, M.C., Brisorgueil, M.J., Ruiz, G., Doucet, E., Hamon, M., Verge, D., 1999. Cellular and subcellular localization of 5-hydroxytryptamine1B receptors in the rat central nervous system: immunocytochemical, autoradiographic and lesion studies. Neuroscience 88, 899-915.
Saulin, A., Savli, M., Lanzenberger, R., 2012. Serotonin and molecular neuroimaging in humans using PET. Amino acids 42, 2039-2057.
Savli, M., Bauer, A., Mitterhauser, M., Ding, Y.S., Hahn, A., Kroll, T., Neumeister, A., Haeusler, D., Ungersboeck, J., Henry, S., Isfahani,

S.A., Rattay, F., Wadsak, W., Kasper, S., Lanzenberger, R., 2012. Normative database of the serotonergic system in healthy subjects using multi-tracer PET. Neuroimage.
Scheperjans, F., Palomero-Gallagher, N., Grefkes, C., Schleicher, A., Zilles, K., 2005. Transmitter receptors reveal segregation of cortical areas in the human superior parietal cortex: Relations to visual and somatosensory regions. Neuroimage 28, 362-379.
Sheard, M.H., 1969. The effect of p-chlorophenylalanine on behavior in rats: relation to brain serotonin and 5-hydroxyindoleacetic acid. Brain research 15, 524-528.
Shepp, L.A., Vardi, Y., 1982. Maximum likelihood reconstruction for emission tomography. IEEE Trans Med Imaging 1, 113-122.
Shiue, C.Y., Shiue, G.G., Mozley, P.D., Kung, M.P., Zhuang, Z.P., Kim, H.J., Kung, H.F., 1997. P-[18F]-MPPF: a potential radioligand for PET studies of 5-HT1A receptors in humans. Synapse 25, 147-154.
Slifstein, M., Laruelle, M., 2001. Models and methods for derivation of in vivo neuroreceptor parameters with PET and SPECT reversible radiotracers. Nucl Med Biol 28, 595-608.
Soubrie, P., 1986. [Serotonergic neurons and behavior]. Journal de pharmacologie 17, 107-112.
Spindelegger, C., Lanzenberger, R., Wadsak, W., Mien, L.K., Stein, P., Mitterhauser, M., Moser, U., Holik, A., Pezawas, L., Kletter, K., Kasper, S., 2009. Influence of escitalopram treatment on 5-HT 1A receptor binding in limbic regions in patients with anxiety disorders. Molecular psychiatry 14, 1040-1050.
Spindelegger, C., Stein, P., Wadsak, W., Fink, M., Mitterhauser, M., Moser, U., Savli, M., Mien, L.K., Akimova, E., Hahn, A., Willeit, M., Kletter, K., Kasper, S., Lanzenberger, R., 2011. Light-dependent alteration of serotonin-1A receptor binding in cortical and subcortical limbic regions in the human brain. The world journal of biological psychiatry : the official journal of the World Federation of Societies of Biological Psychiatry.
Staley, J.K., Malison, R.T., Innis, R.B., 1998. Imaging of the serotonergic system: interactions of neuroanatomical and functional abnormalities of depression. Biol Psychiatry 44, 534-549.
Stein, P., Savli, M., Wadsak, W., Mitterhauser, M., Fink, M., Spindelegger, C., Mien, L.-K., Moser, U., Dudczak, R., Kletter, K., Kasper, S., Lanzenberger, R., 2008. The serotonin-1A receptor distribution in healthy men and women measured by PET and [carbonyl - 11C]WAY-100635. European Journal of Nuclear Medicine and Molecular Imaging 35, 2159-2168.
Takano, H., Ito, H., Takahashi, H., Arakawa, R., Okumura, M., Kodaka, F., Otsuka, T., Kato, M., Suhara, T., 2010. Serotonergic neurotransmission in the living human brain: A positron emission tomography study using [(11)C]dasb and [(11)C]WAY100635 in young healthy men. Synapse 65, 624-633.

Talbot, P.S., Slifstein, M., Hwang, D.R., Huang, Y., Scher, E., Abi-Dargham, A., Laruelle, M., 2012. Extended characterisation of the serotonin 2A (5-HT2A) receptor-selective PET radiotracer 11C-MDL100907 in humans: quantitative analysis, test-retest reproducibility, and vulnerability to endogenous 5-HT tone. Neuroimage 59, 271-285.

Tanaka, E., North, R.A., 1993. Actions of 5-hydroxytryptamine on neurons of the rat cingulate cortex. J Neurophysiol 69, 1749-1757.

Tauscher, J., Verhoeff, N.P., Christensen, B.K., Hussey, D., Meyer, J.H., Kecojevic, A., Javanmard, M., Kasper, S., Kapur, S., 2001. Serotonin 5-HT1A receptor binding potential declines with age as measured by [11C]WAY-100635 and PET. Neuropsychopharmacology : official publication of the American College of Neuropsychopharmacology 24, 522-530.

Tenen, S.S., 1967. The effects of p-chlorophenylalanine, a serotonin depletor, on avoidance acquisition, pain sensitivity and related behavior in the rat. Psychopharmacologia 10, 204-219.

Ter-Pogossian, M.M., Phelps, M.E., Hoffman, E.J., Mullani, N.A., 1975. A Positron-Emission Transaxial Tomograph for Nuclear Imaging (PETT). Radiology 114, 89-98.

Townsend, D.W., 2008. Positron emission tomography/computed tomography. Semin Nucl Med 38, 152-166.

Turkington, T.G., 2001. Introduction to PET instrumentation. J Nucl Med Technol 29, 4-11.

Tzourio-Mazoyer, N., Landeau, B., Papathanassiou, D., Crivello, F., Etard, O., Delcroix, N., Mazoyer, B., Joliot, M., 2002. Automated anatomical labeling of activations in SPM using a macroscopic anatomical parcellation of the MNI MRI single-subject brain. Neuroimage 15, 273-289.

van der Wee, N.J., van Veen, J.F., Stevens, H., van Vliet, I.M., van Rijk, P.P., Westenberg, H.G., 2008. Increased serotonin and dopamine transporter binding in psychotropic medication-naive patients with generalized social anxiety disorder shown by 123I-beta-(4-iodophenyl)-tropane SPECT. Journal of nuclear medicine : official publication, Society of Nuclear Medicine 49, 757-763.

Varnäs, K., Halldin, C., Hall, H., 2004. Autoradiographic distribution of serotonin transporters and receptor subtypes in human brain. Human brain mapping 22, 246-260.

Varnäs, K., Nyberg, S., Halldin, C., Varrone, A., Takano, A., Karlsson, P., Andersson, J., McCarthy, D., Smith, M., Pierson, M.E., Soderstrom, J., Farde, L., 2011. Quantitative analysis of [11C]AZ10419369 binding to 5-HT1B receptors in human brain. J Cereb Blood Flow Metab 31, 113-123.

Wadsak, W., Mien, L., Ettinger, D., 2007. Simple and fully automated preparation of [carbonyl-11C]WAY-100635. Radiochimica Acta 95, 33-38.

Wahl, R.L., Buchnan, J.W., 2002. Principles and practice of positron emission tomography. Lippincott Williams & Wilkins, Philadelphia.

Walker, R.C., Purnell, G.L., Jones-Jackson, L.B., Thomas, K.L., Brito, J.A., Ferris, E.J., 2004. Introduction to PET imaging with emphasis on biomedical research. Neurotoxicology 25, 533-542.
Weissleder, R., Mahmood, U., 2001. Molecular imaging. Radiology 219, 316-333.
Wilson, A.A., Ginovart, N., Hussey, D., Meyer, J., Houle, S., 2002. In vitro and in vivo characterisation of [11C]-DASB: a probe for in vivo measurements of the serotonin transporter by positron emission tomography. Nucl Med Biol 29, 509-515.
Wilson, A.A., Ginovart, N., Schmidt, M., Meyer, J.H., Threlkeld, P.G., Houle, S., 2000. Novel radiotracers for imaging the serotonin transporter by positron emission tomography: synthesis, radiosynthesis, and in vitro and ex vivo evaluation of (11)C-labeled 2-(phenylthio)araalkylamines. J Med Chem 43, 3103-3110.
Windischberger, C., Lanzenberger, R., Holik, A., Spindelegger, C., Stein, P., Moser, U., Gerstl, F., Fink, M., Moser, E., Kasper, S., 2010. Area-specific modulation of neural activation comparing escitalopram and citalopram revealed by pharmaco-fMRI: A randomized cross-over study. Neuroimage 49, 1161-1170.
Winstanley, C.A., Theobald, D.E., Dalley, J.W., Robbins, T.W., 2005. Interactions between serotonin and dopamine in the control of impulsive choice in rats: therapeutic implications for impulse control disorders. Neuropsychopharmacology : official publication of the American College of Neuropsychopharmacology 30, 669-682.
Witte, A.V., Floel, A., Stein, P., Savli, M., Mien, L.K., Wadsak, W., Spindelegger, C., Moser, U., Fink, M., Hahn, A., Mitterhauser, M., Kletter, K., Kasper, S., Lanzenberger, R., 2009. Aggression is related to frontal serotonin-1A receptor distribution as revealed by PET in healthy subjects. Human brain mapping 30, 2558-2570.
Wohlschläger, A.M., Specht, K., Lie, C., Mohlberg, H., Wohlschläger, A., Bente, K., Pietrzyk, U., Stöcker, T., Zilles, K., Amunts, K., Fink, G.R., 2005. Linking retinotopic fMRI mapping and anatomical probability maps of human occipital areas V1 and V2. Neuroimage 26, 73-82.
Zilles, K., Amunts, K., 2010. Centenary of Brodmann's map--conception and fate. Nat Rev Neurosci 11, 139-145.
Zilles, K., Palomero-Gallagher, N., Grefkes, C., Scheperjans, F., Boy, C., Amunts, K., Schleicher, A., 2002. Architectonics of the human cerebral cortex and transmitter receptor fingerprints: reconciling functional neuroanatomy and neurochemistry. European Neuropsychopharmacology 12, 587-599.
Zimmer, L., Riad, M., Rbah, L., Belkacem-Kahlouli, A., Le Bars, D., Renaud, B., Descarries, L., 2004. Toward brain imaging of serotonin 5-HT1A autoreceptor internalization. Neuroimage 22, 1421-1426.

6 Curriculum Vitae

Personal details

Date of Birth	June 23rd, 1979
Place of Birth	Friesach, Austria
Citizenship	Austria
Marital Status	single

Education

2007 – present	Vienna University of Technology, PhD in technical sciences
2007 – present	Research Assistant, Functional, Molecular & Translational Neuroimaging Lab – PET & MRI, Medical University of Vienna
2005 – 2007	University of Vienna, Chinese Studies
2002 – 2005	Vienna University of Technology
2001 – 2002	Project Assistant, Alcatel Austria
1999 – 2002	Vienna University for Applied Sciences
1999	Military Service
1993 – 1998	Technical High School, TGM Wien

Awards

Best Poster Award	*Congress of the German Association for Psychiatry and Psychotherapy,* Berlin, Germany, 2011 November 23-26
Young Scientist Award	*WFSBP 2011*, 10th World Congress of Biological Psychiatry, Prag, Czech Republic, 29 May – 2 June 2011
Forschungspreis 2008	2nd place, *7. Drei-Länder-Symposium der Biologischen Psychiatrie,* October 9 – 11, 2008, Göttingen, Germany
Travel Award	*7. Drei-Länder-Symposium der Biologischen Psychiatrie*, October 9 – 11, 2008*,* Göttingen, Germany
OeFG Travel Awards	„*Österreichische Forschungsgemeinschaft*“ (2008, 2009, 2010, 2011, 2012)

Publications list

Papers

1. Serotonin-1A receptor binding is positively associated with gray matter volume - A multimodal neuroimaging study combining PET and structural MRI
   Kraus C, Hahn A, **Savli M**, Kranz GS, Baldinger P, Höflich A, Spindelegger C, Ungersboeck J, Haeusler D, Mitterhauser M, Windischberger C, Wadsak W, Kasper S, Lanzenberger R.
   NeuroImage *[2011, IF: 5.895]* Epub 2012 Jul 23.

2. Prediction of SSRI treatment response in major depression based on serotonin transporter interplay between median raphe nucleus and projection areas
   Lanzenberger R, Kranz GS, Haeusler D, Akimova E, **Savli M**, Hahn A, Mitterhauser M, Spindelegger C, Philippe C, Fink M, Wadsak W, Karanikas G, Kasper S.
   NeuroImage *[2011, IF: 5.895] 2012 Jul 22;63(2):874-881,* Epub 2012 Jul 22

3. Normative database of the serotonergic system in healthy subjects using multi-tracer PET
   Savli M, Bauer A, Häuseler D, Ding YS, Hahn A, Kroll T, Ungersböck J, Neumeister A, Henry S, Mitterhauser M, Wadsak W, Rattay F, Kasper S, Lanzenberger R
   NeuroImage *[2011, IF: 5.895] 2012 Oct 15;63(1):447-459,* Epub 2012 Jul 9

4. Challenges in the differentiation of midbrain raphe nuclei in neuroimaging research.
   Kranz G, Hahn A, **Savli M**, Lanzenberger R.
   Proceedings of the National Academy of Sciences USA (PNAS) *[2011, IF 9.681], Epub 2012 Jun 18*

5. Imaging Treatment Effects in Depression
   A Höflich, P Baldinger, **M Savli**, R Lanzenberger, S Kasper
   Reviews in the Neurosciences [2011, 2.413], *2012;23(3):227-52*

6. Hormonersatztherapie und deren Wirkung auf Psyche und Gehirn
   Baldinger P, Kranz G, Höflich A, **Savli M**, Stein P, Lanzenberger R, Kasper S.
   Nervenarzt *[2011, IF: 0.681]; Epub 2012 Feb 10*

7. Light-dependent alteration of serotonin-1A receptor binding in cortical and subcortical limbic regions in the human brain

C. Spindelegger, P. Stein, W. Wadsak, M. Fink, M. Mitterhauser, U. Moser, **M. Savli**, LK. Mien, E. Akimova, A. Hahn, M. Willeit, K. Kletter, S. Kasper, R. Lanzenberger
World Journal of Biological Psychiatry *[2010, IF: 2.385], Epub 2011 Nov 23*

8. Serotonin and molecular neuroimaging in humans using PET
Saulin A, **Savli M**, Kasper S, Lanzenberger R
Amino Acids *[2011, IF: 3.248], 2012 Jun; 42(6): 2039-57,* Epub 2011 Sep 24

9. Progesterone Level Predicts Serotonin-1A Receptor Binding in the Male Human Brain
Lanzenberger R, Mitterhauser M, Kranz GS, Spindelegger C, Wadsak W, Stein P, Moser U, **Savli M**, Kletter K, Kasper S.
Neuroendocrinology. [2011, IF: 2.37*6], 2011;94(1):84-8, Epub 2011 May 21*

10. Central 5-HT1A Receptor Binding in Temporal Lobe Epilepsy: A [11C]WAY100635 PET study
E Assem-Hilger, R Lanzenberger, **M Savli**, W Wadsak, M Mitterhauser, LK Mien, E Stögmann, C Baumgartner, K Kletter, S Asenbaum
Epilepsy & Behavior *[2012, IF: 2.335], 2010 Nov;19(3):467-73, Epub 2010 Sept 17*

11. Cortisol plasma levels in Social Anxiety Disorder patients correlate with serotonin-1A receptor binding in limbic brain regions
Lanzenberger R, Wadsak W, Spindelegger C, Mitterhauser M, Akimova E, Mien LK, Fink M, Moser U, **Savli M**, Kranz GS, Hahn A, Kletter K, Kasper S
The International Journal of Neuropsychopharmacology *[2011, IF: 4.578], 2010 Oct;13(9):1129-43, Epub 2010 Jun 2*

12. Regional sex differences in grey matter volume are associated with sex hormones in the young adult human brain
AV Witte, **M Savli**, A Holik, S Kasper, R Lanzenberger
NeuroImage *[2011, IF: 5. 895], 2010 Jan 15; (49):1205–1212, Epub 2009 Sep 28.*

13. Aggression is related to frontal serotonin-1A receptor distribution revealed by positron emission tomography
A.V. Witte, A. Flöel, P. Stein, **M. Savli**, LK. Mien, W. Wadsak, C. Spindelegger, U. Moser, M. Fink, A. Hahn, M. Mitterhauser, K. Kletter, S. Kasper, R. Lanzenberger
Human Brain Mapping *[2011, IF: 5.880], 2009 Aug;30(8):2558-70, Epub 2008 Dec 11.*

14. Lateralization of serotonin-1A receptor distribution in language areas is associated with sex
M. Fink, W. Wadsak, **M. Savli**, P. Stein, U. Moser, A. Hahn, LK. Mien, K. Kletter, M. Mitterhauser, S. Kasper, R. Lanzenberger
NeuroImage *[2011, IF: 5. 895], 2009 Apr 1;45(2):598-605. Epub 2008 Dec 9.*

15. The serotonin-1A receptor distribution in healthy men and women measured by PET
Stein P, **Savli M**, Wadsak W, Mitterhauser M, Fink M, Spindelegger C, Mien LK, Moser U, Kletter K, Kasper S, Lanzenberger R.
Eur J Nucl Med Mol Imaging *[2011, IF: 4.991], 2008 Dec;35(12):2159-68. Epub 2008 Jun 10.*

Educational Journals

1. Bildgebung in der Psychiatrie
Höflich A, Moser U, **Savli M**, Hahn A, Hofer-Irmler I, Kasper S, Lanzenberger R
Clinicum NeuroPsy 4/2010, 18-22

2. Tiefe Hirnstimulation bei Neuropsychiatrischen Erkrankungen: Status quo und Zukunftsperspektiven
Ulrike Moser, Rupert Lanzenberger, **Markus Savli**, Siegfried Kasper
Clinicum NeuroPsy 1/2011

3. Multimodale Bildgebung bei einer organischen depressiven Störung mittels fMRT und PET
M Fink, E Akomova, **M Savli**, R Lanzenberger, S Kasper
J Neuro Neurochir Psychiatr 2011 12(2) p180-182.

Abstracts and Conference Proceedings

1. Anatomical, functional and neurochemical parcellation tool "MULTIPARC" in molecular imaging.
Savli M, Fink M, Mitterhauser M, Stein P, Wadsak W, Spindelegger C, Mien LK, Dudczak R, Kletter K, Kasper S, Lanzenberger R.
Radioactive Isotopes in Clinical Medicine and Research, 28th International Symposium
January 9-12, 2008, Bad Hofgastein, Austria
Nuclear Medicine / Nuklearmedizin. 2007; 46(6): P22 (A170)

2. Multimodal imaging using PET and functional MRI reveals inverse relation between serotonin1A receptor binding and neural activation.
Lanzenberger R, Wadsak W, Stein P, Windischberger C, Mitterhauser

M, Spindelegger C, Mien LK, Fink M, **Savli M**, Dudczak R, Kasper S, Kletter K.
Radioactive Isotopes in Clinical Medicine and Research, 28th International Symposium
January 9-12, 2008, Bad Hofgastein, Austria
Nuclear Medicine / Nuklearmedizin. 2007; 46(6):40 (A162)

3. Lower hypothalamic serotonin-1A receptor binding potential in women revealed by PET and the radioligand [carbonyl-11C]WAY-100635.
Stein P, Spindelegger C, Mitterhauser M, Wadsak W, Moser U, Fink M, **Savli M**, Mien LK, Dudczak R, Kletter K, Kasper S, Lanzenberger R.
Radioactive Isotopes in Clinical Medicine and Research, 28th International Symposium
January 9-12, 2008, Bad Hofgastein, Austria
Nuclear Medicine / Nuklearmedizin. 2007; 46(6):P09 (A166)

4. Regional Relationships of Serotonin Transporter and Serotonin-1A Receptor in Human Brain revealed by PET
M. Savli, D. Haeusler, M. Fink, A. Hahn, C. Spindelegger, U. Moser, L.K. Mien, M. Mitterhauser, W. Wadsak, P. Stein, K. Kletter, S. Kasper, R. Lanzenberger
Neuroreceptor Mapping Conference 2008, July 17-19, 2008, Pittsburgh, USA
NeuroImage, Volume 41, Supplement 2 (2008), T166, P105

5. Serotonin Transporter Availability in Dorsal Raphe Nucleus Predicts Serotonin-1A Receptor Binding in Striatum – A multitracer PET study with [*carbonyl*-11C]WAY and [11C]DASB
R. Lanzenberger, W. Wadsak, **M. Savli**, M. Mitterhauser, M. Fink, LK Mien, A. Hahn, D. Haeusler, C. Spindelegger, U. Moser, P. Stein, K. Kletter, S. Kasper
Neuroreceptor Mapping Conference 2008, July 17-19, 2008, Pittsburgh, USA
NeuroImage, Volume 41, Supplement 2 (2008), T166, P096

6. Absence of Sex Differences in the Serotonin-1A Receptor Binding in Healthy Women and Men Measured by PET
P. Stein, M. Fink, A. Hahn, C. Spindelegger, M. Mitterhauser, W. Wadsak, U. Moser, **M. Savli**, L.K. Mien, R. Lanzenberger, K. Kletter, S. Kasper
Neuroreceptor Mapping Conference 2008, July 17-19, 2008, Pittsburgh, USA
NeuroImage, Volume 41, Supplement 2 (2008), T166, P108

7. Coexpression of Serotonin Transporter and Serotonin-1A Receptor in Human Brain: A multitracer PET study
M. Savli, D. Haeusler, A. Holik, M. Fink, A. Hahn, M. Mitterhauser, W.

Wadsak, K. Kletter, S. Kasper, R. Lanzenberger
21st ECNP Congress, 30 August- 3 September 2008, Barcelona, Spain
European Neuropsychopharmacology, Volume 18, Supplement 4, August 08, Page S259

8. Lateralization of serotonin-1A receptor distribution in language areas revealed by positron emission tomography
M. Fink, **M. Savli**, P. Stein, A. Hahn, C. Spindelegger, M. Mitterhauser, W. Wadsak, K. Kletter, S. Kasper, R. Lanzenberger
21st ECNP Congress, 30 August- 3 September 2008, Barcelona, Spain
European Neuropsychopharmacology, Volume 18, Supplement 4, August 08, Page S266

9. Frontal serotonin-1A receptor distribution is associated with aggression scores in healthy subjects: A positron emission tomography (PET) study with the selective radioligand [11C]WAY100635
A.V. Witte, A. Flöel, P. Stein, **M. Savli**, A. Hahn, M. Fink, M. Mitterhauser, W. Wadsak, S. Kasper, R. Lanzenberger
21st ECNP Congress, 30 August- 3 September 2008, Barcelona, Spain
European Neuropsychopharmacology, Volume 18, Supplement 4, August 08, Page S267-268

10. No Association between Serotonin Transporter and Serotonin-1A Receptor Binding in Limbic Areas revealed by PET
M. Savli, D. Haeusler, A. Holik, M. Fink, A. Hahn, M. Mitterhauser, W. Wadsak, K. Kletter, S. Kasper, R. Lanzenberger
7. Drei-Länder-Symposium der Biologischen Psychiatrie, October 9 – 11, 2008, Göttingen, Germany
Europ. Archives of Psychiatry and Clinical Neuroscience, Vol 258, Suppl 4, Oct 08, P17, P-02-024

11. Okkupanz des zerebralen Serotonintransporters bei Therapie mit selektiven Serotonin-Wiederaufnahmehemmern
Lanzenberger R, Haeusler D, Akimova E, Mien LK, **Savli M**, Fink M, Hahn A, Wadsak W, Mitterhauser W, Dudczak R, Kletter K, Kasper S.
7. Jahrestagung der Österr. Gesellschaft für Nuklearmedizin, 22.-24.1.2009, Salzburg, Austria
7. Annual Congress of the Austrian Society of Nuclear Medicine (OGN) in St. Virgil, Austria
Nuclear Medicine / Nuklearmedizin 2008/6: 152.

12. Serotonin-1A Receptor Binding Potential in Dorsal Raphe Nuclei Predicts Orbitofrontal Reactivity in Healthy Subjects
Hahn A, **Savli M**, Stein P, Mien LK, Holik A, Mitterhauser M, Windischberger C, Wadsak W, Lanzenberger R, Kasper S
ECNP Workshop on Neuropsychopharmacology for Young Scientists in Europe; 5 – 8 March 2009, Nice, France

13. The Increase in Serotonin Transporter Occupancy from single to multiple dosing is associated with treatment outcome in Major Depressive Disorder.
Akimova E, **Savli M**, Häusler D, Moser U, Fink M, Hahn A, Wadsak W, Mitterhauser M, Lanzenberger R, Kletter K, Kasper S.
9th World Congress of Biological Psychiatry (WFSBP), 28 June - 2 July 2009, Paris, France
The World Journal of Biological Psychiatry, Volume 10, Supplement 1 (2009), P218, P-02-004

14. Imaging serotonin-1A receptor asymmetry in language areas using [carbonyl-11C]WAY-100635 and positron emission tomography.
Fink M, **Savli M**, Stein P, Moser U, Hahn A, Spindelegger C, Mien LK, Mitterhauser M, Wadsak W, Kletter K, Kasper S, Lanzenberger R.
9th World Congress of Biological Psychiatry (WFSBP), 28 June - 2 July 2009, Paris, France
The World Journal of Biological Psychiatry, Volume 10, Supplement 1 (2009), P362, P-37-011

15. Amygdala Hyperactivity in Social Anxiety Disorder Induced by Facial Attractiveness.
Hahn A, Holik A, Gerstl F, **Savli M**, Stein P, Fink M, Angleitner P, Windischberger C, Lanzenberger R, Kasper S.
9th World Congress of Biological Psychiatry (WFSBP), 28 June - 2 July 2009, Paris, France
The World Journal of Biological Psychiatry, Volume 10, Supplement 1 (2009), P106, YS-01-001

16. Age-related Change of Serotonin Transporter Binding in Major Depressive Disorder
M Savli, E Akimova, D Häusler, U Moser, M Fink, A Hahn, M Mitterhauser, W Wadsak, R Lanzenberger, S Kasper
15th Annual Meeting of the Organization for Human Brain Mapping (HBM), 18-23 June 2009, San Francisco, California, USA
NeuroImage, Volume 47, Supplement 1 (2009), S49, P215 F-AM

17. Serotonin-1A receptor binding and Reward-dependent Activation are associated within the Human Dorsal Raphe Nucleus as revealed by PET-fMRI
R. Lanzenberger, A. Hahn, C. Windischberger, W. Wadsak, A. Holik, F. Gerstl, **M. Savli**, U.Moser, L.K. Mien, E. Akimova, M. Mitterhauser, K. Kletter, E. Moser, S. Kasper
15th Annual Meeting of the Organization for Human Brain Mapping (HBM), 18-23 June 2009, San Francisco, California, USA
NeuroImage, Volume 47, Supplement 1 (2009), S176, P638 SU-PM

18. Anxiety Scores are Related to Amygdala Activity Induced by Facial Attractiveness and Emotional Expressions
A Hahn, A Holik, F Gerstl, **M Savli**, P Stein, E Akimova, P Angleitner, C Windischberger, S Kasper, R Lanzenberger
15th Annual Meeting of the Organization for Human Brain Mapping (HBM), 18-23 June 2009, San Francisco, California, USA
NeuroImage, Volume 47, Supplement 1, (2009), S48, P191 F-AM

19. Reduced serotonin transporter availability in patients with major depression
M Savli, E Akimova, D Häusler, M Fink, A Hahn, U Moser, M Mitterhauser, W Wadsak, R Lanzenberger, S Kasper
5th PhD-Symposium, 17-19 June 2009, Medical University of Vienna, Austria

20. Effect of escitalopram treatment on the relationship of pre- to postsynaptic serotonin-1A receptors in anxiety disorders
Hahn A, Lanzenberger R, Fink M, Stein P, Mien LK, **Savli M**, Akimova E, Mitterhauser M, Wadsak W, Kasper S
22nd European College of Neuropsychopharmacology (ECNP) Congress, 12th – 16th September 2009, Istanbul, Turkey
European Neuropsychopharmacology, Vol 19, Suppl. 3, Sept. 2009, S607

21. Imaging gender differences in serotonin-1A receptor lateralization in language areas of healthy subjects using PET
Fink M, Lanzenberger R, **Savli M**, Spindelegger C, Moser U, Mitterhauser M, Wadsak W, Stein P, Hahn A, Kletter K, Kasper S
22nd European College of Neuropsychopharmacology (ECNP) Congress, 12th – 16th September 2009, Istanbul, Turkey
European Neuropsychopharmacology, Vol 19, Suppl. 3, Sept. 2009, S311

22. Elevation of Serotonin Transporter Occupancy during escitalopram or citalopram treatment correlates with positive clinical outcome in Major Depressive Disorder
E Akimova, **M Savli**, D Häusler, U Moser, M Fink, C Spindelegger, A Hahn, W Wadsak, M Mitterhauser, R Lanzenberger, K Kletter, S Kasper
22nd European College of Neuropsychopharmacology (ECNP) Congress, 12th – 16th September 2009, Istanbul, Turkey
European Neuropsychopharmacology, Vol 19, Suppl. 3, Sept. 2009, S424

23. Serotonin-1A receptor binding potential in dorsal raphe nuclei predicts orbitofrontal reactivity in healthy subjects
Hahn A, **Savli M**, Stein P, Mien LK, Holik A, Mitterhauser M, Windisch-

berger C, Wadsak W, Lanzenberger R, Kasper S
22nd European College of Neuropsychopharmacology (ECNP) Congress, 12th – 16th September 2009, Istanbul, Turkey
European Neuropsychopharmacology, Vol 19, Suppl. 3, Sept. 2009, S182

24. Enhanced association of pre- to postsynaptic serotonin-1A receptors through escitalopram treatment in anxiety disorder patients
Hahn A, Lanzenberger R, Spindelegger C, Stein P, Mien LK, **Savli M**, Akimova E, Mitterhauser M, Wadsak W, Kasper S
26th AGNP Symposium (Arbeitsgemeinschaft für Neuropsychopharmakologie und Pharmakopsychiatrie), 7th - 10th October 2009, Munich, Germany

25. [11C]WAY-100635 and [18F]FDG PET in temporal lobe epilepsy
S. Asenbaum, E. Assem-Hilger, **M. Savli**, M. Hoffmann, K. Mien, M. Mitterhauser, W. Wadsak, R. Lanzenberger
22nd Annual European Association of Nuclear Medicine (EANM) Congress, 10-14 October 2009, Barcelona, Spain.
Eur J Nucl Med Mol Imaging (2009) 36 (Suppl 2):S158 –S193, OP175

26. Preoperative Evaluation of Temporal Lobe Epilepsy using [11C]WAY-100635 and [18F]FDG PET
S. Asenbaum, E. Assem-Hilger, **M. Savli**, M. Hoffmann, L. Mien, M. Mitterhauser, W. Wadsak, K. Kletter, R. Dudczak, R. Lanzenberger
Radioactive Isotopes in Clinical Medicine and Research, 29th International Symposium
January 16-19, 2010, Bad Hofgastein, Austria
Nuclear Medicine / Nuklearmedizin 2009: 48(6): P31 (A153)

27. Seasonal alterations of serotonin-1A receptor binding in the healthy human brain
C. Spindelegger, P. Stein, W. Wadsak, M. Fink, M. Mitterhauser, U. Moser, **M. Savli**, LK. Mien,
E. Akimova, A. Hahn, M. Willeit, K. Kletter, S. Kasper, R. Lanzenberger
18th EPA European Congress of Psychiatry, Munich, Germany, Feb 27 - March 2, 2010.

28. Serotonin Transporter Availability in Raphe Nuclei quantified with PET predicts Treatment Response to S-Citalopram in Major Depressive Disorder
Akimova E, Lanzenberger R, **Savli M**, Häusler D, Wadsak W, Spindelegger C, Moser U, Fink M, Mitterhauser M, Kletter K, Kasper S
ECNP Workshop on Neuropsychopharmacology for Young Scientists in Europe, 4 – 10 March 2010, Nice, France

29. Segmentation of [carbonyl-11C]WAY-100635 PET Brain Images using

Linear Discriminant Analysis
A Hahn, **M Savli**, C Spindelegger, LK Mien, W Wadsak, M Mitterhauser, G Kranz, C Windischberger, S Kasper, R Lanzenberger
16th Annual Meeting of the Organization for Human Brain Mapping, 6-10 June 2010, Barcelona, Spain

30. Serotonin-1A, -2A Receptors and Transporter Distribution in Brodmann Areas – Multitracer PET study
M Savli, A Bauer, D Häusler, A Hahn, M Fink, LK Mien, F Rattay, M Mitterhauser, W Wadsak, S Kasper, R Lanzenberger
16th Annual Meeting of the Organization for Human Brain Mapping, 6-10 June 2010, Barcelona, Spain

31. Serotonin transporter occupancy in single and multiple dosing of S-citalopram
M Savli, R Lanzenberger, D Häusler, M Fink, C Spindelegger, U Moser, M Mitterhauser, E Akimova, W Wadsak, LK Mien, S Kasper
XXVII Congress of the CINP, 6-10 June 2010, Hongkong, China
The International Journal of Neuropsychopharmacology, June 2010, Vol 13, Suppl S1, P-14-027

32. Serotonin Transporter Availability predicts clinical outcome in patients with Major Depressive Disorder. [11C] DASB PET Study
E Akimova, R Lanzenberger, **M Savli**, D Häusler, M Fink, C Spindelegger, U Moser, M Mitterhauser, W Wadsak, LK Mien, S Kasper
XXVII Congress of the CINP, 6-10 June 2010, Hongkong, China
The International Journal of Neuropsychopharmacology, June 2010, Vol 13, Suppl S1, P-03-001

33. Multitracer PET Imaging of the Serotonin Transporter, Serotonin-1A and -2A Receptor Distribution in the Living Human Brain
Savli M., Bauer A., Häusler D., Kroll T., Hahn A., Rattay F., Mitterhauser M., Wadsak W., Kasper S., R. Lanzenberger
8th International Symposium on Functional Neuroreceptor Mapping of the Living Brain (NRM), 22-24 July 2010, Glasgow, Scotland, UK
NeuroImage, Volume 52, Supplement 1, Aug 2010, S73-74, P017

34. Segmentation of [^{11}C]DASB and [*carbonyl*-^{11}C]WAY-100635 PET brain images using linear discriminant analysis
A. Hahn, **M. Savli**, C. Spindelegger, D. Häusler, W. Wadsak, M. Mitterhauser, S. Kasper, R. Lanzenberger
8th International Symposium on Functional Neuroreceptor Mapping of the Living Brain (NRM), 22-24 July 2010, Glasgow, Scotland, UK
NeuroImage, Volume 52, Supplement 1, Aug 2010, S155-56, P086

35. Serotonin Transporter Occupancy in Median Raphe Nucleus quantified with PET predicts treatment response to S-Citalopram in Major

Depressive Disorder
Akimova E, Lanzenberger R, **Savli M**, Häusler D, Wadsak W, Spindelegger C, Moser U, Fink M, Mitterhauser M, Kletter K, Kasper S
23nd European College of Neuropsychopharmacology (ECNP) Congress, 12th – 16th September 2009, Amsterdam, The Netherlands European Neuropsychopharmacology, Vol 20, Suppl. 3, Sept. 2010, S389

36. Multitracer PET Imaging of the Serotonergic System
Savli M, Bauer A, Häusler D, Kroll T, Hahn A, Kranz GS, Rattay F, Mitterhauser M, Wadsak W, Kasper S, Lanzenberger R.
10th International Forum on Mood and Anxiety Disorder (IFMAD), Nov 17-19, 2010, Vienna, Austria

37. Multimodal Imaging of an Astrocytoma affecting the Amygdalar Region.
Fink M, Moser U, Pezawas L, **Savli M**, Stein P, Hahn A, Spindelegger C, Wadsak W, Windischberger C, Mitterhauser M, Kasper S, Lanzenberger R.
19th European Congress of Psychiatry (EPA), March 12-15, 2011, Vienna, Austria

38. Database of MNI Stereotactic Coordinates for Deep Brain stimulation targets in Neuropsychiatric Disorders
Moser U, **Savli M**, Lanzenberger R, Kasper S.
19th European Congress of Psychiatry (EPA), March 12-15, 2011, Vienna, Austria

39. Attenuated Serotonin Transporter Association between Midbrain and Nucleus Acccumbens in Major Depression.
Hahn A, Akimova E, Häusler D, Philippe C, **Savli M**, Baldinger P, Höflich A, Zgud S, Mitterhauser M, Wadsak W, Lanzenberger R, Kasper S.
19th European Congress of Psychiatry (EPA), March 12-15, 2011, Vienna, Austria

40. In vivo molecular imaging reveals distinct distributions of the serotonin transporter, the major inhibitory and excitatory serotonin receptors.
Savli M, Bauer A, Häusler D, Kroll T, Hahn A, Kranz GS, Rattay F, Mitterhauser M, Wadsak W, Kasper S, Lanzenberger R.
19th European Congress of Psychiatry (EPA), March 12-15, 2011, Vienna, Austria

41. Serotonin-1A receptor distribution in the subgenual anterior cingulate cortex is associated with regional grey matter volume in the striatum and temporal areas.
Kraus C, **Savli M**, Hahn A, Baldinger P, Höflich A, Mitterhauser M, Windischberger C, Wadsak W, Kasper S, Lanzenberger R.
19th European Congress of Psychiatry (EPA), March 12-15, 2011, Vi-

enna, Austria

42. Are there structural brain changes following 10 days of SSRI administration investigated by voxel-based morphometry?
Baldinger P, **Savli M**, Kranz G, Höflich A, Kraus C, Windischberger C, Kasper S, Lanzenberger R
19th European Congress of Psychiatry (EPA), March 12-15, 2011, Vienna, Austria

43. Prediction of steady-state occupancy of the serotonin transporter based on single-dose ccupancy: A [11C]DASB PET study.
Höflich A, Philippe C, **Savli M**, Baldinger P, Kranz GS, Müller S, Häusler D, Zgud S, Kraus C, Wadsak W, Mitterhauser M, Lanzenberger R, Kasper S.
19th European Congress of Psychiatry (EPA), March 12-15, 2011, Vienna, Austria

44. Area-specific occupancy of the serotonin transporter by Escitalopram and Citalopram in MDD
Akimova E, Lanzenberger R, **Savli M**, Häusler D, Wadsak W, Spindelegger C, Moser U, Fink M, Mitterhauser M, Kasper S.
19th European Congress of Psychiatry (EPA), March 12-15, 2011, Vienna, Austria

45. The Impact of Software Motion Correction on PET Drug Occupancy Studies.
Savli M, Hahn A, Häusler D, Philippe C, Baldinger P, Höflich A, Kraus C, Kranz GS, Zgud S, Akimova E, Wadsak W, Mitterhauser M, Lanzenberger R, Dudczak R, Kasper S.
10th International Conference on Quantification of Brain Function with PET, May 24-28, 2011, Barcelona, Spain

46. Imaging of an Astrocytoma affecting the Amygdala Region – A Multimodal Approach
Fink M, Moser U, Pezawas L, **Savli M**, Stein P, Hahn A, Spindelegger C, Wadsak W, Windischberger C, Mitterhauser M, Kasper S, Lanzenberger R.
10th World Congress of Biolog. Psychiatry (*WFSBP), 29 May – 02 June 2011, Prague, Czech Republic*

47. Can the Median Raphe Nucleus predict Clinical Outcome in Patients with Major Depression? A [11C]DASB PET study
Savli M, Hahn A, Häusler D, Baldinger P, Höflich A, Kraus C, Wadsak W, Mitterhauser M, Lanzenberger R, Dudczak R, Kasper S.
10th World Congress of Biolog. Psychiatry (*WFSBP), 29 May – 02 June 2011, Prague, Czech Republic*

48. Reduced Serotonin Transporter Association between Raphe Region and Ventral Striatum in Major Depressive Disorder
A Hahn, R Lanzenberger, D Häusler, C Philippe, **M Savli**, P Baldinger, A Höflich, C Kraus, E Akimova, M Mitterhauser, W Wadsak, S Kasper
10th World Congress of Biolog. Psychiatry (*WFSBP), 29 May – 02 June 2011, Prague, Czech Republic*

49. Inhibitory serotonergic neurotransmission correlates positively with cortical grey matter volume as revealed by PET and MRI
Kraus C, Hahn A, **Savli M**, Höflich A, Baldinger P, Kranz GS, Zgud S, Losak J, Mitterhauser M, Wadsak W, Windischberger C, Kasper S, Lanzenberger R.
10th World Congress of Biolog. Psychiatry (*WFSBP), 29 May – 02 June 2011, Prague, Czech Republic*

50. Molecular Imaging of the Serotonergic System – Serotonin, an important Effector in modulating Emotions
C Kraus, **M Savli**, A Hahn, A Höflich, P Baldinger, M Mitterhauser, W Wadsak, S Kasper, R Lanzenberger
12th International Neuropsychoanalysis Congress, June 24-26 2011, Berlin, Germany

51. A positive Correlation Between Inhibitory Serotonergic Neurotransmission and Grey Matter Volume
Kraus C, Hahn A, **Savli M**, Mitterhauser M, Wadsak W, Windischberger C, Kasper S, Lanzenberger R.
7th PhD Symposium, 15-16th June 2011, Vienna Austria

52. Serotonin-A receptor binding in the dorsal raphe nucleus is associated with hippocampal grey matter volume.
Kraus C, Hahn A, **Savli M**, Höflich A, Baldinger P, Kranz GS, Mitterhauser M, Wadsak W, Kasper S, Lanzenberger R.
24th European College of Neuropsychopharmacology (ECNP) Congress, 3-7 September 2011, Paris, France

53. Rapid gray matter density changes after selective serotonin reuptake inhibitor administration revealed by voxel-based-morphometry.
Savli M, Baldinger P, Kranz GS, Höflich A, Kraus C, Losak J, Windischberger C, Kasper S, Lanzenberger R.
24th European College of Neuropsychopharmacology (ECNP) Congress, 3-7 September 2011, Paris, France

54. The Impact of Median Raphe Nucleus Serotonin Transporter Binding on Depression: A [11C]DASB PET study
Savli M, Hahn A, Häusler D, Baldinger P, Höflich A, Kraus C, Wadsak W, Mitterhauser M, Lanzenberger R, Dudczak R, Kasper S.
International Society for Neuroimaging in Psychiatry (ISNIP), 7-10 Sep-

tember 2011, Heidelberg

55. The serotonin-1A, -2A receptor and transporter distribution in the living human brain: a multitracer PET study.
    Savli M, Bauer A, Häusler D, Kroll T, Hahn A, Rattay F, Mitterhauser M, Wadsak W, Kasper S, Lanzenberger R.
    The 15th World Congress of Psychiatry (WPA), Buenos Aires, 18-22 September, 2011

56. Multimodal neuroimaging detects serotonin-1A receptor mediated neuroplasticity in humans.
    Kraus C, Hahn A, **Savli M**, Baldinger P, Höflich A, Kranz GS, Losak J, Mitterhauser M, Wadsak W, Windischberger C, Kasper S, Lanzenberger R.
    24th IGB Workshop, Regulation of Neural Gene Expression from Development to Disease, 16-19 October 2011 Capri, Italy

57. Lower Median Raphe Serotonin Transporter Availability indicate superior treatment outcome in Depression:A [11C]DASB PET study
    Savli M, Hahn A, Häusler D, Baldinger P, Höflich A, Kraus C, Wadsak W, Mitterhauser M, Dudczak R, Kasper S, Lanzenberger R
    Congress of the German Association for Psychiatry and Psychotherapy (DGPPN), Berlin, Germany, 2011 November 23-26

58. Molecular neuroimaging biomarkers to predict antidepressant treatment response in major depressive disorder
    Lanzenberger R, Kranz GS, **Savli M**, Hahn A, Mitterhauser M, Spindelegger C, Wadsak W, Kasper S
    Australasian cognitive neuroscience conference, 21st Meeting of the Australasian Society for Psychophysiology, 9 – 12 Dec 2011, Sydney, Australia.

59. [^{18}F]FE@SUPPY – Final countdown?
    Haeusler D, Kuntner C, **Savli M**, Hoerleinsberger WJ, Nics L, Zeilinger M, Lanzenberger R, Langer O, Shanab K, Spreitzer H, Dudczak R, Wadsak W, Mitterhauser M.
    Radioactive Isotopes in Clinical Medicine and Research; 11 –14 January 2012, Bad Hofgastein, Austria

60. Serotonin-1A Receptor related Morphogenic Signaling is Associated with Regional Brain Volumes and Network Neuroplasticity
    C Kraus, **M Savli**, A Hahn, P Baldinger, A Höflich, M Mitterhauser, C Windischberger, W Wadsak, S Kasper, R Lanzenberger
    20th EPA European Congress of Psychiatry, Prague, 3-6 March 2012

61. Multimodal neuroimaging with PET and MRI to investigate the relation between serotonergic neurotransmission and regional brain volumes.

Kraus C, **Savli M**, Hahn A, Höflich A, Baldinger P, Wadsak W, Windischberger C, Mitterhauser M, Kasper S, Lanzenberger R.
ECNP Workshop on Neuropsychopharmacology for Young Scientists in Europe, 15-18 March 2012, Nice, France

62. Serotonin transporter ratio between raphe and projection areas predict SSRI treatment response in major depression
Kranz GS, Haeusler D, Akimova E, **Savli M**, Hahn A, Mitterhauser M, Spindelegger C, Wadsak W, Lanzenberger R, Kasper S.
ECNP Workshop on Neuropsychopharmacology for Young Scientists in Europe, 15-18 March 2012, Nice, France

63. Normal database of the serotonergic system in healthy subjects using multi-tracer PET
Savli M, Bauer A, Häuseler D, Ding YS, Hahn A, Kroll T, Ungersböck J, Neumeister A, Henry S, Mitterhauser M, Wadsak W, Rattay F, Kasper S, Lanzenberger R
18th Annual Meeting of the Organization for Human Brain Mapping (HBM), June 10-14, 2012, Beijing, China

64. Reduced insula activation associated with electric acupuncture: A placebo-controlled fMRI study
Chang JL, **Savli M**, Gao Y, Losak J, Zhu D, Hahn A, Zhong HZ, Tan ZJ, Lanzenberger R
18th Annual Meeting of the Organization for Human Brain Mapping (HBM), June 10-14, 2012, Beijing, China

65. A Normative database of the serotonergic system in healthy subjects using multi-tracer PET
Kraus C, Mitterhauser M, Bauer A, Ding Y-S, Henry S, Rattay F, **Savli M**, Lanzenberger R.
8th PhD Symposium, June 13-14, 2012, Vienna, Austria

66. Higher-order principles in distribution patterns of serotonergic receptor subtypes revealed by PET.
Attaripour Isfahani S, Wadsak W, Bauer A, Ding Y-S, Henry S, Rattay F, Lanzenberger R, **Savli M**
8th PhD Symposium, June 13-14, 2012, Vienna, Austria

67. Moleculare connectivity in patients with unilateral temporal lobe epilepsy investigated with [^{18}F]FDG PET.
Vanicek T, Hahn A, Asenbaum S, Assem-Hilger E, **Savli M**, Kranz G, Baldinger P, Lanzenberger R
8th PhD Symposium, June 13-14, 2012, Vienna, Austria

68. Brodmann Area database of the serotonergic system in healthy subjects using multi-tracer PET

M. Savli, W. Wadsak, A Bauer, YS Ding, A Hahn, A Neumeister, M. Mitterhauser, S Attaripour-Isfahani, P Baldinger, R. Lanzenberger
9th International Symposium on Functional Neuroreceptor Mapping of the Living Brain (NRM), 9-11 August 2012, Baltimore, USA

69. Interaction of inhibitory and excitatory receptors of the serotonergic system: A multi-tracer PET study
M. Savli, M. Mitterhauser, YS Ding, A Hahn, A Neumeister, A Bauer, W. Wadsak, S Attaripour-Isfahani, A Höflich, R. Lanzenberger
9th International Symposium on Functional Neuroreceptor Mapping of the Living Brain (NRM), 9-11 August 2012, Baltimore, USA

70. Treatment response in major depression predicted by serotonin transporter interplay
R Lanzenberger, G Kranz, D Häusler, E Akimova, **M Savli**, A Hahn, M Mitterhauser, C Spindelegger, W Wadsak, S Kasper
9th International Symposium on Functional Neuroreceptor Mapping of the Living Brain (NRM), 9-11 August 2012, Baltimore, USA

71. Whole brain relationship of serotonergic receptors
Savli M, Mitterhauser M, Ding YS, Hahn A, Neumeister A, Bauer A, Wadsak W, Attaripour-Isfahani S, Höflich A, Lanzenberger R
25th European College of Neuropsychopharmacology (ECNP) Congress, 13-17 October 2012, Vienna, Austria

72. Molecular connectivity in patients with unilateral temporal lobe epilepsy investigated with [18F]FDG PET
Vanicek T, Hahn A, Solá R, Asenbaum S, Assem-Hilger E, **Savli M**, Kranz G, Baldinger P, Kasper S, Lanzenberger R
25th European College of Neuropsychopharmacology (ECNP) Congress, 13-17 October 2012, Vienna, Austria

73. Prediction of SSRI treatment response in major depression based on serotonin transporter binding ratios
Kranz G, Lanzenberger R, Häusler D, Philippe C, **Savli M**, Hahn A, Mitterhauser M, Spindelegger C, Wadsak W, Kasper S
25th European College of Neuropsychopharmacology (ECNP) Congress, 13-17 October 2012, Vienna, Austria

Vienna, September 2012